TÉCNICO LISBOA

Cooperation of Humans and Robots Underwater

André Mendes Potes

Thesis to obtain the Master of Science Degree in

Electrical and Computer Engineering

Supervisor: Professor David Alexandre Cabecinhas
Professor António Manuel dos Santos Pascoal

Examination Committee

Chairperson: Professor João Fernando Cardoso Silva Sequeira
Advisor: Professor David Alexandre Cabecinhas
Member of the Committee: Doutor Pedro António Duarte Marques Lourenço

December 2021

Declaration: I declare that this document is an original work of my own authorship and that it fulfills all the requirements of the Code of Conduct and Good Practices of the Universidade de Lisboa.

Declaração: Declaro que o presente documento é um trabalho original da minha autoria e que cumpre todos os requisitos do Código de Conduta e Boas Práticas da Universidade de Lisboa.

Acknowledgements

The development of this thesis was not possible without some important people present in my life.

I want to express my deepest gratitudes towards my Advisor and Professor David Cabecinhas whose help and perseverance were essential to the beginning of such an important step towards my course completion and future career. I do not think it would be possible to achieve this work progression without his guidance and availability at any time of the day.

I also want to say a huge thank you to Professor António Pascoal for his interest and expertise in judging our progression and making sure that we are deeply motivated for the work ahead of me, both during classes but also in the DSOR meetings.

A big hug to my colleagues Rita and Gonçalo for their support during the MARETEC course in the Summer times, whose work and helping hand was crucial to this thesis development.

Also, my huge thank for all the collaboration with my colleagues from DSOR whose help is undoubtedly valuable, specially from Marcelo, David Souto, João Cruz and João Quintas.

A special thanks to my parents, sister, and close friends who supported me through this academic journey and always pushing for the best of me during stressful times, making sure to easy my mind and distract me whenever it was needed the most.

As a final remark, I would like to thank Fundação para a Ciência e Tecnologia (FCT) trough project H2020 EU Marine Robotics Research Infrastructure Network [ID731103] and the Blue Roses project [863619], co-funded by the European Maritime and Fisheries fund of the European Union, for partially funding and supporting this work.

Abstract

In underwater environments, human divers face enormous challenges commonly related with poor visibility, lack of orientation, heavy equipment, limited breathing time and pressure-related issues. This does not only hinder the diver's work performance, but also increases the probabilities of occurring accidents. With this in mind, the present work addresses the problem of enabling cooperative strategies between the diver and autonomous underwater vehicle (AUV) aiming to increase task safety and efficiency levels. From a practical perspective, our work contributes by proposing a cooperation architecture between a diver and the AUV guidance, navigation and control systems. Under this cooperation framework, we present state of the art solutions to localize and track the diver via algorithms and on board sensors of the AUV and follow up by designing its control system. And from a theoretical perspective, the derivation of the controllers exploit nonlinear Lyapunov based techniques and geometric control analysis tools, achieving robust properties and performance that are proved formally. Simulations results are presented and discussed, in the presence of measurement noise, constant ocean current disturbances and uncertainty in the model parameters of our vehicle, that illustrate the performance and robustness achieved with the proposed control system in a realistic cooperative scenario with a diver. Future work is highlighted, suggesting subsequent directions on this relatively new field of cooperation between diver and robots and the control problems faced while analyzing the stability of our control system.

Keywords: Autonomous underwater vehicles, Diver-robot interaction, Target tracking, Geometric control, Stability of nonlinear systems, Path following.

Resumo

Mergulhadores em ambientes submarinos são confrontados com enormes desafios como fraca visibilidade, falta de sentido de orientação, dependência de equipamentos de respiração, que potencialmente afeta o desenvolvimento do trabalho do mergulhador e aumenta as probabilidades de ocorrer acidentes. Tendo isto em mente, o trabalho presente aborda o problema de criar estratégias de cooperação entre mergulhadores e veículos submarinos autónomos (AUV), com o intuito de aumentar níveis de segurança e eficiência. Numa perspetiva prática, o nosso trabalho contribui com a proposta de uma arquitetura de cooperação com um mergulhador, através dos sistemas de navegação e controlo de um AUV. Neste enquadramento, apresentamos soluções de estado da arte relacionadas com a localização e seguimento de um mergulhador via sensores e algoritmos implementados no veículo, seguido pelo desenho do sistema de controlo do mesmo. Finalmente, numa perspetiva teórica, os controladores são projetados explorando técnicas de análise Lyapunov de sistemas não linear e controlo geométrico, alcançado soluções finais robustas provadas formalmente. Apresentam-se resultados de simulações realizadas com o objetivo de provar o desempenho das mesmas soluções, na presença de ruído, incerteza de parâmetros do modelo do veículo e correntes oceânicas, num cenário realístico em cooperação com um mergulhador. Por fim, delineámos um plano de trabalhos futuro neste relativamente novo tema de trabalho e os problemas embebidos na teoria de controlo, que se encontraram aquando o desenvolvimento do nosso trabalho.

Palavras-Chave: Controlo geométrico, Estabilidade de sistemas não lineares, Interação robot-mergulhador, Seguimento de caminho, Seguimento de alvos, Veículos submarinos autónomos.

Contents

List of Figures

List of Tables

List of Acronyms

LTI	Linear time-invariant
PID	Proportional-Integral-Derivative
PD	Proportional-Derivative
SNAME	Society of Naval Architects and Marine Engineers
NED	North-East-Down
UUV	Unmanned Underwater Vehicle
AUV	Autonomous Underwater Vehicle
UAV	Unmanned Aerial Vehicle
ASV	Autonomous Surface Vehicle
AMRV	Autonomous Marine Robotic Vehicle
ROV	Remotely Operated Vehicle
DVL	Doppler Velocity Log
IMU	Inertial Measurement Unit
POM	Position-only Measurements
PVM	Position-Velocity Measurements
VRU	Vertical Reference Unit
AHRS	Attitude and Heading Reference System
USBL	Ultra-Short Baseline
LBL	Long Baseline
SBL	Short Baseline
SSS	Side-Scan Sonar
GNSS	Global Navigation Satellite System
MIMO	Multiple-Input-Multiple-Output
DOF	Degrees of Freedom
FLS	Forward-Looking SONAR
MEMS	Microelectromechanical Systems
SONAR	Sound Navigation and Ranging
aISS	Almost Globally Input-to-state Stable
ISS	Input-to-state Stable
IOS	Input-to-output Stable

AGAS	Almost Globally Assymptotically Stable
GAS	Globally Assymptotically Stable
GES	Globally Exponentially Stable

Chapter 1

Introduction

Diving has been around since humanity started to explore the ocean waters, from harvesting marine resources to fulfilling our innate human curiosity. At initial times, these activities were performed by divers with only bared hands and without much of the equipment and strategies that characterize present diving operations. During this maturation process, it was found through experience that diving is not an activity that is easily carried out as most terrestrial activities, and ultimately requires extreme caution and standardized procedures to minimize the dangerous risks faced by divers. But in the end, the output product of these operations allowed multiple discoveries of new materials, fauna, flora, the inner workings of our planet, provided answers to the many mysteries of mankind evolution and, most of all, prompted the development of new technology and the harvest our oceans energy and minerals. Nowadays, divers are subject to rigorous training and the existence of new underwater tools and equipment greatly benefits the development of their underwater work. However, risks are still present, no matter the diver experience or used gear. In a recent European study of safety measures during scuba diving operations [1], it was found that the most common risks faced by divers during these types of missions are related to oxygen depletion, equipment failure, nitrogen narcosis, inaccessibility to emergency facilities underwater, poor visibility and a lack of sense of direction. In addition, most divers are accompanied by buddy divers to reduce these risks during operation. Although important and necessary, these procedures can increase the cost of diving operations significantly and also their complexity. But rescinding this factor can result in an increased and higher probability of accidents, or worse, fatalities [2]. For that reason, there has been a recent interest in the development of new strategies and work ethics to carry out these diving operations, mainly those that are made solo, opening the question of whether the use of cooperative mechanisms between divers and robots can potentiate operation efficiency, reduce extra material, personnel and, above all, attenuate the risks faced by the diver on such operations. In addition to this thought-provoking question, the development and implementation of such cooperative mechanisms raise several challenges and opportunities for the control community. As highlighted in [3], the marine environment represents a challenging framework where novel applications will continue to set further requirements for future generations of marine robots and their enabling systems. Therefore, applications of these cooperative mechanisms will surely result in novel solutions to guidance, navigation and control problems, but also raise new challenges that will enable carrying out safely and efficiently these same solutions, resulting in a cyclical

research and development phase boosting innovation and contributing to the overall human experience. In underwater missions, the use of robots can be made in an autonomous approach with the use of Autonomous Marine Robotic Vehicle (AMRV)s (e.g., Autonomous Underwater Vehicle (AUV)s, Autonomous Surface Vehicle (ASV)s), or via Remotely Operated Vehicle (ROV) with the help of a human operator. Although there are certain advantages and disadvantages on both types of robots, AMRVs do have an advantage over ROVs: the foregoing of tether cables and increased precision in achieving certain mission objectives on their own, removing the human element out of the equation. With available data and information of the surrounding environment as well as the task at hand, there exist systematic and rigorous solutions to achieve the mission requirements with well-defined behaviours, founded on control and navigation theory [4]. ASVs are known to be a useful type of autonomous vehicle towards the execution and support of marine missions (see, for example, [5]–[9], and references therein) but their working environment is focused solely on the water surface. So, within the scope of this thesis, the cooperation mechanisms between divers and robots will be focused on an AUV platform which can both cover the surface and depths of the ocean environment.

1.1 Problem Definition

Given the above introduction and brief motivation to the theme of cooperation between AUVs and divers during diving operations, we now proceed to better formulate the problem at hand in a two-fold approach, that is, both from a practical and theoretical point of view.

From a practical perspective, this thesis focuses on expanding the theme of cooperation between AUV and divers and discuss possible cooperation strategies, highlighting different solutions that enable them and identifying their benefits to the diver and possible constraints. These strategies aim to reduce the risks faced by divers during different types of diving operations and/or augment their underwater capabilities via the use an AUV in the loop. However, it raises the following problems that need to be addressed:

- There is no universal cooperation method that an AUV performs alongside a diver. Many different types of diving operations exist and therefore various cooperation strategies need to be identified, that may or may not be suitable for these scenarios.
- For the AUV to perform the cooperation strategy, there must be a way to know the diver whereabouts, be it absolute or relative to the AUV position. This, by itself, is not straightforward as underwater environments pose many challenges in the design and control of AUVs, from the nonexistence of Global Navigation Satellite System (GNSS) signals to low-visibility and accentuated attenuation of electromagnetic waves [10], [11].
- To design the control system for the AUV, a navigation and control architecture must be formulated in which the cooperation strategy can be implemented.

Finally, from a theoretical viewpoint, the design of the control system for a single AUV poses a myriad of challenges, namely:

- The dynamics of marine vehicles are often complex and cannot be simply ignored or drastically simplified for control design purposes.

- For our AUV to reach arbitrary positions and attitudes references, different control laws for position and attitude must be addressed independently.
- In classical approaches to attitude control (e.g., local parameterization of rotation matrices, such via Euler angles) there is no global continuous feedback solution due to geometric singularities [12]. Since our vehicle must attain arbitrary attitude references, other attitude stabilization control laws must be addressed that offer global stability properties.
- Many AUVs control systems are usually separated into the dynamic and kinematic controller, facilitating their respective implementation in what is known as an inner-outer loop architecture [13], [14]. However, this their closed-loop interconnection is not guaranteed to be stable, raising the need to carefully study their interconnection stability properties.

In summary, we address the problem of *designing a 6 Degrees of Freedom (DOF) dynamic and kinematic control system for a single AUV within a cooperation framework system that will enhance the diverse capabilities and/or reduce associated risks with diving operations.*

1.2 State of the Art

Some of the above-mentioned problems have already been discussed in the literature and numerous solutions can be found, with some tackling partially different formulations of the problem at hand and others with solutions that can be adapted to the problems studied in this thesis. We will introduce representative state of the art works, whose solutions and presented challenges serve as a basis of support and guidance of our work developed onward.

1.2.1 Diver-Robot Interaction

It is worth mentioning some projects, works and developed robotic platforms that have been carried out towards the development and research of cooperation frameworks between AMRVs and divers, serving as a basis of support to the work carried out in this thesis. We will discuss some of these works in chronological order, mentioning relevant advancements and challenges of project/work individually.

The European project CO3-AUVs (Cooperative Cognitive Control for Autonomous Underwater Vehicles) [15] was carried out in 2009-2012 with the main objective of studying, developing and testing tools and algorithms towards more robust and intelligent coordination and cooperative control of AUVs as well as ASVs. The tasks at hand consisted of 3D mapping and perception, cooperative situation awareness, deliberation and navigation as well as behavioural control within restrictive underwater communications, a prevalent challenge in underwater environments. The results and achievements attained in this project were then extended with the development and testing of diver assistance scenarios, namely the integration and field test evaluation of the systems required for cooperative navigation and motion control of single/multiple Autonomous Marine Robotic Vehicle (AMRV) working together with a human in the loop. This demo was motivated by an operational constraint where a diver starts from a simple support boat after she/he has thrown a set of small AMRVs equipped with GPS receivers and hydrophones in the water. Then, the AMRVs will guide and follow the diver keeping position

at the geometric centre on top of the diver, via estimates of the diver location with acoustic channels and pingers (that the diver possesses), using trilateration techniques. The diver then sees the heading information of the desired underwater location bearing's, via a set of LEDs display in their goggles, whose information is provided via an acoustic channel by the AMRVs. In Fig. 1.1 we can observe the diver-robot mission scenario interpretation. The experimental tests proved the viability of the concept set forth for combined robot-assisted diving operations using cooperative path-following techniques with multiple marine vehicles. Future work in deeper waters will aim at improving at making the overall system more ergonomic and efficient, via different acoustic and visual techniques of navigation and towards using lesser agents in the loop.

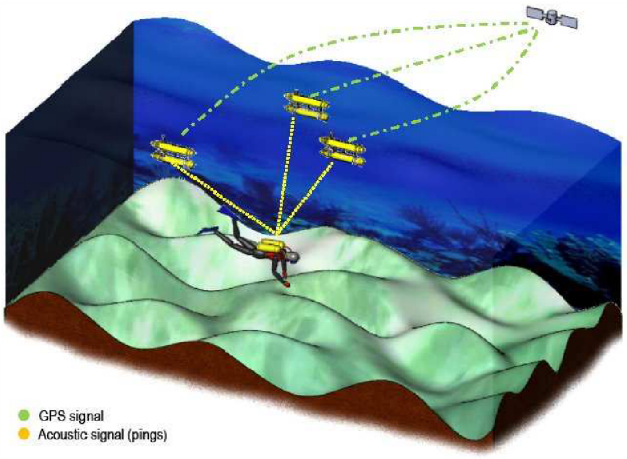

Figure 1.1: Illustration of the interaction between humans and AUVs in the CO3-AUVs project (obtained from [15]).

CONMAR (Cognitive robotics: cooperative control and navigation of multiple marine robots for assisted human diving operations) [16] was a European project coordinated by Instituto Superior Técnico with the main objective to contribute to the area of cooperative navigation in marine environments, with special emphasis on mission scenarios with human divers in the loop. Much like the project CO3-AUVS, discussed earlier, the tasks addressed in the project were motivated by a larger mission concept whereby the vehicles are asked to supervise the diver and guide him/her along a pre-planned path by issuing heading commands that the diver must follow. Central to the implementation of such a system, capable of estimating the position of the diver underwater, is the correct placement of the companion vehicles. To study this issue, and in parallel with the task described above, research was done on the problem of optimal sensor placement for target positioning in three dimensions, with the restriction that the sensors be placed at the water surface. A solution to this problem involved the computation of so-called Cramér-Rao-Bounds to compute the best positioning performance that can be achieved with any unbiased target position estimator. This culminated in the development of a prototype of a tracking system to assist human divers that has good potential to further be enhanced and witness the transition from the laboratory to the real world.

Another major project towards the diver-robot interaction underwater was project ICARUS (Integrated Components for Assisted Rescue and Unmanned Search operations) [17] carried out in the years of 2012-2016 with the main objective of increasing the situational awareness of humanitarian crises, such that more work can be done in a shorter amount of time. It is impossible to provide one solution which fits all needs, as every crisis is different, therefore the project aims to provide an integrated proof-of-concept solution, to be evaluated by a

board of expert end-users that can ensure that operational needs are addressed, with assistance unmanned air, ground and sea vehicles, equipped with victim detection sensors. More specific to the context of human-robot interaction, ICARUS results and findings pointed out that, in search and rescue diving operations, an efficient and rapid search for human survivors maximizes the chances of survival. In this regard, unmanned vehicles equipped with sensing technology are an excellent choice for this task, which have numerous advantages compared to classical human search and rescue teams. Additionally, it was proposed the development and employment of survival capsules that can be adapted to ASVs and, with the help of other unmanned vehicles (e.g., AUVs, UAVs, etc.) and extra sensors, gather information and reach identified survival victims. Although this project concerned a more detailed planning approach towards eventual catastrophes and reducing their social/economic impact, it discussed some important aspects and cooperation strategies that can benefit said operations, evident from the fact that unmanned vehicles can possess efficient and complex equipment towards search and rescue mission, motivating their use and the development of autonomous cooperation algorithms. However, as is the nature of these operations, search and rescue missions can vary greatly in complexity and characteristics therefore it is quite difficult to come up with general solutions. The framework that this project developed will help define the adequate strategies and possible solutions towards increasing the survival probabilities of victims.

The European project CADDY (Cognitive Autonomous Diving Buddy) [18], carried out in the span of 3 years (2014-2017) was also important, being very focused on the cooperation between divers and robots within a framework of a diving buddy which is a critical concept in diving operations. The project aims to establish an innovative set-up between a diver and companion AUVs and ASVs that exhibit cognitive response through learning, interpreting, and adapting to the diver's presence, physical state, and actions, in a cooperative scenario as shown in Fig. 1.2. More specifically, the desired behaviour can be categorized on 3 fronts:

1. Observation - The robot buddy can observe the diver with onboard sensors, be it via visual or acoustic signals.

2. Interpretation - The robot buddy possesses in-built algorithms towards reconnaissance of gestures and visual queues signalled by the diver, much like a diver buddy would communicate with another diver underwater.

3. Guidance - The robot can guide the diver in an underwater environment while maintaining a close visual range, both from the diver and the sensors equipped in him/her.

The project development resulted in solutions regarding areas of control, navigation, and planning, but mainly constructed a bridge between underwater guidance, navigation and control theory and machine learning algorithms, in which cooperation structures between divers and robots have benefited immensely. With the use of an ASV it is possible to locate a diver underwater maintaining a centred geometrical position on top of the diver, much like the CO3-AUVs project, via control positioning systems and acoustic pingers. Additionally, this information is relayed to another buddy AUV which maintains proximity with the diver and performs position and attitude control (this requires the AUV buddy to be fully actuated, which translates into a more complex and costly robot platform). The buddy AUV is then able to observe the diver and interpret their behaviour

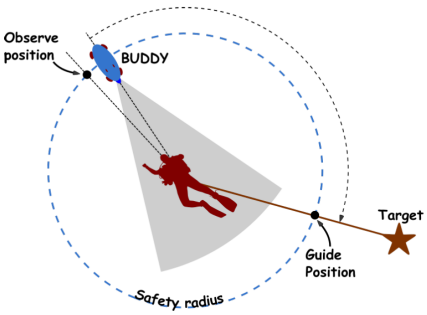

(a) The geometric distribution of BUDDY, the diver and the desired target point or observation position. (obtained from [18]).

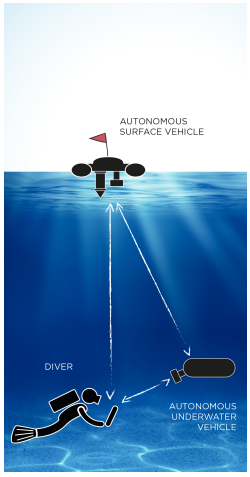

(b) Concept demonstrating the relation between two unmanned vehicles which collaborate with a single diver (obtained from [18]).

Figure 1.2: Project CADDY approach to diver-robot cooperation.

from machine learning algorithms that were developed using a previously obtained data set from diver gestures. These tasks allow the buddy AUV to accomplish the mission requirements of observation (1), interpretation (2) and guidance (3).

Built on top of CADDY project development, many recent works have extended their results and deliverables towards enhancing autonomous diver-AUV via image processing and machine learning techniques. In [19], the authors proposed a sophisticated gesture-based communication system for an AUV that allows divers to tell the robot to help them with certain tasks. The gesture-based language (CADDIAN) was developed based on standardized and aggregated diver gestures, with an alphabet, syntax, and semantics to ensure logical coherence. Following that, a hierarchical classification strategy based on stereo images is shown for hand gesture identification. This stops the AUV from performing motions that are unneeded, infeasible, or potentially dangerous. Other authors took a different approach but with the same principles in [20], where gesture recognition algorithms were implemented on a AUV to dynamically reconfigure mission tasks and parameters. On the other hand, in [21] the authors resorted to focusing on recognizing the diver faces so that AUVs will be able to engage in collaborative tasks with the correct person in human-robot teams and ensure that instructions are accepted from only those authorized to command the robots. Finally, in [22], the authors derived a multiple diver tracking-by-detection algorithms based on a convolutional neural network (for diver detection) and a tracking algorithm from images obtained by the AUV, resulting in accurate identification of multiple divers during tracking.

Lastly, it is worth mentioning the Ocean One project [23] carried out by Standford University in 2016. Albeit not hugely correlated with the framework of cooperation, but instead more focused on the development of a robot that could handle specific and complex tasks underwater that are usually carried out by a diver, this has proved to be an extremely useful companion/buddy to the diver himself/herself. The project main goal was more broad towards the challenge of accessing oceanic depths and whose solution was a bimanual force-controlled humanoid robot denoted as Ocean One that affords immediate and intuitive haptic interaction in oceanic environments.

Figure 1.3: Ocean One diving in the Mediterranean at 15 m, interacting with the diver in a compliant and safe manner (obtained from)[23]).

The Ocean One concept is to create a robotic humanoid with a high degree of autonomy in physical interaction, as shown in Fig. 1.3, connected to a human expert through an intuitive interface. The robot is designed with advanced skills to interact with its environment. The human typically instructs the robot through high-level cognitive guidance but can intervene at any level of operation. This is made possible by building a rich interface for the human operator, one that provides visual and haptic feedback together with a user command centre (UCC) that displays data from other sensors and sources. Ocean One's accomplishments mark the beginning of a new level of man-machine cooperation. Future work foresees robotic avatars that will search for and acquire materials in hazardous and inhospitable settings, maintain support equipment at remote sites, or build infrastructure for monitoring underwater environments.

1.2.2 Single Vehicle Motion Control

The control of an AUV towards autonomous cooperation with a diver can be tackled from different perspectives, each with unique solutions. In summary, our control problem, as mentioned before in Section 1.1, consists in designing adequate controllers that can control the vehicle kinematics and dynamics in position and attitude, independently. This requires a vehicle that can control both with its actuators, that is, being fully actuated, therefore our thesis will focus solely on these types of vehicles. The problem of controlling the vehicle's kinematic components in both position and attitude of the vehicle is by no means a new control problem. Starting with the former, this consists in positioning the vehicle on the desired point in 3-dimensional space and this problem can be formulated in different control objectives. One can approach this problem by formulating it as a *set-point regulation* (or *point stabilization*) problem which concerns the basic and critical motion control for the vehicle to stabilize at the desired reference chosen to be constant. A guidance system provides these desired references via auxiliary sensor data, weather data, obstacle and collision avoidance data, or other means of information, which is then pre-processed to generate a feasible point towards motion control. Then, the controller referred to as *regulator*, produces the necessary inputs to drive the vehicle state towards these references. Examples of this kind of controller are constant depth, trim, heel and speed controllers. There has been much research regarding this type of control problem, in the context of underwater vehicles [24]–[26]

and usually, these types of problems are easy to define and the respective controller are easily implemented. However, many stability problems might arise when coupling both this guidance system and the controller itself, where the separation of guidance and autopilot functions may not yield stability [27]. In addition, constant input or set-points reference constrain our control objective to basic formulations and does not leave room for other possible formulations such as course-changing manoeuvres, speed-changing and attitude control. Another formulation is the *trajectory tracking* problem, whose control objective is to force the vehicle to reach and follow a time parameterized reference curve. These allow a more broad and different type of definitions to be used in terms of tracking certain reference signals. For underwater vehicle systems, the trajectory-tracking problem is now reasonably well understood and applied in recent works [28], [29]. However, as is well known in the marine robotics literature [27] this may lead to situations where the AUV faces strong ocean currents and the vehicle stalls with almost no control authority. Furthermore, trajectory tracking control often leads to jerky vehicle motion when attempting to meet the time-restricted spatial requirements. With this, a similar but intrinsically different formulation arises known as *path-following* problems whose control objective is to also force the vehicle to follow a geometric path but without an associated timing law. With this, a smoother convergence to a path is achieved, and the control signals are less likely pushed to saturation [27]. Additionally, in non-minimum phase system, path-following schemes do not suffer from zero-dynamic stability performance limitations [30]. For land robots, these methodologies are well known and established, usually deriving the controller at a kinematic level [31]. However, in marine robotics, the same can not be applied as a result of highly non-linear dynamics and coupling terms, such as hydrodynamic damping, Coriolis-centripetal forces, etc [32], related to the surrounding water environment. In [33], [34], a path-following scheme was developed, where the work [31] was extended to deal with the underwater vehicle dynamics. However, the extension has an associated problem: *the initial position of the vehicle is restricted to lie inside a tube around the path, the radius of which must be smaller than the smallest radius of curvature that is present in that path*. It is possible to bypass this problem with an additional degree of freedom that controls the progression rate of the virtual particle [35]. In our work, we extend the *path-following* problem and generalize it to a *moving path-following* problem that consists of steering the robotic vehicle along *a-priori* specified geometric path expressed with respect to a moving target frame [36]. The present thesis builds the positioning controller and respective stability analysis on these previous results.

The second problem concerns the task of changing the vehicle attitude to stabilize at a certain reference. This problem can be regarded as a *set-point regulation* problem of attitude stabilization of a rigid body, where the state space of the attitude dynamics are defined in $SO(3)$, the space of rotation matrices where $SO(3)$ stands for the Special Orthogonal group of 3D matrices. Specifically, on $SO(3)$, it is possible to parameterize such rotation matrices using Euler angles, which facilitate the approach and design of attitude controllers, by transforming the state space into a Euclidean vector space [37], which becomes more intuitive and simple to derive control laws. However, such approaches only guarantee local stability, do not assure trajectories from approaching singularity zones (e.g., gimbal lock, pitch) or even interpolation between points. Another way to represent such parameterization is the use of quaternions [38], which cover the map of rotation matrices in $SO(3)$ providing a globally non-singular parameterization of $SO(3)$. However, such control solutions can exhibit unwinding behaviour, that is, the solution is easy to define in $SO(3)$ but is not globally well defined,

which may result in a system rotating unnecessarily through large angles to reach a certain configuration, even though it may start near it [39]. Additionally, systems evolving in this space face topological obstructions not allowing the existence of GAS equilibrium points [39]. Therefore, one must relax this definition to design attitude controllers and define the existence of AGAS equilibrium points [40]. In loose terms, this corresponds to saying the equilibrium point is stable and all solutions except for those starting in a certain set of measure zero, converge asymptotically to that point. A set of measure zero is considered thin and negligible in both a measure-theoretical and a topological sense. In practical terms, this assumption is innocuous since the slightest disturbance or sensor noise will prevent system trajectories from remaining on this thin-set. For a more refined definition of AGAS refer to [41]. In [42] the authors propose an *Almost Globally Assymptotically Stable* (AGAS) controller design for attitude stabilization and the present thesis builds on top of these results to achieve the desired configuration related to the mission requirements without the risk of creating attitude singularities and unwinding phenomena.

The solutions discussed so far formulate our problems of position and attitude stabilization control, whose solutions come in the form of different controllers that provide the necessary kinematic inputs (e.g, velocities) for the vehicle to follow. Since an underwater vehicle obeys certain dynamical constraints, it does not follow these reference inputs immediately. Classical solutions usually make use of Proportional-Integral-Derivative (PID) controllers, inverse dynamics, or other motion control solutions, whose equilibrium points satisfy certain stability conditions in closed-loop form with vehicle dynamics. To facilitate our stability analysis and controller derivation between the kinematic and dynamic level, the concept of inner-outer loop was formulated [14]. It was initially used in the aircraft control literature, to provide a convenient approach design for the outer-loop position and attitude controllers, as well as the inner-loop controller whose outputs are the forces and torques of the vehicle actuation, accomplishing the speed requirements. It is known that such control schemes exhibit a fast-slow temporal scale separation [13], [14] which yields simple "rules of thumb" for controller tuning, rooted in singular perturbation theory [43], providing the advantages such as: i) the structure of the outer loop controller does not depend on the vehicle's dynamics, ii) convenient way to derive control laws in a general approach to use in various vehicles. Caution must be taken on the design of these types of control architectures because, even if each individual controlled system satisfies robust and asymptotic stability properties, the interconnection of both might not be stable under the same conditions [14]. For that, different state of the art stability analysis tools exist to deal with such situation and carefully analyses them, mostly rooted in the *Input-to-state Stable* (ISS) and *Input-to-output Stable* (IOS) notions [43]–[45] and variations of these, e.g., *Almost Globally Input-to-state Stable* (aISS) [46], [47], ISS with restrictions [48]. With this, our thesis motion control problem is tackled by following this decomposition of the kinematics and dynamics into an inner-outer loop approach, where the inner loop forces the vehicle to move at the desired speed, provided by the outer loop, which takes into account the kinematics task of position and attitude stabilization, and carefully analyzing the different stability conditions in which both systems work together in unison.

1.3 Main Contributions

This thesis presents a series of cooperation frameworks between divers and robots in underwater diving operations, and position and attitude controllers are derived for a single AUV under the proposed cooperation architecture. These results are kept generalized so that they can be applied to any fully-actuated AUV, from the kinematic to a dynamical level. Given this, our key contributions are:

- **AUV Modeling** - A full 6 DOF mathematical model representing the kinematics and dynamics of an AUV taking into the underwater dynamics, in which our control system will be implemented upon.
- **Diver-Robot Cooperation** - A review on different types of diving operations, associated risks and tasks performed, and possible cooperation frameworks between robots and divers that enhance mission performance and security.
- **Diver Tracking** - Discussion of different technologies and implementations towards diver tracking, and obtain the kinematic components of a diver, that is, position and velocity. A Kalman diver tracking filter and a cooperation architecture were proposed under the listed cooperation frameworks and diver tracking formulations, in which the control system will be inserted to promote cooperative strategies with the diver.
- **Motion Control** - A control system is proposed to stabilize both position and attitude of an AUV at arbitrary references, extended to the vehicle dynamic level and within the working environment of the cooperation architecture. Additionally, a thorough stability analysis of the inner-outer loop interconnection allowed us to apply state of the art input-to-state notions of stability on systems evolving in distinct spaces.

1.4 Thesis Outline

The structure of this thesis is as follows:

Chapter 2 contains the mathematical theoretical preliminaries of non-linear control that will be recalled along with the derivation of the AUV control system.

Chapter 3 introduces a generalised mathematical model that describes an underwater vehicle motion used in this work, that will be later taken into account for control design purposes and simulations.

Chapter 4 introduces the different cooperation frameworks between divers and robots that are possible to introduce in various diving operations and presents classical and recent efforts towards solving the diver tracking problem, in which a diver position and velocity are estimated. An architecture for navigation and control of an AUV is proposed to enable cooperative behaviour with a diver.

Chapter 5 derives dynamic and kinematic control laws for the motion control of the AUV within the proposed cooperation architecture and analyses the properties of the closed-loop system.

Chapter 6 presents the simulations that were made to test and demonstrate the controller performance and its stability properties, devised in the previous chapters.

Chapter 7 summarizes the results obtained and suggests the directions of further investigation.

Chapter 2

Theoretical Preliminaries

In this chapter, we introduce some mathematical notations and definitions used throughout this thesis, as well as important non-linear control tools for stability analysis of the control problems discussed in Chapter 5. After defining the notation in Section 2.1, we give a brief overview of the theory of non-linear stability theory in Section 2.2.

2.1 Mathematical Groundwork and Notations

To facilitate the interpretation of mathematical expressions, we use bold symbols and letters to reference vectors or matrices, and normal script for scalars. Moreover, vectors are represented in lower case, whereas matrices are represented in upper case. $\boldsymbol{I}_n$ represents the $n \times n$ identity matrix, where $n > 0$ denotes a positive integer. A block diagonal matrix is represented as diag$(A1, ..., An)$.If x is a scalar, $|x|$ denotes its absolute value. If $\boldsymbol{x}$ is a vector, $\|\boldsymbol{x}\|$ denotes its norm. The norms used in this thesis are the class of p-norms defined by

$$\|\boldsymbol{x}\|_p = (|x_1|^p + \cdots + |x_n|^p)^{(1/p)}$$

where $p \geq 1$ is a real number, and $x_i, \quad i = 1, \cdots, n$ refers to the ith element of $\boldsymbol{x}$. Additionally, the asymptotic norm and (essential) supremum norm are denote by, respectively, with $\|\boldsymbol{x}\|_a = \lim_{t\to\infty} \|\boldsymbol{x(t)}\|$ and $\|\boldsymbol{x}\|_\infty = \sup_{t\geq 0} \|\boldsymbol{x}(t)\|$. For simplicity of notation, except when explicitly stated, $\|\cdot\|$ denotes the Euclidean 2-norm.

Respectively, for an arbitrary $n \times m$ matrix $\boldsymbol{A}$, if the p-norm for vectors is used, the corresponding (induced) norm is defined as

$$\|\boldsymbol{A}\|_p = \sup_{\boldsymbol{x}\neq\boldsymbol{0}} \frac{\|\boldsymbol{Ax}\|_p}{\|\boldsymbol{x}_p\|}$$

where $\boldsymbol{0}$ denotes the zero vector. In the special case of euclidean 2-norm and square $n \times n$ matrices, we have the following inequality

$$\lambda_{\mathsf{min}}(\boldsymbol{A}) \leq \|\boldsymbol{A}\|_2 \leq \lambda_{\mathsf{max}}(\boldsymbol{A})$$

where λ_{min} and λ_{max} denote, respectively, the smallest and largest eigenvalues of matrix $\boldsymbol{A}$.

We denote $\boldsymbol{S} : \mathbb{R}^n \mapsto \mathbb{S}$ as the cross-product operator, where $\mathbb{S} = \{A \in \mathbb{R}^{n\times n} : \boldsymbol{A} = -\boldsymbol{A}^T\}$ denotes the space of $n \times n$ skew-symmetric matrices. Note that $\boldsymbol{S}$ verifies $\boldsymbol{S}(\boldsymbol{a})\boldsymbol{b} = \boldsymbol{a} \times \boldsymbol{b}$, where $\boldsymbol{a}, \boldsymbol{b} \in \mathbb{R}^n$ and $\times$ is the vector cross product.

2.2 Stability Theory: A Brief Overview

Stability theory concerns the stability of linear and non-linear systems, more specifically, the stability of equilibrium points. There exist different notions of stability for such systems, and even more, these systems can be categorized into two types: *autonomous* and *non-autonomous* systems. Throughout this thesis, only the former is considered, as they only depend on the trajectories and are not explicitly dependent on time. Some theorems and definitions are introduced and borrowed from Khalil, in the book *Nonlinear Systems*, which are important to the development and design of control solutions to the problems described in Chapter 5. Finally, some stability notions and theorems showed in this chapter are applied to a general *non-autonomous* systems but can still be applied to *autonomous* systems, since it is only a matter of considering the independence of time, as is the case for the considered systems throughout this thesis, without loss of generality.

2.2.1 *Autonomous* Systems

Consider the following *autonomous* system

$$\dot{\boldsymbol{x}} = \boldsymbol{f}(\boldsymbol{x}) \tag{2.1}$$

where $\boldsymbol{f} : D \Rightarrow \mathbb{R}^n$ is locally Lipschitz in $\boldsymbol{x}$, that is, satisfies the following inequality

$$\|\boldsymbol{f}(\boldsymbol{x}) - \boldsymbol{f}(\boldsymbol{y})\| \leq L \|\boldsymbol{x} - \boldsymbol{y}\|, \quad L > 0 \tag{2.2}$$

The origin is an equilibrium point of (2.1), that is, $\boldsymbol{f}(\boldsymbol{0}) = \boldsymbol{0}$. By shifting the origin of the system, we may assume that the equilibrium point of interest occurs at $\boldsymbol{x} = \boldsymbol{0}$. If multiple equilibrium points exist, then the stability of each one is studied by appropriately shifting the origin, without loss of generality.

Definition 1 (Equilibrium Points)**.** *The equilibrium point $\boldsymbol{x} = \boldsymbol{0}$ of (2.1) is:*

- ***stable** (in the sense of Lyapunov) if, for each $\epsilon > 0$, there exists a $\delta(\epsilon) > 0$ such that*

$$\|\boldsymbol{x}(0)\| < \delta \Rightarrow \|\boldsymbol{x}(t)\| < \epsilon, \quad \forall t \geq t_0 \tag{2.3}$$

- ***unstable** if it is not stable*
- ***asymptotically stable** if it is stable and δ can be chosen such that*

$$\|\boldsymbol{x}(0)\| < \delta \Rightarrow \lim_{t\to\infty} \boldsymbol{x}(t) = \boldsymbol{0} \tag{2.4}$$

Notice that, there is no explicit dependence in time for the above-mentioned stability definitions. Now, we can proceed to state the following Lyapunov's stability theorem, on which important theorems for this thesis work are built upon.

Theorem 1 (Lyapunov Stability)**.** *Let $\boldsymbol{x} = \mathbf{0}$ be an equilibrium point of* (2.1) *and $D \subset \mathbb{R}^n$ be a domain that contains $\boldsymbol{x} = \mathbf{0}$. Let $V : [0, \infty) \times D \to \mathbb{R}$ be a continuously differentiable function such that*

$$V(\mathbf{0}) = \mathbf{0}, \quad V(\boldsymbol{x}) > 0 \text{ in } D \backslash \{\mathbf{0}\} \tag{2.5}$$

$$\dot{V}(\boldsymbol{x}) \leq \mathbf{0} \in D \tag{2.6}$$

Then, $\boldsymbol{x} = \mathbf{0}$ is stable. Moreover, if

$$\dot{V}(\boldsymbol{x}) < \mathbf{0} \text{ in } D \backslash \{\mathbf{0}\} \tag{2.7}$$

then $\boldsymbol{x} = \mathbf{0}$ is asymptotically stable.

A continuously differentiable function $V(\boldsymbol{x})$ satisfying (2.5) and (2.6) is called a *Lyapunov function*. The concept of *asymptotically stable* equilibrium points can further be extended to the case when $D = \mathbb{R}^n$, as stated by the following theorem.

Theorem 2 (Lyapunov Global Asymptotic Stability)**.** *Suppose assumptions of Theorem 1 are satisfied with inequalities* (2.5) *and* (2.6) *strengthened with*

$$V(\mathbf{0}) = \mathbf{0}, \quad V(\boldsymbol{x}) > 0, \quad \forall \boldsymbol{x} \neq \mathbf{0} \tag{2.8}$$

$$\dot{V}(\boldsymbol{x}) < \mathbf{0}, \quad \forall \boldsymbol{x} \neq \mathbf{0} \tag{2.9}$$

and also satisfying

$$\|\boldsymbol{x}\| \Rightarrow \infty \Rightarrow V(\boldsymbol{x}) \Rightarrow \infty \tag{2.10}$$

then, $\boldsymbol{x} = \mathbf{0}$ is Globally Assymptotically Stable *(GAS).*

In robotics, and more generally in control theory, it is always interesting to have *asymptotically stable* equilibria as we want the system to evolve to a certain point, and not merely remain nearby. In Theorem 1, it only proves local stability, whereas in Theorem 2 it describes a global behaviour for the equilibria, for all initial conditions in $\mathbb{R}^n$, a stronger and desirable condition.

2.2.2 *Non-autonomous* Systems

Moving from *autonomous* systems towards *non-autonomous* systems, analyzing stability becomes less straightforward from the fact that the solution of *non-autonomous* systems depends not only on the initial time t_0 but also subsequent time t. To cope with this analysis it is necessary to use some comparison functions, known as class $\mathcal{K}$, class $\mathcal{K}_\infty$ and class $\mathcal{KL}$ functions, facilitating the proofs further ahead. Refer to [43] for an overview of the respective definitions.

Consider the following *non-autonomous* system

$$\dot{\boldsymbol{x}} = \boldsymbol{f}(t, \boldsymbol{x}) \tag{2.11}$$

where $\boldsymbol{f}$ is piecewise continuous in t and locally Lipschitz in $\boldsymbol{x}$, that is, satisfies the following inequality

$$\|\boldsymbol{f}(t, \boldsymbol{x}) - \boldsymbol{f}(t, \boldsymbol{y})\| \leq L \|\boldsymbol{x} - \boldsymbol{y}\| \tag{2.12}$$

for all $(t, \boldsymbol{x})$ and $(\boldsymbol{t}, \boldsymbol{y})$ in some neighborhood of $(t_0, \boldsymbol{x}_0)$. The origin is an equilibrium point if

$$\boldsymbol{f}(t, \boldsymbol{0}) = \boldsymbol{0}, \quad \forall t \geq 0 \tag{2.13}$$

Definition 2 (Equilibrium Points)**.** *The equilibrium point $\boldsymbol{x} = \boldsymbol{0}$ of* (2.11) *is:*

- ***stable*** *(in the sense of Lyapunov) if, for each $\epsilon > 0$, there exists a $\delta(t_0, \epsilon) > 0$ such that*

$$\|\boldsymbol{x}(t_0)\| < \delta \Rightarrow \|\boldsymbol{x}\| < \epsilon, \quad \forall t \geq t_0 \tag{2.14}$$

- ***unstable*** *if it is not stable*
- ***uniformly stable*** *if, for each $\epsilon > 0$, there exists a $\delta(\epsilon) > 0$ independent of time t_0 such that* (2.14) *is satisfied.*
- ***asymptotically stable*** *if it is stable and there is a positive constant $c(t_0)$ such that $\boldsymbol{x} \Rightarrow \boldsymbol{0}$ as $t \Rightarrow \infty, \quad \forall \|\boldsymbol{x}(t_0) < c\|$*
- ***uniformly asymptotically stable*** *if it is uniformly stable and there exists a positive constant c independent of time t_0, such that for all $\|\boldsymbol{x}(t_0)\| < c$, $\boldsymbol{x}8(t) \Rightarrow \boldsymbol{0}$ as $t \Rightarrow \infty$, uniformly in t_0, that is, for each $\eta > 0$, there exists $T(\eta) > 0$ such that*

$$\|\boldsymbol{x}(t)\| < \eta, \quad t \geq t_0 + T(\eta), \quad \|\boldsymbol{x}(t_0)\| < c \tag{2.15}$$

- ***exponentially stable*** *if there exists positive constants c, k, and λ such that*

$$\|\boldsymbol{x}(t)\| \leq k \|\boldsymbol{x}(t_0)\| \exp^{-\lambda(t-t_0)}, \forall \|\boldsymbol{x}(t_0)\| < c \tag{2.16}$$

It is possible to observe the main distinction of stability between *autonomous* and *non-autonomous* is that in the former case δ is independent of time t_0. In other words, stability for *non-autonomous* systems take into account the uniformity in time, a concept which guarantees the equilibrium point stability at initial times, so that equation (2.14) may hold for all t_0. For the case of *autonomous* this is already taken into account, as the system is not explicitly dependent on time, as seen in (2.1).

It is important to note that the definitions of *asymptotic stability* do not quantify the rate of convergence. There is a strong form of stability that demands an exponential rate of convergence.

Theorem 3 (Lyapunov Exponential Stability). *Let $\boldsymbol{x} = \mathbf{0}$ be an equilibrium point for* (2.11) *and $D \subset \mathbb{R}^n$ be a domain that contains $\boldsymbol{x} = \mathbf{0}$. Let $V : [0, \infty) \times D \Rightarrow \mathbb{R}$ be a continuously differentiable function such that*

$$k_1 \|\boldsymbol{x}\|^a \leq V(t, \boldsymbol{x}) \leq k_2 \|\boldsymbol{x}\|^a \tag{2.17}$$

$$\dot{V}\big|_{\dot{\boldsymbol{x}} = \boldsymbol{f}(\boldsymbol{x})} = \frac{\partial V_d}{\partial t} + \frac{\partial V_d}{\partial \boldsymbol{x}} f(t, \boldsymbol{x}) \leq -k_3 \|\boldsymbol{x}\|^a \tag{2.18}$$

$\forall t \geq 0$ and $\forall \boldsymbol{x} \in D$, where k_1, k_2, k_3 and a are positive constants. Then $\boldsymbol{x} = \mathbf{0}$ is exponentially stable. If the assumptions hold globally, then $\boldsymbol{x} = \mathbf{0}$ is Globally Exponentially Stable *(GES).*

Exponential stability is a strong notion of stability, in particular, due to the association of such conditions being more robust to perturbations to the system and essential in terms of control algorithms, especially adaptive control algorithms [49].

In some cases, it will not be possible to prove the stability of certain equilibrium points due to disturbances in the system. In such cases concepts related to boundedness are important, especially in perturbation theory [43].

Theorem 4 (Lyapunov Boundedness). *Let $D \subset \mathbb{R}^n$ be a domain that contains the origin and $V : [0, \infty) \times D \Rightarrow \mathbb{R}$ be a continuously differentiable function such that*

$$\alpha_1(\|\boldsymbol{x}\|) \leq V(t, \boldsymbol{x}) \leq \alpha_2(\|\boldsymbol{x}\|) \tag{2.19}$$

$$\dot{V}\big|_{\dot{\boldsymbol{x}} = \boldsymbol{f}(\boldsymbol{x})} = \frac{\partial V}{\partial t} + \frac{\partial V}{\partial \boldsymbol{x}} f(t, \boldsymbol{x}) \leq -W_3(\boldsymbol{x}), \forall \|\boldsymbol{x}\| \geq \mu > 0 \tag{2.20}$$

$\forall t \geq 0$ and $\forall \boldsymbol{x} \in D$, where $\alpha_1(\boldsymbol{x})$ and $\alpha_2(\boldsymbol{x})$ are class $\mathcal{K}$ functions and $W_3(\boldsymbol{x})$ is a continuous positive definite function. Take $r > 0$ such that $B_r \subset D$ and suppose that

$$\mu < \alpha_2^{-1}(\alpha_1(r)) \tag{2.21}$$

Then, there exists a class $\mathcal{KL}$ function β and for every initial state $\boldsymbol{x}(t_0)$, satisfying $\|\boldsymbol{x}(t_0)\| \leq \alpha_2^{-1}(\alpha_1(r))$, there is $T \geq 0$ (dependent on $\boldsymbol{x}(t_0)$ and μ) such that the solution of (2.11) *satisfies*

$$\|\boldsymbol{x}\| \leq \beta(\|\boldsymbol{x}(t_0)\|, t - t_0), \forall t_0 \leq t \leq t_0 + T \tag{2.22}$$

$$\|\boldsymbol{x}\| \leq \alpha_1^{-1}(\alpha_2(\mu)), \forall t \geq t_0 + T \tag{2.23}$$

Moreover, if $D = \mathbb{R}^n$ and $\alpha - 1$ belongs to class $\mathcal{K}_\infty$, then (2.22) *and* (2.23) *hold for any initial state $\boldsymbol{x}(t_0)$, with no restriction on how large μ is.*

The inequalities above (2.22) and (2.23) show that $\boldsymbol{x}$ is uniformly ultimately bounded with the *ultimate bound* of $\alpha_2^{-1}(\alpha_1(r))$. If $D = \mathbb{R}^n$ and α^{-1} belongs to class $\mathcal{K}_\infty$, then $\boldsymbol{x}$ is *Globally Uniformly Ultimately Bounded*. Moreover, if the system is *autonomous*, it is possible to drop the notion of uniformity and state that the trajectories of (2.1) are *ultimately bounded*, depending on the achieved conditions mentioned in Theorem 4.

2.2.3 Input/Output Systems

Until this point, we have only dealt with systems with no inputs and outputs. However, depending on the context, the system at hand might be influenced by other systems outputs or external disturbances. Moreover, the same system produces a certain output that might influence other systems being studied. Therefore, when studying certain systems interconnections, and disturbances or noise influencing the system, it is useful to represent a system input/output mechanism and study the stability and properties of the said system under these contexts.

Consider the following system

$$\dot{\boldsymbol{x}} = \boldsymbol{f}(t, \boldsymbol{x}, \boldsymbol{u}) \tag{2.24}$$

where $\boldsymbol{f} : [0, \infty) \times D \times D_u \Rightarrow \mathbb{R}^n$ is assumed to be locally Lipschitz in $\boldsymbol{x}$ and $\boldsymbol{u}$, inputs being measurable locally essentially bounded maps $\boldsymbol{u} : [0, \infty) \Rightarrow \mathbb{R}^m$, for some positive integers n, m, $D \subset \mathbb{R}^n$ a domain that contains the origin and $D_u \subset \mathbb{R}^m$ a domain that contains $\boldsymbol{u} = \boldsymbol{0}$. The *unforced* system associated with system (2.24) is considered as follows

$$\dot{\boldsymbol{x}} = \boldsymbol{f}(t, \boldsymbol{x}, \boldsymbol{0}) \tag{2.25}$$

Suppose system (2.25) has a GAS origin. One would assume that bounded inputs result in bounded state trajectories, as well as output, as is the case for linear systems with GAS equilibria [50]. But this property is not true for non-linear systems, such as our case, where solutions might diverge even for some inputs that converge to zero [44]. Therefore, this motivates the concept of *Input-to-state Stable* (ISS), that is, for any bounded input $\boldsymbol{u}$, the state $\boldsymbol{x}$ will also be bounded.

Definition 3 (Input-to-State Stability)**.** *The system* (2.24)*is said to be ISS if there exists a class $\mathcal{KL}$ function β and a class $\mathcal{K}$ function γ such that for any initial state $\boldsymbol{x}(t_0)$ and any bounded input $\boldsymbol{u}$ the solution $\boldsymbol{x}$ exists for all $t \geq t_0$ and satisfies the following condition*

$$\|\boldsymbol{x}\| \leq \gamma(\|\boldsymbol{u}\|_\infty) + \beta(\|\boldsymbol{x}(t_0)\|, t - t_0) \tag{2.26}$$

In some cases the ISS condition cannot be satisfied for any $\boldsymbol{x}(t_0)$ and $\boldsymbol{u}$. To address these class of problems, in [48], [51] the authors define the concept of ISS with restrictions on the initial states and/or inputs, that can be summarized in the following definition.

Definition 4. *The system* (2.24) *is said to be ISS with restrictions $\mathcal{X} \Rightarrow \mathbb{R}^n$ and $\Delta > 0$ on the initial state $\boldsymbol{x}(t_0)$ and the input $\boldsymbol{u}$, respectively, if there exist a class $\mathcal{KL}$ function and a class $\mathcal{K}$ function γ such that for any initial state $\boldsymbol{x}(t_0) \in \mathcal{X}$ and any bounded input function $\boldsymbol{u}$ satisfying $\|\boldsymbol{u}\| < \Delta$ the solution $\boldsymbol{x}$ exists for all $t \geq t_0$ and satisfies* (2.26)*.*

Then, the following theorem provides a Lyapunov framework to prove that (2.24) satisfies the ISS condition.

Theorem 5. *Let $V : [0, \infty) \times D \Rightarrow \mathbb{R}$ be a continuously differentiable function such that*

$$\alpha_1(\|\boldsymbol{x}\|) \leq V(t,\boldsymbol{x}) \leq \alpha_2(\|\boldsymbol{x}\|) \tag{2.27}$$

$$\dot{V}\big|_{\dot{\boldsymbol{x}}=\boldsymbol{f}(\boldsymbol{x})} = \frac{\partial V}{\partial t} + \frac{\partial V}{\partial \boldsymbol{x}} f(t,\boldsymbol{x}) \leq -W_3(\boldsymbol{x}), \forall\, \|\boldsymbol{x}\| \geq \rho(\|\boldsymbol{u}\|) > 0 \tag{2.28}$$

$\forall (t,\boldsymbol{x},\boldsymbol{u}) \in [0,\infty) \times \mathbb{R}^n \times \mathbb{R}^m$, *where* α_1, α_2 *are class* $\mathcal{K}_\infty$ *functions,* ρ *is a class* $\mathcal{K}$ *function, and* $W_3(\boldsymbol{x})$ *is a continuous positive definite function on* $\mathbb{R}^n$. *Then, the system* (2.24) *is ISS with* $\gamma = \alpha_1^{-1}(\alpha_2(\rho))$.

It is useful to also study the ISS condition of systems in cascade connections

$$\dot{\boldsymbol{x}}_1 = \boldsymbol{f}_1(\boldsymbol{x}_1, \boldsymbol{x}_2) \tag{2.29}$$

$$\dot{\boldsymbol{x}}_2 = \boldsymbol{f}_2(\boldsymbol{x}_2) \tag{2.30}$$

Suppose that both $\dot{\boldsymbol{x}}_1 = \boldsymbol{f}_1(\boldsymbol{x}_1, \boldsymbol{0})$ and (2.30) have GAS equilibrium points at the origin. It is possible to analyze the stability of the overall cascade connection equilibrium points, with the help of the following lemma.

Lemma 1. *Under the stated assumptions, if the system* (2.29)*, with* $\boldsymbol{x}_2$ *as input, is ISS and the origin of* (2.30) *is GAS, then the origin of the cascade system* (2.29) *and* (2.30) *is GAS.*

Until now, it was only discussed the ISS concept, related to the system state concerning the input. In certain models, the output might not be the state itself but other functions of the input and state of the system. Consider the following input-output model

$$\dot{\boldsymbol{x}} = \boldsymbol{f}(t,\boldsymbol{x},\boldsymbol{u}), \quad \boldsymbol{y} = \boldsymbol{h}(t,\boldsymbol{x},\boldsymbol{u}) \tag{2.31}$$

where, in addition to (2.24), $\boldsymbol{h} : [0,\infty) \times D \times D_u \Rightarrow \mathbb{R}^p$ is a continuous function of the system state $\boldsymbol{x}$ and input $\boldsymbol{u}$ with $\boldsymbol{h}(\boldsymbol{0}) = \boldsymbol{0}$ and output $\boldsymbol{y}$ taking values in $\mathbb{R}^p$, for some positive integer p.

The concept of *Input-to-output Stable* (IOS) arises to provide a stability analysis framework in the space of input and output signals, applied to models like (2.31). There exist many definitions of IOS but all of them work in the space of signals norm, known in the literature as *normed spaces*, which provide a measure of the size of the signal. In the context of this thesis and further proofs, we will work in the signal space of $\mathcal{L}_\infty$, the set of all bounded functions with the supremum norm $\|u\|_\infty$.

This norm is usually related to problems of finding maximum absolute, tracking error and the problem of control saturation [45]. Note that, since we only work in the space of supremum norm space $\mathcal{L}_\infty$ we can drop the subscript ∞ and simply refer to it as the space $\mathcal{L}$. Within this space, the input-output relation can be represented by

$$y = Hu \tag{2.32}$$

where H is some mapping/operator, from one norm space to another, specifying y in terms of u. With this, we can then proceed to define IOS.

Definition 5 (Input-to-Output Stability). *A mapping H is $\mathcal{L}$ stable if there exists a class $\mathcal{K}$ functions α, defined on $[0, \infty)$, and a nonnegative constant β such that*

$$\|Hu\|_\infty = \|y\|_\infty \leq \alpha(\|u\|_\infty) + \beta \tag{2.33}$$

Additionally, it is finite-gain $\mathcal{L}$ stable if, instead, there exists nonnegative constants γ and β such that

$$\|Hu\|_\infty = \|y\|_\infty \leq \gamma \|u\|_\infty + \beta \tag{2.34}$$

An useful relationship between ISS and IOS can be made, in a Lyapunov framework, via the following theorem.

Theorem 6. *Consider the system 2.31 with $D = \mathbb{R}^n$ and $D_u = \mathbb{R}^m$. Suppose also that*

- *The system $\dot{\boldsymbol{x}} = \boldsymbol{f}(t, \boldsymbol{x}, \boldsymbol{u})$ is proven to be ISS.*
- *$\boldsymbol{h}$ satisfies the following inequality*

$$\|\boldsymbol{h}(t, \boldsymbol{x}, \boldsymbol{u})\| \leq \alpha_6(\|\boldsymbol{x}\|) + \alpha_7(\|\boldsymbol{u}\|) + \eta, \quad \forall (t, \boldsymbol{x}, \boldsymbol{u}) \in [0, \infty) \times \mathbb{R}^n \times \mathbb{R}^m \tag{2.35}$$

for some class $\mathcal{K}$ functions α_6, α_7 and a nonnegative constant η.

Then, for each $\boldsymbol{x}(0) \in \mathbb{R}^n$, the system (2.31) *is $\mathcal{L}$ stable.*

Finally, when studying the stability of interconnected systems in a feedback form, that is, the output of one system is the input of another and vice-versa, it is useful to use the formalism of IOS in the sense of this connection being finite-gain $\mathcal{L}$ stable. Then, the following theorem, known in the literature as *small-gain* theorem, provides a simple condition to prove that the interconnection is IOS.

Theorem 7 (Small-gain Theorem). *Consider two system H_1 and H_2 and suppose that both are finite-gain $\mathcal{L}$ stable, that is*

$$\|y_1\|_\infty \leq \gamma_1 \|u_1\|_\infty + \beta_1 \tag{2.36}$$

$$\|y_2\|_\infty \leq \gamma_2 \|u_1\|_\infty + \beta_2 \tag{2.37}$$

where β_1 and β_2 a nonnegative constant bias terms. Then, the feedback connection of both system is finite-gain $\mathcal{L}$ stable if $\gamma_1 \gamma_2 < 1$.

The theorems and definitions presented in this chapter prove and give sufficient conditions for certain stability criteria, and will be the basis of support for the derivation of controllers and accomplish the requirement. It does not, however, give a "prescription" for determining the Lyapunov function $V(\boldsymbol{x}, t)$. Since the theorem only gives sufficient conditions, the search for a Lyapunov function establishing the stability of equilibria could be arduous. In Chapter 5 we will discuss the problem of controlling the vehicle in a cooperative framework, with diverse control problems, describing the specifications and designing control laws that solve the mentioned problems. For that, respective proofs will guide the reader to find a suitable Lyapunov function to derive the control law and apply it to these theorems to prove stability conditions.

Chapter 3

Underwater Robots Modelling

Autonomous robots that operate in underwater environments require immense dexterity and rely on huge amounts of external information to safely and efficiently carry out the intended missions. As a result, careful work is needed in the design and implementation of such machines. In this Chapter we discuss and obtain a mathematical model for a generic marine vehicle moving in three-dimensional space, thus requiring a 6 DOF description. We start by defining the different frames of reference in Section 3.1 that are used to represent the state of an underwater vehicle and then proceed to obtain the kinematic equations of motion of the vehicle without taking into account the forces and moments at play, in Section 3.2. Afterwards, we analyze the external forces that affect the vehicle motion, formulating the dynamics equations of motion of an arbitrary underwater vehicle, ending up with a set of equations in vectorial form for the vehicle kinematics and dynamics. This chapter follows the marine standard notation and practice, based on [32].

3.1 Reference Frame and Motion Variables

To describe the motion of a vehicle in space, one must first introduce coordinates in which to express the vehicle variables such as position, velocity and acceleration, and the frame where these coordinates apply.

To accurately describe the motion of the vehicle it is enough to use two reference frames, as shown in Fig. 3.1, with their respective notations.

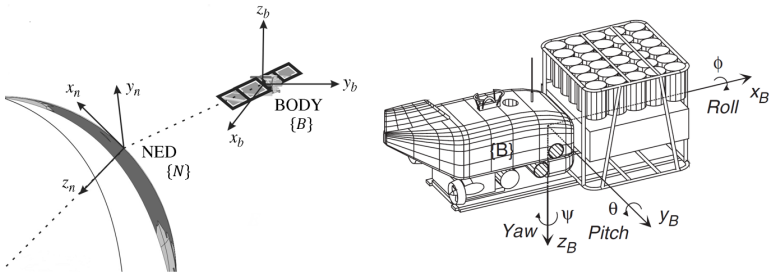

Figure 3.1: Vehicle body frames and respective motion variables notation (adapted from [32]), as well as AUV motion variables and respective nomenclature (obtained from [24]).

These two frames are known as *body-fixed* frame $\{B\} = (x_b, y_b, z_b)$ and *inertial* frame or *NED* frame (*North-East-Down (NED)* frame) $\{N\} = (x_n, y_n, z_n)$. The first frame is a moving frame fixed to the vehicle,

whose origin describes its position and orientation relative to the *inertial* frame. On the other hand, the second frame is assumed to be a fixed tangent plane to the surface of the Earth, where the x axis points to the true North, the y axis point towards East and the z axis points downwards to the center of the Earth.

That being said, we now define the necessary nomenclature to describe the motion variables of underwater vehicles:

Position of $\{B\}$ measured in $\{N\}$	$\boldsymbol{p} = \begin{bmatrix} x \\ y \\ z \end{bmatrix} \in \mathbb{R}^3$	Attitude of $\{B\}$ w.r.t $\{N\}$ expressed in $\{N\}$	
Linear velocity of $\{B\}$ w.r.t $\{N\}$ expressed in $\{B\}$	$\boldsymbol{v} = \begin{bmatrix} u \\ v \\ w \end{bmatrix} \in \mathbb{R}^3$	Angular velocity of $\{B\}$ w.r.t $\{N\}$ expressed in $\{B$	
Body-fixed forces in $\{B\}$	$\boldsymbol{f} = \begin{bmatrix} X \\ Y \\ Z \end{bmatrix} \in \mathbb{R}^3$	Body-fixed moments in $\{B\}$	

Table 3.1: Description of position, velocity and forces of actuation on the vehicle, under SNAME notation.

where $\mathbb{R}^3$ is the *Euclidean space* of three dimensions. Additionally, we can specify these motion variables in a more compact form as:

$$\boldsymbol{\eta} = \begin{bmatrix} \boldsymbol{p} \\ \boldsymbol{\Theta} \end{bmatrix} \in \mathbb{R}^6, \quad \boldsymbol{\nu} = \begin{bmatrix} \boldsymbol{v} \\ \boldsymbol{\omega} \end{bmatrix} \in \mathbb{R}^6, \quad \boldsymbol{\tau} = \begin{bmatrix} \boldsymbol{f} \\ \boldsymbol{m} \end{bmatrix} \in \mathbb{R}^6 \tag{3.1}$$

where $\boldsymbol{\eta}$ denotes position and orientation (in Euler angles) of the vehicle with respect to $\{N\}$, $\boldsymbol{\nu}$ denotes the linear and angular velocities expressed in $\{B\}$ with respect with $\{N\}$ and $\boldsymbol{\tau}$ represents the forces and moments acting on the vehicle expressed in $\{B\}$.

Throughout work, we choose the centre of gravity (CG) to coincide with the origin of $\{B\}$, facilitating the study and design of controllers for the vehicle motion since the other way around would involve simple but additional steps of taking this translation into account.

Having this notation in mind, we can now proceed to develop the kinematic and dynamic equations of motion of an underwater vehicle, under these mathematical nomenclatures.

3.2 Kinematics

The *kinematics* of a vehicle, as mentioned before, concerns the geometrical aspects of a single point motion through a 3-dimensional space, without taking into account the forces of motion dynamics. Specifically, we will cover the relationships between velocities expressed in the *body-fixed* frame with the corresponding variables expressed in the *inertial* frame.

3.2.1 Linear Velocity Transformation

In guidance, navigation and control application it is customary to decompose the *body-fixed* velocities $\boldsymbol{v}$ in the *inertial* frame using the Euler angles $[\phi, \theta, \psi]$ (roll, pitch and yaw, respectively) representation. One can use a rotation matrix $\boldsymbol{R}$ to transform vectors expressed in a certain frame into the same vector expressed in another frame. We define the nomenclature of $\boldsymbol{R}_b^n \in SO(3)$ to represent the transformation of a vector expressed in $\{N\}$ into the same vector expressed in $\{N\}$, where $SO(3) := \{\boldsymbol{R} \in \mathbb{M}_{3\times 3} : \boldsymbol{R}\boldsymbol{R}^T = \boldsymbol{I}_3, \det(\boldsymbol{R}) = 1\}$ and $\mathbb{M}(n, m)$ represents the space of $n \times m$ real valued matrices, with $n > 0$ and $m > 0$. Given the notion of rotation matrix represented as $\boldsymbol{R}$, following the zyx convention for Euler angles, one can define $\boldsymbol{R}_b^n$ to be equivalent to consecutive rotations in the zyx axis, which is mathematically equivalent to

$$\boldsymbol{R}_b^n := \boldsymbol{R}_{z,\psi}\boldsymbol{R}_{y,\theta}\boldsymbol{R}_{x,\phi} \tag{3.2}$$

where $\boldsymbol{R}_{z,\psi}\boldsymbol{R}_{y,\theta}\boldsymbol{R}_{z,\phi}$ denote the principal rotation matrices around the three dimensional axis, defined as

$$\boldsymbol{R}_{z,\psi} = \begin{bmatrix} 1 & 0 & 0 \\ 0 & c\phi & -s\phi \\ 0 & s\phi & c\phi \end{bmatrix}, \quad \boldsymbol{R}_{y,\theta} = \begin{bmatrix} c\theta & 0 & s\theta \\ 0 & 1 & 0 \\ -s\theta & 0 & c\theta \end{bmatrix}, \quad \boldsymbol{R}_{x,\phi} = \begin{bmatrix} c\psi & -s\psi & 0 \\ s\psi & c\psi & 0 \\ 0 & 0 & 1 \end{bmatrix} \tag{3.3}$$

where, for compactness, we let $c\cdot = \cos(\cdot)$ and $s\cdot = \sin(\cdot)$.

We can expand (3.2) and define the velocity transformation matrix as follows

$$\boldsymbol{R}_b^n(\boldsymbol{\Theta}) = \begin{bmatrix} c\psi c\theta & -s\psi c\phi + c\psi s\theta s\phi & s\psi s\phi + c\psi c\phi s\theta \\ s\psi c\theta & c\psi c\phi + s\phi s\theta s\psi & -c\psi s\phi + s\theta s\psi c\phi \\ -s\theta & c\theta s\phi & c\theta c\phi \end{bmatrix} \tag{3.4}$$

With this, the *body-fixed* linear velocity can be expressed in the *inertial* frame as

$$\dot{\boldsymbol{p}} = \boldsymbol{R}_b^n(\boldsymbol{\Theta})\boldsymbol{v} \tag{3.5}$$

where $\dot{\boldsymbol{p}}$ is the *inertial* linear velocity vector.

3.2.2 Angular Velocity Transformation

Likewise, we can obtain the transformation matrix related to the angular velocity vector from *body-fixed* to *inertial* frame, also known as the Euler rate vector, given by

$$\dot{\boldsymbol{\Theta}} = \boldsymbol{T}_b^n(\boldsymbol{\Theta})\boldsymbol{\omega} \tag{3.6}$$

$$\boldsymbol{T}_b^n = \begin{bmatrix} 1 & s\phi t\theta & c\phi t\theta \\ 0 & c\phi & -s\phi \\ 0 & s\phi/c\theta & c\phi/c\theta \end{bmatrix} \tag{3.7}$$

where $t\cdot = \tan(\cdot)$. An important aspect to take into account using $\boldsymbol{T}_b^n$ is the fact that it is undefined for pitch angles of $\theta = \pm 90°$. However, there are ways to solve this problem, such as using Quaternions parameterization instead of Euler angles, avoiding singularity issues, or defining our attitude in the space of rotation matrices $SO(3)$. Each strategy has their own pros and cons as previously mentioned in Chapter 1 but for simplicity purposes we will leave the angular kinematic equations via parameterization using Euler angles.

3.2.3 Six DOF Kinematic Equation

Grouping together both Linear and Angular velocity transformations we can derive the full *kinematic* equation for a six DOF vehicle in vector form as

$$\dot{\boldsymbol{\eta}} = \boldsymbol{J}(\boldsymbol{\eta})\boldsymbol{\nu} \Leftrightarrow \begin{bmatrix} \dot{\boldsymbol{p}} \\ \dot{\boldsymbol{\Theta}} \end{bmatrix} = \begin{bmatrix} \boldsymbol{R}_b^n(\boldsymbol{\Theta}) & \boldsymbol{0}_{3x3} \\ \boldsymbol{0}_{3x3} & \boldsymbol{T}_b^n(\boldsymbol{\Theta}) \end{bmatrix} \begin{bmatrix} \boldsymbol{v} \\ \boldsymbol{\omega} \end{bmatrix} \tag{3.8}$$

3.3 Dynamics

Having studied and mathematically defined the geometric transformation of a single point motion through three-dimensional space, we need to identify how this motion is affected by external forces, following the Newton-Euler formulation in the *body-fixed* frame. Such motion can be produced by actuator forces, such as propellers or other types of thrusters, restoring forces, due to the hydrostatic nature of submerged vehicles in water, and the hydrodynamic forces due to the motion of the vehicle itself through a water medium. The objective of this study is to then establish an underwater vehicle equations of motion based on Newton's law [32] in vector form, given by

$$\boldsymbol{M}\dot{\boldsymbol{\nu}}_r + \boldsymbol{C}(\boldsymbol{\nu}_r)\boldsymbol{\nu}_r + \boldsymbol{D}(\boldsymbol{\nu}_r)\boldsymbol{\nu}_r + \boldsymbol{g}(\boldsymbol{\eta}) + \boldsymbol{g}_0 = \boldsymbol{\tau} \tag{3.9}$$

where

- $\boldsymbol{M}$ is the system inertia matrix, corresponding to the rigid-body inertia and added mass terms.
- $\boldsymbol{C}(\boldsymbol{\nu}_r)$ is the Coriolis-centripetal matrix, corresponding to the rigid-body and added mass Coriolis and centripetal terms.
- $\boldsymbol{D}(\boldsymbol{\nu}_r)$ is the hydrodynamic damping matrix terms due to viscous friction and damping. Typically both linear and quadratic drag are considered.
- $\boldsymbol{g}(\boldsymbol{\eta})$ and $\boldsymbol{g_0}$ are vectors of hydrostatic forces, associated with gravity and buoyancy, and restoration forces due to ballast systems, respectively.
- $\boldsymbol{\tau}$ is the vector of forces and moments from the thrusters.
- $\boldsymbol{\nu}_r = \boldsymbol{\nu} - \boldsymbol{\nu}_c$ is the relative velocity of the vehicle in water, where $\boldsymbol{\nu}_c = [u_c, v_c, w_c, 0, 0, 0]^T$ is the generalised ocean current velocity vector of an irrotational fluid, with u_c, v_c and w_c are expressed in $\{B\}$.

We approach the generalised *dynamics* equation of motion of the vehicle taking ocean currents into account, being $\boldsymbol{\nu}_r$ the relative velocity vector of the marine craft with water.

The system inertia matrix $\boldsymbol{M}$ can be expressed in vector form as the sum of two parts

$$\boldsymbol{M} = \boldsymbol{M}_{RB} + \boldsymbol{M}_A \tag{3.10}$$

where $\boldsymbol{M}_{RB}$ is the rigid-body system inertia matrix and $\boldsymbol{M}_A$ is the rigid-body added mass matrix.

The concept of added mass in $\boldsymbol{M}_A$ concerns the hydrodynamics of the vehicle, more specifically, the inertia that is added into the system caused by the displacement of a volume of fluid, water in our case, due to the motion of the vehicle. These terms can be neglected on land robots, however, because we are working in an underwater environment, the same can not apply. To simplify our work during control design using Lyapunov function candidates as a sum of kinetic and potential energy, we assume that the system inertia matrix $\boldsymbol{M}$ has constant potential coefficients, implying the following property [32, Property 7.1]:

Property 1 (System Inertia Matrix)**.** *The system inertia matrix $\boldsymbol{M}$ is unique and satisfies*

$$\dot{\boldsymbol{M}} = 0, \quad \boldsymbol{M} = \boldsymbol{M}^T > 0$$

The total hydrodynamic damping matrix can be expressed as a sum of linear and non-linear terms

$$\boldsymbol{D}(\boldsymbol{\nu}_r) = \boldsymbol{D} + \boldsymbol{D}_n(\boldsymbol{\nu}_r) \tag{3.11}$$

where $\boldsymbol{D}$ takes into account potential damping and possible skin friction and $\boldsymbol{D}_n(\boldsymbol{\nu}_r)$ represents the non-linear quadratic damping and higher-order terms. Additionally, $\boldsymbol{D}(\boldsymbol{\nu}_r)$ satisfies the following dissipation property [32, Property 6.3]:

Property 2 (Hydrodynamic Damping Matrix)**.** *For a rigid-body moving through a water medium, the hydrodynamic damping matrix will be real, nonsymmetric and strictly positive:*

$$\boldsymbol{D}(\boldsymbol{\nu}_r) > 0, \quad \forall \boldsymbol{\nu_r} \in \mathbb{R}^6 \tag{3.12}$$

In other words,

$$\boldsymbol{x}^T \boldsymbol{D}(\boldsymbol{\nu}_r)\boldsymbol{x} > 0, \quad \forall \boldsymbol{x} \neq \boldsymbol{0} \tag{3.13}$$

The Coriolis-centripetal matrix $\boldsymbol{C}$ appears due to the rotation of the body with respect to the *inertial* frame. Likewise, the system inertia matrix can be expressed as a sum of two parts

$$\boldsymbol{C}(\boldsymbol{\nu}) = \boldsymbol{C}_{RB}(\boldsymbol{\nu}) + \boldsymbol{C}_A(\boldsymbol{\nu}) \tag{3.14}$$

where $\boldsymbol{C}_{RB}$ is the rigid-body system Coriolis-centripetal matrix and $\boldsymbol{C}_A$ is the hydrodynamic added mass matrix related to rotation of the body in the surrounding fluid.

The Coriolis-centripetal matrix $\boldsymbol{C}$ is not unique and is chosen such that it is skew-symmetric, i.e $\boldsymbol{C} = -\boldsymbol{C}^T$, allowing us to simplify the equations. Letting the system inertia matrix be partitioned as $\boldsymbol{M} = \begin{bmatrix} \boldsymbol{M}_{11} & \boldsymbol{M}_{12} \\ \boldsymbol{M}_{21} & \boldsymbol{M}_{22} \end{bmatrix}$,

we recall from [32, Theorem 3.2]:

Theorem 8 (Coriolis–Centripetal Matrix from System Inertia Matrix)**.** *Let $\boldsymbol{M}$ be a 6×6 system inertia matrix defined as*

$$\boldsymbol{M} = \boldsymbol{M}^T = \begin{bmatrix} \boldsymbol{M}_{11} & \boldsymbol{M}_{12} \\ \boldsymbol{M}_{21} & \boldsymbol{M}_{22} \end{bmatrix}$$

where $\boldsymbol{M}_{21} = \boldsymbol{M}_{12}^T$. Then, the Coriolis–centripetal matrix can always be parameterized such that $\boldsymbol{C}(\boldsymbol{\nu}) = -\boldsymbol{C}^T(\boldsymbol{\nu})$ by choosing

$$\boldsymbol{C}(\boldsymbol{\nu}) = \begin{bmatrix} \mathbf{0}_{3x3} & -\boldsymbol{S}(\boldsymbol{M}_{11}\boldsymbol{v} + \boldsymbol{M}_{12}\boldsymbol{\omega}) \\ -\boldsymbol{S}(\boldsymbol{M}_{11}\boldsymbol{v} + \boldsymbol{M}_{12}\boldsymbol{\omega}) & -\boldsymbol{S}(\boldsymbol{M}_{21}\boldsymbol{v} + \boldsymbol{M}_{22}\boldsymbol{\omega}) \end{bmatrix} \tag{3.15}$$

Having described the *kinematics* and *dynamics* equations of motion of an underwater vehicle in vector form, given by (3.16) and (3.17), respectively, we can proceed to apply these concepts to a real model of an existing six DOF AUV, expanding and developing the motion dynamic matrices.

3.3.1 Model Equations in Vector Form

To sum up all of the work developed in this chapter, we recall the obtained *kinematics* and *dynamics* equations of motion in vector form

$$\dot{\boldsymbol{\eta}} = \boldsymbol{J}(\boldsymbol{\eta})\boldsymbol{\nu} \tag{3.16}$$

$$\boldsymbol{M}\dot{\boldsymbol{\nu}}_r + \boldsymbol{C}(\boldsymbol{\nu}_r)\boldsymbol{\nu}_r + \boldsymbol{D}(\boldsymbol{\nu}_r)\boldsymbol{\nu}_r = \boldsymbol{\tau} \tag{3.17}$$

where each term and variable is previously defined and applied to an AUV, where our work will be focused on. Additionally, throughout the work carried out in this thesis, we simplify the notation of our vehicle rotation matrix, by considering $\boldsymbol{R}_v$ to represent the rotation matrix from $\{B\}$ to $\{N\}$, that is, $\boldsymbol{R}_v = \boldsymbol{R}_n^b$.

Chapter 4

Underwater Cooperation between Diver and AUV

This chapter is dedicated to reviewing and studying the cooperation mechanisms between an AUV and a diver. In Section 4.1 we briefly discuss different types of diving operations and possible cooperation strategies between AUVs and divers. In Section 4.2 we present state-of-the-art algorithms that provide essential information of the diver absolute/relative position underwater. In Section 4.3, we extend incorporate these results in a tracking filter to obtain filtered components of the diver kinematic components. We finalize this chapter with the proposal of a generalized cooperation architecture to be implemented on an AUV in Section 4.4.

4.1 Cooperation Frameworks

The world of diving operations is complex and can be categorized in many different ways. In this section, we discuss diving operations that are carried out by professional divers excluding training or personal/recreational diving operations, as our work is focused on the use of delicate and costly equipment (e.g., robots) that requires time and planning beforehand. Within some margin of flexibility, we can divide the professional diver operations into several categories, discuss their associated risks, and possible cooperation strategies with AUVs. The key takeaways from these discussions will serve as basis of support to our cooperation architecture proposal in Section 4.4. In Appendix A a table is presented with a brief summary of the discussion held in this section.

4.1.1 Commercial/Industrial Diving

These types of diving operations concern the aspects of engineering in underwater environments such as building, repair, examination, or maintenance. Examples of such operations can be:

- Offshore diving where divers work towards the support of the oil and gas industry.
- Maintenance, repair and cleaning of vessels without the need for lifting or docking at a special structure, or even prepare the vessel itself towards raising.
- Laying pipelines or communication lines underwater.

- Hazmat diving, which is one of the most dangerous diving operations, where the diver works in contaminated underwater environments for repair, sampling, maintenance, or pollution clean up.

- Salvage and retrieval of sunken ships, cargo, aircraft or other vehicles and structures.

Usually, these types of operations are methodically planned and occur periodically, from half an hour to 2 hours. They do not occur sporadically but instead are part of projects that span over months or even years, depending on the scale and complexity, with dives occurring many times throughout the project/work carried out. For example, in Norfolk, Virginia, United States of America, a commercial diving company provided underwater marine construction services towards a coal pier, and the 13 divers performed 400 dives in a 9-month long project [52]. On the other hand, NEOSUB, a diving operation service company, participated in a huge sub-aquatic project in Portugal that undertook 5 years [53].

In all types of diving operations, diver usually face common risks such as low visibility, decompression sickness, nitrogen narcosis, ocean currents and a general lack of orientation. However, specific to commercial diving, there also exists added risks due to the mission nature itself. Divers are usually accompanied by other diver "buddies", and are equipped with specialized equipment such as a diving bell, a decompression chamber, and/or other life support equipment, reducing the diver overall mobility. For example, in saturation diving, these situations are more pronounced as the diver stays underwater for prolonged hours. Additionally, in commercial diving, the divers may handle specialized tools, e.g., underwater torch, high-pressure water jet cleaning tools, etc, and working in dangerous environments, e.g., polluted/contaminated water, heavy and delicate underwater cables, tight spaces, rig propulsion systems, etc, some of which would be a real challenge to work with even if they were above ground.

The implementation and use of cooperative schemes between AUVs and divers in commercial/industrial diving operations might mitigate some of the aforementioned risks and enhance certain task operations. For example, observation and monitoring of a diver could provide some sort of visual coverage and, with the help of additional sensors implanted on the diver suit, the robot could serve as a monitoring station and send information to the surface, establishing a communication link between the diver and the outside world eliminating the need for additional cabling connect to the diver. Additionally, it would allow the AUV to plan missions according to the diver underwater, in a more adaptive and responsive approach. Recent works regarding chain link communication between robots have proven to be an efficient way of establishing underwater communication, via the use of different unnamed underwater/surface autonomous vehicles in a cooperative control framework [54]–[58]. Another useful cooperation scheme is the use of robots as means of carrying the necessary tools and essential systems and taking away the burden from the diver, allowing him/her to work underwater with more ease and flexibility. Or the AUV might perform the actual task as well, by drilling the necessary screws or turning certain valves that require strength and dexterity. The authors in [59] derive certain control frameworks towards the development of autonomous manipulation tasks, under the scope of the DexROV Horizon 2020 project, such as inspecting the surface of a pipeline.

4.1.2 Scientific Diving

In scientific diving, contrary to commercial/industrial diving, concerns the pursuit of knowledge and research development related to science. Examples of scientific dive operations can consist of:

- Sampling and observation of biological organisms and geophysical phenomenon *in situ*.
- Underwater archaeology and geology.
- Retrieval and maintenance of scientific equipment.
- Underwater mapping and registration of important local features for seabed characterization.

Like commercial/industrial diving operations, these types of missions operate as part of projects that usually span over weeks and months or years. But contrary to commercial/industrial diving, the divers are usually scientists first and professional divers second. For example, in 2010, the Centre for Scientific Diving of the Alfred Wegener Institute (AWI) conducted studies of impacts of artificial structures on fish and macroinvertebrate communities in the subtidal zone (depths of 5 to 10 meters), with several diving operations performed sporadically since then, to conduct scientific experiments near these implanted artificial structures [60]. Usually, those dives only occurred whenever further investigation was required by the research development. Another example is an expedition to Neumayer III, a German research facility in Antarctica, where it was found that, towards investigation and research of Antarctica's sub-ice ecosystem, in situ approaches through diving and custom-designed incubation systems or sensor arrays were essential [61].

Despite the scientific nature of these types of diving operations, there is always the need for diver buddies and support teams above water to ensure a safe diving mission. Moreover, there are still associated risks besides the usual risks transversal to all diving operation types, as mentioned before. However, these are comparatively fewer compared with commercial/industrial diving as the work performed is done under favourable conditions, do not need to be accomplished under tight timelines and/or profitability, and do not involve using large and complex equipment. Another risk associated with some scientific diving operations is related to the human factor disturbance in the area of research. For example, underwater archaeology operations require extreme care with the handling of equipment and objects of interest and usually involve surveying the area previously. Or with biology-related research dives, it is of utmost importance to avoid disturbing the surrounding fauna and flora, otherwise risk ruining the samples, invalidating the data.

Cooperation schemes between divers and robots, might still prove to be essential tools towards conducting a better performance of underwater scientific and research tasks. In seabed mapping or underwater observation missions, the robot can be an excellent tool via acoustic or visual sensory equipment and using a diver as a supervisor to the robot can result in efficient sample gathering and surveying task t. If turbidity or lack of navigation capabilities impedes successful diving operations, it is possible to use a robot as means of guiding the diver towards the mission site or even provide some sort of lighting and tools assistant, as mentioned previously in commercial/industrial diving operations.

4.1.3 Media Diving

Media diving operations, as the name suggests, is a branch of diving operations concerning underwater cinematography and photography. It can overlap some of the aforementioned styles of diving operation as it provides some sort of coverage towards those said operations, with the main objective of documenting underwater research and investigation tasks related to oceanography, engineering, cinema and television industry, etc other types of science.

Besides some of the usual risks of diving operations in general, above mentioned, media diving operations fall into the same category of risks related to science diving operations. Some additional or different than usual tasks that media divers perform usually are concerned with up keeping and using specialized recording equipment such as high definition video cameras in underwater housings, with special underwater lighting, and remote camera. Therefore, there could be some risks associated with the handling of equipment during such diving operations, but do not pose an added risk to the diver. Finally, because media divers themselves are accompanied by other divers, the need to navigate accurately and know the whereabouts is almost non-existent therefore the lack of underwater navigation and sense of orientation does not pose a risk towards the media diver.

Relative to possible cooperation schemes and benefits/risks associated, there needs to be some considerations taken into account. As media diving operations require special knowledge relative to camera work and filming, the robot itself must carry the necessary algorithms to perform such tasks. This is not new to the world of robotics and filming, as there are already commercially available technologies that implement these assignments, with discussions in the cinema industry literature relative to the advancements and benefits/downsides of robot operating cameras [62]. Therefore, one could have the robot operating as an underwater filming station where the diver could command the vehicle to perform specific manoeuvres around a certain site, motivated by recent developments in gesture-based algorithms and computer vision [18].

4.1.4 Military Diving

Finally, military and public safety diving operations concern the tasks performed by military personnel in underwater environments. These tasks can range from a multitude of tasks, such as:

- Search and rescue/recovery.
- Explosive ordnance disposal.
- Reconnaissance, sabotage or infiltration.
- Hydro-graphic surveys.

Concerning risks, it is straightforward to expect that military diving operations are risky by nature, from working with nearby explosive devices to diving in unknown and "enemy" territory, owing to the nature of war. Such operations lack the time and non-urgency to prepare and plan the mission beforehand, safety checks, and require the diver to adapt easily and possess a huge underwater expertise. However, the same serves as a counter-acting point towards decreasing the associated risks with these types of dives, as compared to

other types of diving operations. A study made by the Poland Military Institute of Medicine [63] analyzed and concluded that the major factors of increased number of accidents included diving frequency, adaptation to higher pressure conditions and overestimation of one's skills in undertaking challenges, and that a model of military diving training provides a much higher guarantee of diving safety as compared with some models used in scientific or media diving.

Nevertheless, there will always be a risk associated with the deactivation of explosive devices underwater or infiltration/reconnaissance diving mission therefore the use of AUVs might prove an useful cooperation tool. In underwater reconnaissance, sabotage or infiltration operations, AUVs may dive alongside a diver, carrying additional tools of observation, with the diver performing initial reconnaissance and investigation, and make the decisions towards a better inspection, or move to another location. Finally, in search and rescue missions, AUVs can be useful to accompany the diver as there will always be some degree of visibility issue that always plague these environments.

4.2 Diver Localization

In guidance, navigation and control literature, the problem of *localization* concerns the position estimation of an entity in the surrounding environment relative to a certain frame. This is an important problem in the present marine robotics scene, which has witnessed growing interest due to the demand for increasingly more accurate control and navigation systems for autonomous operations. It is also a challenging problem as these environments usually are in the presence of ocean currents, sensor bias, noise, access to Global Navigation Satellite System (GNSS) signals is impracticable, and position fixes utilizing this system require the vehicle to resurface periodically [64]. More specific to the problem of localization is the *target localization* problem which concerns the estimation of a target position, e.g., diver, object, robot, dock, animal, via measurements accessed by an agent from its sensors. Such framework is suited in the context of cooperation schemes between divers and robots underwater since it benefits and enhances the cooperative behaviour of an autonomous vehicle by obtaining important information of the whereabouts of the diver. In this Section, we intended to briefly present and discuss some works done towards solving this *target localization* problem, under cooperative schemes between divers and robots underwater. We do not discuss the topics of obtaining velocity components of a target as they usually are obtained via filtering processes with position measurements, and raw velocity measurements of an underwater target from onboard sensors are not common.

4.2.1 LBL/SBL Systems

A customary approach towards the localization of targets is the use of fixed beacons, spread out in the working environment. One common known example of such localization method is the GNSS where a constellation of satellites resort to the principles of triangulation and clock synchronization towards locating a desired object via electromagnetic signals. However, it is well known in maritime literature that the propagation of electromagnetic waves underwater is heavily damped in water and hence can not be detected by the receiver in most cases of interest. As an alternative, acoustic waves are highly used in underwater localization systems due to their propagation properties and high range of normal operation. Then, it is possible to use sets of

beacons that are placed on buoys or other surfaces that perform similar localization methods as satellites do via triangulation and clock synchronization, or other geometric methodologies. There exists various solutions such as LBL, SBL, USBL or even single range measurements. However, in this section, we will discuss the LBL and SBL systems as they are closely related, with minor differences in application, and the rest are worth mentioning in a separate context, mentioned next.

Relative to LBL systems, the position is determined via interrogation of three or more fixed transducers (beacons) separated by large distances (long baselines). These transducers can either be fixed on the seabed (classical LBL systems) or fixed to buoys with access to GNSS signals (mobile LBL systems), as shown in Fig. 4.1. These transducers are deployed at the ocean floor and their geometric topology needs to be accurately calibrated. The distances between the transducers, their depth information and the known position of the host vessel (or buoys) are used to set up a local inertial frame using which the target position is estimated. Then, an equipped transducer in the desired target (e.g., diver, AUV, etc) pings each of the transducers in the LBL system in a round-robin fashion. The travel times from the response signals are used to estimate its position via geometric methods such as trilateration.

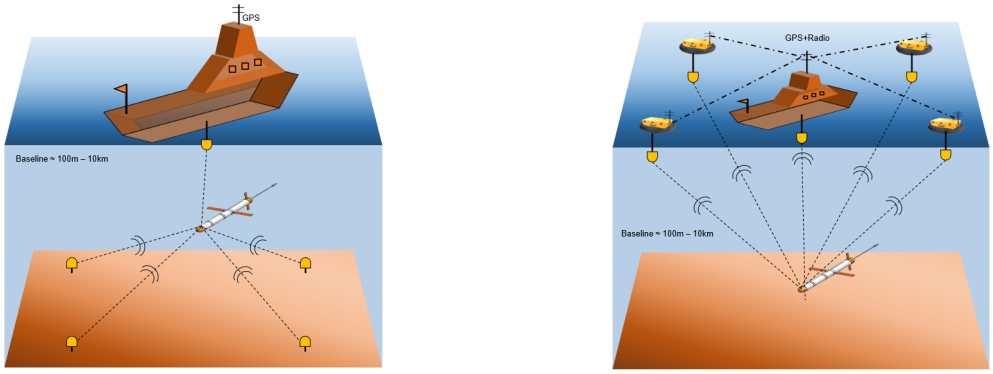

(a) Classical LBL systems.

(b) Mobile LBL systems.

Figure 4.1: Two main implementation approaches of LBL systems (obtained from [65]).

The same applies to the SBL systems, with the difference of the transducers being located in a boat or other platform instead of being fixed on the ocean floor, as shown in Fig. 4.2,. Usually, the baseline length is measured in meters, instead of hundreds of meters for the LBL systems, hence the *short* designation. The position is then calculated relative to an inertial known position of the host vessel and requires precise calibration of the transducer array. Depth sensors onboard the AUV is used in conjunction with the acoustic travel times to obtain 3D position information. Because any range and bearing available from the SBL system is with respect to the receivers mounted on the vessel, a SBL system needs additional tools such as Vertical Reference Unit (VRU), gyroscope and surface navigation system (e.g., GNSS) to provide a position on an inertial reference system.

The LBL system is well known in the literature and proven to be a robust solution towards solving localization problems, especially in deep water mission and over large areas of operation [64], providing an alternative solution to GNSS systems, SBL systems, or inertial navigation systems. In [66], the authors implemented a simple LBL system using high-precision calibrated underwater beacons as references, highlighting the need for calibration in the actual beacon known positions as they can induce errors in the estimation itself. This process

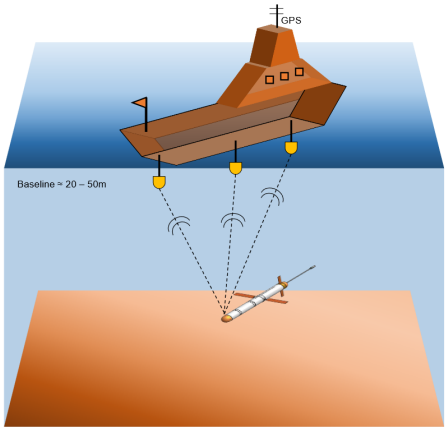

Figure 4.2: Implementation approach of a SBL system. (obtained from [65]).

is an important source of error and if done improperly deeply impacts the accuracy of the system accuracy [65]. However, LBL implementations can be complex due to the need for physical beacons with the known position being built on-site, sometimes unfeasible for divers to fixate the beacons due to extreme depths. If it is required to move location, this constrains the whole portability/mobility of the navigation system, being difficult to implement such a solution in a single vehicle towards the localization of a target (e.g., diver).

On the other hand, SBL systems are also known in the literature for quite some time, and require the agents to operate in the close vicinity of the ship or platform of choice and have a lesser range than LBL systems [67]. However, they are easier to deploy and operate and are favoured for research operations centred around a host vessel or other chosen platform, with the performance similar to LBL systems. The accuracy of the estimate is largely dependent on the length of the baseline. Generally, the farther apart the transducers, the better the accuracy [68]. In [69] the authors describe a SBL system used to track SPURV III, a Self-Propelled Underwater Research Vehicle, that consisted of a triangular array of hydrophones mounted beneath the ship's hull. Reference works [67] are other examples of SBL systems implementation. Despite this, it is still hard to minimize the use of agents in the estimation of the desired target position using SBL techniques, such as a scenario of using a single vehicle to track a driver's position.

4.2.2 USBL Systems

An USBL acoustic system consists of an acoustic ranging mechanism composed of a small array of transducers, usually with a baseline on the order of centimetres hence the name *ultra-short*, that computes the position of a target in the reference frame of the vehicle, based on the travel time of acoustic signals emitted by the transponder. Due to the proximity of the sensors in the receiving array, it is capable of measuring more accurately the time-difference-of-arrival (TDOA) of the acoustic waves at the receivers compared to the actual travel times between the transmitters and receivers [70]. As depicted in Fig. 4.3, the position of the transponder in the vehicle reference frame is given by

$$\boldsymbol{r}^B = \boldsymbol{R}_v^T(\boldsymbol{p}_t - \boldsymbol{p}) \tag{4.1}$$

where $\boldsymbol{r}^B \in \mathbb{R}^3$ represent the target position in $\{B\}$ and $\boldsymbol{p}_t \in \mathbb{R}^3$ is the target position in $\{N\}$.

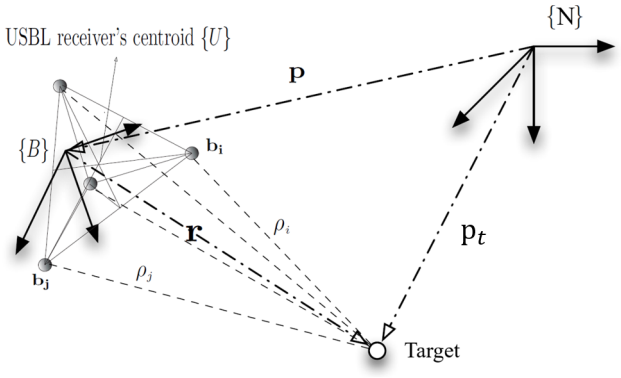

Figure 4.3: An USBL system with i receivers, with a representation of the sensor frame $\{U\}$ centroid, the body-fixed frame $\{B\}$ attached to the vehicle with the USBL system, and an inertial frame $\{N\}$ (adapted from [71]).

The overall objective of this system is to compute the target's position based on range measurements between a transponder implanted on a target and the receivers in the USBL receiving array. These distances between the transponder and receivers installed on-board the vehicle (as measured by the receivers) can be simply written in $\{B\}$ as follows

$$\rho_i = \left\| \boldsymbol{b}_i - \boldsymbol{r}^B \right\| = \| \boldsymbol{p}_t - \boldsymbol{p} - \boldsymbol{R}_v \boldsymbol{b}_i \| \tag{4.2}$$

where $\boldsymbol{b}_i \in \mathbb{R}^3$ denotes the position of the receiver in $\{B\}$.

It is possible to obtain a range/direction of the transponder byways of approximating the acoustic waves in the classical approach, that is, acoustic waves from far away can be perceived as planar waves coming to the receivers. This implies that in close-range operations (e.g., the robot operating near the diver) the approximation might fail and increase the error in the estimates but as a rule of thumb, the planar wave approximation is considered to yield satisfactory results at distances approximately 10 times larger than the baseline of the receiving array [64]. Then, using such approximation, it is possible to obtain an estimate of the transponder's direction d_r via a weighted least squares estimation problem [71], that we will not expand here for simplicity purposes, but it will ultimately allow us to access the relative position of the target expressed in $\{U\}$ as follows

$$\boldsymbol{r}_r = \rho_r \boldsymbol{d}_r \tag{4.3}$$

where ρ_r is the range of the transponder computed by just averaging the measured ranges from all receivers (since it is assumed that the receivers array are all equally distanced to the origin of $\{U\}$).

Additionally, if the vehicle's position $\boldsymbol{p}$ is know, it is only a matter rearranging equation (4.1) towards finding the target's inertial location underwater $\boldsymbol{p}_t$. These types of systems provide good accuracy and estimation of position in a small navigation environments, i.e., a docking station, laboratory tank, close-range control, where there is a need for precision to avoid collisions with the environment/agents. In those situations, an USBL system at certain operation frequencies of 200 kHz can perform with errors in centimeters range [64], as long as it satisfies a distance of 3 meters or above with respect to the target. Additionally, USBL systems offer

the advantage of not requiring a sea floor transponder array, which increases the mobility of a robot without requiring the use of fixed-structures in the environment such as the ones used in LBL/SBL systems.

In [72], the authors derived a non-linear navigation filter with the use of an USBL system alongside a DVL sensor which aimed to estimate a transponder position. The USBL system in these solutions is usually referred to be in an "inverted" implementation, being abbreviated as iUSBL, where the actual target position estimation process happens inside the working vehicle. The filter satisfied useful properties such as GAS as error dynamics, validating the theory behind such systems and their overall performance in a low-complexity environment by only coupling AUV with an USBL system and a transponder in the sea-floor (in theory, this could be a moving target). However, this work assumes the transponder was fixed and not moving, therefore the convergence properties may not hold. In another work [73], the authors located (and tracked) a moving target (diver) via measurements from an USBL system and, additionally, used a FLS whose measurements were transformed into a picture for post-processing and not only detect the target but also serve as an additional measurement in the tracking filter, fusing both data. Finally, in [74] the author developed a tracking system based on multiple USBL systems towards the tracking of multiple targets and additional measures from an inertial system, fusing the information in a sensor fusion approach.

Despite all of this, USBL systems possess certain disadvantages, namely that the positioning accuracy and robustness is not as good comparatively for LBL systems [64]. The reason is that multiple sensors needed for the receiver array require to be located at an equal distance with each other, as mentioned before, so small errors in this positioning can introduce additional errors. Finally, USBL systems usually have blind-spot regions for certain azimuth and elevation angles of the receiver array, not receiving signal due to either obstruction or simply the way the structure is implemented. And, as with the other acoustic positioning systems, the non-uniformity of the underwater environment can cause signal refraction and reflections that have an impact on both USBL and other acoustic positioning systems, i.e LBL systems, SBL systems, SONAR, etc.

4.2.3 Visual Based Localization

Another strategy used towards localization of targets is via the use of optical sensors (e.g., cameras) or acoustic imaging sensors (e.g., SONAR). They can provide additional information about the surrounding environment and objects that are not accessible using traditional acoustic sensor arrays, such as the ones discussed before, and are relatively easy to implement as their structure is not complex and can be easily integrated into an AUV. The theory behind vision-based algorithms is well known and still in research, in what is commonly known in the robotics literature as Image Processing and Computer Vision theory, with many different examples to show in the terrestrial and aerial applications. This field is promising and relatively new in the Marine Robotics literature due to the increase in onboard computing power to process all the data and computation regarding Image Processing and Computer Vision algorithms. The process of position determination in visual-based tracking intends to locate the area of the target in each measured frame from the visual sensor of choice. With this, we will discuss some works carried out recently concerning the vision-based localization of targets or other objects, as there is not a specific architecture in such algorithms, beginning with optical-based target localization, followed with acoustic-imaging target localization.

Optical Sensors

A possible solution in vision-based localization strategies is the use of visual landmarks implanted on the desired target, e.g., a diver, dock, etc. In [75] the authors approached the problem of detecting a target based on visual data from a camera, and position the robot relative to the target, in a tracking fashion. We are only concerned about the detection itself since this is the part where the desired locations of the target are obtained. This is done via two artificial coloured lighting sources mounted on the desired target, followed by a two-step segmentation process (luminescence and reference pixel values), obtaining a set of candidate pixels. Finally, assuming the scene is parallel to the vehicle, these pixels are transformed into vertical and horizontal relative positions based on the pinhole imaging theory, which takes into account the camera resolution factor, projection angle and pixel size. Such systems are capable of achieving high accuracy but require a pre-installed infrastructure.

An alternative approach is the use of a camera or set of cameras to identify features in the environment or targets for the AUV mission. The use of visual data from a camera is an attractive method for underwater sensing and it is especially effective in close range detection. But this data is usually characterized by their poor visibility because the light is attenuated as it travels in the water and the resulting scenes are poorly contrasted and hazy. Therefore, a usual strategy when using such measurements is to first apply a colour restoration algorithm [76]. Afterwards, it is possible to obtain useful information from these measured images. Similarly, the authors in [77] decided to approach the problem target localization in two parts: detection and tracking. The first one consists in solving a detection and recognition problem, separating all the visual data into the desired object to then apply a tracking solution. The authors show that a *template-based* approach, whose detection results of the desired objects were more successful than a *feature-based* approach, although this is dependent on the actual object of interest. Then, with the desired objects detected, two tracking algorithms were proposed: *Optical flow* and *Mean shift* tracking. The former consists of estimating the positions of the image points by calculating the flow velocities in two consecutive frames. However, this algorithm relies on features to then obtain the required image points and, as mentioned before, feature extraction algorithms are not reliable as compared to template matching algorithms. The *mean shift* tracking algorithm consists in creating a colour histogram of the interest area and the mean of the histogram is shifted to locate the position of the interest area. This latter solution obtained more reliable results since this one can work on both detection algorithms and is particularly effective towards tracking non-rigid objects. Note that, the word "track" used here refers to visual tracking and is not to be confused with the problem of *target tracking* which we will discuss later in Section 4.3, but instead refers to the act of positioning the camera to maintain a visual reference.

In [78] the authors perform a similar approach that focuses on the control of a micro-AUV that follows the desired object based on camera images. However, the difference relies on a more complex vision system that has different steps. The first performs a pre-processing of the raw image with different filters, e.g., Gaussian blurring to remove *salt-pepper* noise, histogram equalization, etc. Then, the data is separated into colour and shape for each object via HSV filtering (Hue, Saturation and Value), followed by the creation of groups of blobs. Each blob has its centroid computed, whose coordinates serve as a position towards the navigation system, on which the control law will follow up.

The optical localization systems we have discussed here all have a problem in common which is the fact they do not work in poor-visibility conditions, a recurrent scenario in underwater environments. If such a situation occurs, most of these algorithms' performances are drastically reduced. Moreover, optical sensors do not scale well with distance in these environments and have a limited field of view, reason why they are mostly known to be applied in close-distance scenarios. Additionally, during diving operations, it is common to also occur the appearance of bubbles in the surrounding water from the breathing system embedded in the divers. These systems are usually present in scientific, media and military diving operations, except for commercial diving operations where the diver is usually breathing through a cabled system (e.g., saturation diving), as explained in Section 4.1. These bubbles may be disregarded at first glance, but it is known in the literature that they interfere with visual and acoustic algorithms performance reducing, as mentioned in [5] during the work developed on the CADDY project.

Acoustic Imaging

Another implementation of vision-based target localization is through the use of acoustic imaging sensors, e.g., Multibeam SONAR, FLS, as shown in Fig. 4.4. While cameras and other optical sensors give low-precision visibility in a limited field of view as mentioned before, acoustic imaging sensors are an attractive alternative method for underwater sensing, which is especially effective for long-range tracking. Moreover, these types of technologies have been around for more time, before the huge advances in Image Processing and Computer Vision theory, and were usually the go-to technologies in underwater autonomous operations, therefore the research in these areas tends to be more robust. For example, in [79], from 1995, the authors derived a diver localization algorithm from a sequence of images obtained from a FLS working in both time and frequency domain to segment a moving object from a static one. This allowed the facilitation of feature extraction procedures in later steps of an arbitrary architecture (e.g., computer vision and image processing algorithms based on features) and simplifies the localization of the desired target since we are focused on moving ones (e.g., a diver). Now, in more recent works, it is possible to obtain extra information from these acoustic images, not only the distance but also extra features. We will discuss some recent works done in this area, as similarly done for the target localization via optical sensor measurements

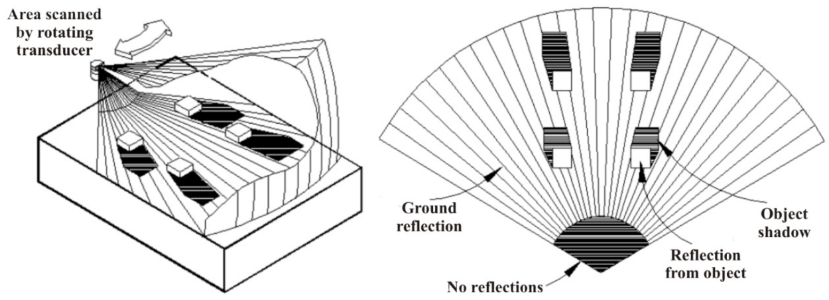

Figure 4.4: Typical image from a acoustic image sensor, such as a FLS or a Multibeam SONAR (obtained from [80]).

In a more recent work[80] the authors propose a similar framework to the frameworks present in optical target localization. More specifically, certain features were extracted from raw FLS images via traditional image processing techniques such as segmentation and media-filtering, followed by feature extractions from machine

learning techniques. Finally, the authors implemented a Particle Filter towards solving a Bayesian problem of the probability of the target position is in the image frames.

Another work developed with the use of acoustic images was done in [81] where the authors resorted to an imaging SONAR data set towards visually tracking a moving object, obtaining an inertial position of the same object. These images were followed by typical image processing techniques of noise removal and smoothed out, followed by labelling algorithm resulting in a set of pixels of the image where the object is located, equal to the before-mentioned works. Then, in a later stage, it is possible to convert these pixels to the corresponding range and bearing measured from the sonar. Using the orientation of the sonar and the position of a nearby research vessel, the range and bearing were geo-referenced to inertial coordinates of the target position.

Acoustic imaging sensors tend to be more complex relative to image sensors, not only in terms of structure but also the actual raw data we obtain from them. Working with this data can be more difficult as the scattering capability of different parts of the target surface is different, which is affected by the shape, material, and relative position between target and sensor. The incident angle of an acoustic wave is also changed with target movement, so different regions may be generated for the same target in the acoustic image, and they often appear to be unconnected regions in acoustic vision. Additionally, similar to acoustic positioning systems, energy plays a major factor, as reducing the energy cost means sacrificing certain tracking accuracy [82]. Moreover, the number of transducers on an acoustic imaging sensor that can be packed in an array is physically restricted because of the limitations of transducer size. Thus the resolution of an acoustic image is lower, and the grey level of the target area is generally smaller, so it is more difficult to find some details of targets inside it [81].

4.2.4 Single Source Range Measurements

Until now, we have discussed concepts of localization of target based on different sensors, from traditional acoustic arrays of sensors such as LBL, SBL, USBL, to vision-based systems. Most of the time these methods rely on complex structures, sensors that are usually costly, e.g., SONARs, require complex algorithms and architectures related to Image Processing or Computer Vision theory, or not even working in certain conditions of visibility and distance. As an alternative, particular emphasis has been recently placed on the use of range measurements to a single source as a cost-efficient solution to improve the performance of navigation systems and extrapolate that information to estimate a target's position. This is easily obtained via the use of acoustic/electromagnetic transponders, that are cheap and easy to implement in an underwater platform/robot [83]. In the literature, this is known as single range localization and relatively recent works have highlighted their performance and viability towards marine robotics. Following the same structure as before, we will briefly discuss the theory behind this concept and present some works realized towards its development.

The concept of single range localization (or sometimes referred to as source localization in the literature), roughly speaking, considers an agent that has access to range measurements from a set of sensors and aims to estimate the position of a source, and can be either via electromagnetic or acoustic propagation. This concept is similar to triangulation/trilateration discussed before in Section 4.2.1 and Section 4.2.2 but with the difference of only having available a single range measurement. Then, via certain excitation conditions, such as the agent motion around the source, it is possible to design an observable filter, that is, roughly

speaking, with certain measurement and velocity conditions of the agent it is possible to estimate the state variables associated with the inertial position of the target itself, satisfying certain stability conditions of the observer error dynamics. In Fig. 4.5 it is possible to observe an agent (e.g., an AUV) performing a specific motion around the target to obtain reliable estimates of a target inertial position estimate from single range measurements between the agent and the target.

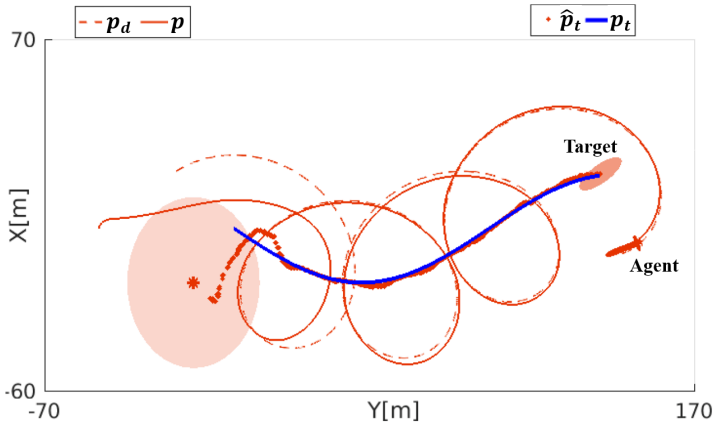

Figure 4.5: An AUV (represented in red, with true and desired position $\boldsymbol{p}$ and $\boldsymbol{p}_d$, respectively) performs a certain motion around a target (represented in blue, with true and estimated position $\boldsymbol{p}_t$ and $\hat{\boldsymbol{p}}_t$, respectively) in order to obtain reliable estimates of its position (adapted from [84]).

Although not in the context of target localization, pioneering works in marine robotics literature used single range measurement towards vehicle navigation in underwater scenarios. In [85], the authors solved the navigation problem of localizing a vehicle's inertial position via single range measurements from a transducer with a known position, knowing the vehicle's velocity relative to the fluid, given by the range measurement model

$$r(t) = \|\boldsymbol{p}(t) - \boldsymbol{p}_t(t)\| \in \mathbb{R} \tag{4.4}$$

where $\boldsymbol{p}_t$ is the target/transponder inertial position.

The solution came in the form of prescribed motions of the vehicle based on the observability analysis of an AUV non-linear kinematics equations of motion in 2D linearized about arbitrary trajectories. It was found that only certain trajectories allowed the system to be locally observable and consequently design an observer based on these conditions found from the observability analysis. The authors results found that the estimated trajectory closely follows the true trajectory except along turns, which is due to the mismatch between the kinematic model of AUV motion and actual AUV dynamics during turning manoeuvres.

In a more recent work [86], the authors tackled a similar problem of single range measurement but instead towards estimating the position of a target via an agent that has access to range measurements between one another. The authors followed an identical approach but this time provided an analysis of the observability of a non-linear time-varying system, instead of linearizing the system in arbitrary trajectories. This was possible through the use of state augmentation, preserving the analysis properties, effectively making possible the characterization of the final system as a linear time-varying system, deriving the necessary observability conditions. This resulted in better converge properties of the observer error dynamics, even in more tight

manoeuvres. Working on top of these results, the authors in [84] also performed a similar strategy but with the added possibility of using multiple agents to not only localize a target but also pursue it. These added agents relax the necessary conditions in which the target system is observable, allowing more possible motions to be performed by the agents. The same authors described the target's motion model in 3 scenarios for a single target:

Scenario A: Target is stationary/fixed:

$$\dot{\boldsymbol{p}}_t(t) = \mathbf{0}.$$

Scenario B: Target moves with unknown constant velocity vector:

$$\dot{\boldsymbol{p}}_t(t) = \boldsymbol{u}_t(t),\ \dot{\boldsymbol{u}}_t(t) = \mathbf{0}.$$

Scenario C: Target moves with unknown constant acceleration vector:

$$\dot{\boldsymbol{p}}_t(t) = \boldsymbol{u}_t(t),\ \dot{\boldsymbol{u}}_t(t) = \boldsymbol{a}_t(t),\ \dot{\boldsymbol{a}}_t(t) = \mathbf{0}.$$

According to these scenarios, there exist certain conditions in which the position of the target is uniquely determined. The conditions are briefly discussed in the following results obtained from the aforementioned works:

- In Scenario A, the target is "observable" if the agent velocity $\boldsymbol{v} \neq \mathbf{0}$ and the agent changes its velocity vector $\boldsymbol{v}$ direction at least once in $[t_0, t_f]$, that is, performs an exciting trajectory. For an under-actuated vehicle, this translates to changing at least once the heading angle ψ. In the same scenario, the target is "unobservable" if the agent moves along any straight line, that is, performs a non-exciting trajectory. In Fig. 4.6 it is possible to visualize some of the mentioned exciting and non-exciting trajectories.
- In Scenario B and C, the target is "unobservable" even if the agent is moving with nonzero acceleration, e.g., $\boldsymbol{u}(t) = \alpha(t)\boldsymbol{u}_t$ where $\dot{\alpha}(t) \neq 0$ and $\boldsymbol{u}_t$ is the target's velocity. In the 2D case, "cycloid-type" trajectories are sufficient conditions for the target's position to be "observable", as shown in Fig. 4.7. For the 3D case, "helix-type" trajectories also provide sufficient conditions for the target's position to be "observable".

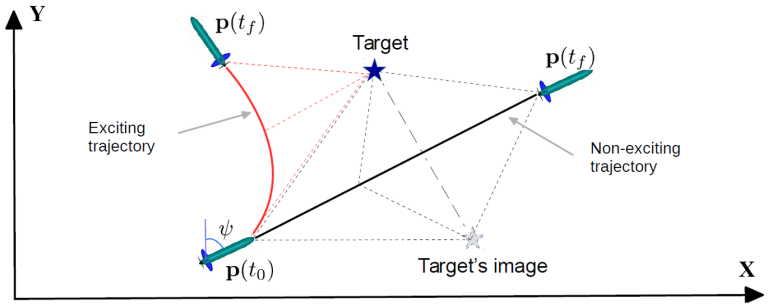

Figure 4.6: Exciting and non-exciting trajectories in which the target's position is or is not observable, respectively, in Scenario A (adapted from [87]).

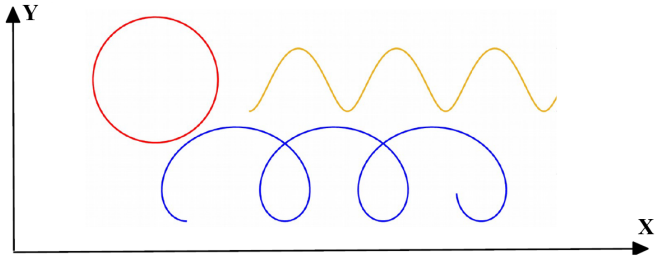

Figure 4.7: Cycloid-type trajectories in which the observability conditions are satisfied in Scenario B and C (adapted from [87]).

In multiple agents scenarios, the observability conditions are similar to a single agent scenario, with the added differences of certain agents having fewer restrictions of movement. For example, in Scenario A, using 2 agents, the target is "unobservable" if agent 1 moves along a straight line towards agent 2. For more detailed explanations on the conditions and the respective results for multiple agents refer to [87].

These types of solutions make it possible to achieve convergence properties in terms of the target's position estimate error dynamics and are well defined in terms of what and what does not provide good stability properties, in terms of the agent's motion. However, this does not come without its drawbacks. These solutions require the agent(s) to perform prescribed motions, constraining our approach towards enabling diver cooperation strategies whereas in the other mentioned systems such as USBL, these types of constraints do not exist. As mentioned before, these motion constraints might be relaxed with the use of more agents in the working scenario, but this does not only increases the overall system complexity but also the associated cost.

4.2.5 Summary

Given these state-of-the-art systems and algorithmic solutions towards diver localization in underwater scenarios, we will briefly summarize what was discussed and key conclusions:

Traditional and robust ways to localize a target in underwater scenarios consist of the use of an array of transducers disposed of in specific geometries, similar to GNSS systems. Such systems can be implemented in different arrangements, from long-short distanced beacons referred to as LBL systems and SBL to closely located beacon implementations mounted on the working platforms, referred USBL systems. These come with robust algorithms related to trilateration and triangulation techniques, capable of estimating a target's position accurately. However, LBL and SBL systems require complex infrastructures and mounting platforms and reduce their use to the location where they are implemented. As for the more mobile case of USBL systems, these are more costly and require precise geometric implementation of acoustic arrays, and have certain regions of non-operability in terms of signal propagation due to how these systems are constructed.

Other solutions arise in terms of visual-based localization systems, such as optical sensors or acoustic imaging sensors. These solutions are usually implemented using Image Processing and Computer Vision techniques, an area of intensive investigation and which has seen major improvement with the increase in computational power units. However, as for the case of optical sensors, due to the high damping on underwater electromagnetic propagation, these solutions only work in close operations with the target and the algorithms can be sometimes highly complex with no stability properties well-defined relative to the target's position estimate error dynamics.

As for the acoustic imaging sensors, these can operate in significantly higher distances with the target due to the properties of acoustic propagation. However, these types of sensor measurement are highly noisy and require some machinery to pre-process the data, as well as the sensors themselves being bulky and costly to implement in AUV platforms.

Finally, single range measurement algorithms have been studied motivated by the simple complexity behind such systems as they only require a set of transducers to work, or other sensors that provide relative distances between the target and the working vehicle, known as the agent. The theory behind such systems is well established with proven good stability conditions in terms of the target's position estimate error dynamics. However, these solution conditions require constraining the motion of the agent which reduces drastically the overall mobility of the agent itself, diminishing the cooperation capabilities between the diver and AUV.

4.3 Diver Tracking

With the concept of *target localization* established, we now proceed to study estimation solutions towards obtaining kinematic components of a moving target, e.g., a diver, in an *on-time* procedure where fast processing is mandatory in real-time applications. More specifically, we want to study filters that take on measurement data relative to a diver location, such as the solutions discussed in Section 4.2, and obtain filtered data relative to position, velocity, and/or acceleration of the target, depending on the requirements. This is especially advantageous as the position measurements are prone to error, noise, and are available with low frequency, a prevalent issue in underwater sensors. The problem of estimating the position, velocity and acceleration of a target, commonly abbreviated as the target's trajectory, is known in the literature as a *target tracking* problem, which aims to estimate the state of a target over time, translating into the design of filter solutions. The main difference between *tracking* and *localization* is that the latter can be seen as an *one-time* application where the quality of the information (i.e., the accuracy of the estimation of the target position) is the only issue, whereas the former aims to propagate this information along the target's trajectory in time. A variety of state-of-the-art solutions exist in the literature for the tracking problem distinguished by the characteristics of the target, environment, and available technology [88].

As such, in the context of cooperative solution between divers and AUVs, this Section will discuss the design approach of a model that captures a diver's kinematic components in underwater operations, as well as the measurement model itself whose measurements are considered to be only relative to position via the solutions discussed in 4.2. These approaches are well studied in the literature of *target tracking* and the predominant paradigm is to use a stochastic estimation approach. These can range from simple Kalman filters and their variants of extended/unscented Kalman filters, or even particle filters. However, we will only focus on a Kalman filter approach since it is a well known reliable and simple solution in the literature, and our main focus is not on the tracking solution on an arbitrary target (e.g., aerial, terrestrial, etc) but is known *a-priori* as being divers. These will allow paying more detailed attention to the actual procedure towards the design and implementation of the filter, highlighting the effects of different choices of parameters, e.g., noise covariance, measurement model, etc. Ultimately, the filter derivation will provide the necessary information of the target's kinematic components for our controller derived in Chapter 5, with some assumptions made throughout.

4.3.1 Process and Measurement Model

The diver's dynamic model captures parameters, such as position or velocity, whose description is necessary for the implementation of a filter that provides us with these states. On the other hand, the measurement model is related to the process model but captures the dynamics of the measurement states via onboard sensors. There are various approaches to the design of a model that best fits the moving target's behaviour, as well as the respective measurements, and it is well known in the literature of robotics, with examples ranging from remote monitoring systems that accurately track moving cars or robots to guidance systems. In general, underwater tracking is modelled with a system state, which describes the evolution of the system in discrete time, and measurement process with the following form

$$\boldsymbol{x}_k = \boldsymbol{f}(\boldsymbol{x}_{k-1}, \boldsymbol{u}_{k-1}) + \boldsymbol{w}_k \tag{4.5a}$$

$$\boldsymbol{z}_k = \boldsymbol{h}(\boldsymbol{x}_k) + \boldsymbol{v}_k \tag{4.5b}$$

where k is a time index, $f(\cdot) : \mathbb{R}^{n+m} \rightarrow \mathbb{R}^n$ is a non-linear function of the state vector $\boldsymbol{x} \in \mathbb{R}^n$ and the input vector $\boldsymbol{u}_k \in \mathbb{R}^m$, $h(\cdot) : \mathbb{R}^n \rightarrow \mathbb{R}^q$ is a non-linear function that yields the measurement taken at time k with the target at a given state $\boldsymbol{x}_k$, $\boldsymbol{z}_k \in \mathbb{R}^q$ the measurement vector taken at time k, $\boldsymbol{w}_k \in \mathbb{R}^n$ is the process noise sequence, $\boldsymbol{v}_k \in \mathbb{R}^q$ is the measurement noise that models map errors and sensor noise, and n,m,q are positive constants.

Relative to the structures of the target motion models, a review of tracking filter applications showed that the structure used for underwater target tracking is usually similar, with some slight differences in the implementation of models and matrices [89]. These models are described as a state-space time-invariant process and there are three frequently used target motion models: constant velocity (CV) model, constant acceleration (CA) model and turning model. The most popular and common approach [90] is to consider the target dynamics with having a constant velocity (CV) between each sampling time, that is, in each iteration, the filter integrates the velocity of the target and adds it to the last estimated position according to the sampling time. Empirically, this is compatible with the notion that a diver performs underwater whose acceleration is almost non-existent and turning manoeuvres do not occur rapidly. This matter will be further discussed in Section 4.3.2. Since we are dealing with second-order systems, as mentioned before, that is, the state vector assumes the position and velocity components of the target, defined as

$$\boldsymbol{x} = [\boldsymbol{p}_t^T, \boldsymbol{v}_t^T]^T \in \mathbb{R}^6 \tag{4.6}$$

where $\boldsymbol{p}_t \in \mathbb{R}^3$ and $\boldsymbol{v}_t \in \mathbb{R}^3$ denote the target's inertial position and inertial linear velocity, respectively, following the same notation referenced throughout this thesis. With this, we can proceed to define a constant velocity (CV) target model, expressed as follows

$$\boldsymbol{x}_k = \boldsymbol{\Phi}\boldsymbol{x}_{k-1} + \boldsymbol{w}_k \tag{4.7}$$

where $\mathbf{\Phi}$ denotes the transition matrix from $(k-1)T_s$ to kT_s, taking the following form

$$\mathbf{\Phi} = \begin{bmatrix} 1 & 0 & 0 & T_s & 0 & 0 \\ 0 & 1 & 0 & 0 & T_s & 0 \\ 0 & 0 & 1 & 0 & 0 & T_s \\ 0 & 0 & 0 & 1 & 0 & 0 \\ 0 & 0 & 0 & 0 & 1 & 0 \\ 0 & 0 & 0 & 0 & 0 & 1 \end{bmatrix} \tag{4.8}$$

with T_s being the sampling time interval. We assume the noise $\boldsymbol{w}_k$ corrupting our system is additive white Gaussian noise, with zero mean and time-invariant covariance matrix $\boldsymbol{Q}$.

Finally, the structure of the measurement model depends on the context of the work and how we measure the states of our system. Since we are working with a second-order system, we can consider a measurement model structure in the form of Position-only Measurements (POM) or Position-Velocity Measurements (PVM). Target POM are predominant in the literature and some systems/sensors have been briefly discussed in Section 4.2 that can obtain such measurements. On the other hand, target PVM are not so common since they are designed for sensors (e.g., Doppler radar for aerial target tracking) or filters systems (e.g., sensor fusion systems) that can measure both position and velocity of a target simultaneously. For the sake of simplicity and without loss of generalization, we assume that we only have access to position measurements provided by some type of system mentioned in 4.2. With this in mind, we can represent our measurement model in a POM system, taking the following form

$$\boldsymbol{z}_k = \boldsymbol{H}\boldsymbol{x}_k + \boldsymbol{v}_k \tag{4.9}$$

where $\boldsymbol{z}_k \in \mathbb{R}^3$ denotes the measurement vector, and $\boldsymbol{H}$ the measurement matrix defined as

$$\boldsymbol{H} = \begin{bmatrix} 1 & 0 & 0 & 0 & 0 & 0 \\ 0 & 1 & 0 & 0 & 0 & 0 \\ 0 & 0 & 1 & 0 & 0 & 0 \end{bmatrix} \tag{4.10}$$

and $\boldsymbol{v}_k$ represent the noise corrupting our position measurements defined as additive white Gaussian noise, with zero mean and time-invariant covariance matrix $\boldsymbol{R}$.

4.3.2 Filter Parameter Design

The next natural step is to define and design the parameters of the filter itself, that is, design how the noise relates and affects the system state, as well as the sensor measurements, defined by the covariance matrices $\boldsymbol{Q}$ and $\boldsymbol{R}$, respectively. This can be thought of as the "tuning knobs" of the filter and designing them appropriately can result in a filter that describes adequately a target's motion.

Regarding the process noise $\boldsymbol{w}$, the elements of its covariance matrix $\boldsymbol{Q}$ are regarded as design parameters, not model parameters. Thus, we must know how to appropriately design them, a question that is not straightforward as one might think as pointed out by the authors in [91]. They have to be chosen to meet

certain requirements usually concerning bandwidth, response time, and steady-state errors. And it is not known in general how the design of covariance matrix elements are related to important performance parameters such as bandwidth. Bearing this in mind, we remind that all these aspects are not taken into account fully on the design of the filter parameters, namely the definition of process noise covariance and the filter requirements, as these can be a matter of discussion in future works, not on the scope of this thesis. With this, in conventional tracking systems, a common model of process noise design is the *random acceleration* (RA) model [91], with the covariance matrix taking the following structure

$$\boldsymbol{Q} = \begin{bmatrix} T_s^2/4 & 0 & 0 & T_s/2 & 0 & 0 \\ 0 & T_s^2/4 & 0 & 0 & T_s/2 & 0 \\ 0 & 0 & T_s^2/4 & 0 & 0 & T_s/2 \\ T_s/2 & 0 & 0 & 1 & 0 & 0 \\ 0 & T_s/2 & 0 & 0 & 1 & 0 \\ 0 & 0 & T_s/2 & 0 & 0 & 1 \end{bmatrix} \sigma_q^2 T_s^2 \tag{4.11}$$

The appropriate selection of σ_q is important because this parameter directly determines the performance of the tracking filter with the CV model. There is no definitive method of determining its actual value, however, following the reasoning in [91], the authors view it as a standard deviation parameter of a Gaussian sequence that models the target acceleration $\boldsymbol{w}_q$, assumed to be constant during the sampling interval T_s, a common practice in the literature. Intuitively, we can treat this as random fluctuations on position and velocity data due to small accelerations, as pointed out by the authors in [36] on the implementation of a diver velocity filter.

Finally, relative to the measurement covariance matrix $\boldsymbol{R}$, this is also a matter of discussion in terms of the implementation and the values to be used. As pointed out in [89], $\boldsymbol{R}$ is a representative parameter of the Kalman filter and is usually estimated from analyzing the specifications of sensing equipment. For arbitrary users, this is difficult to grasp or get a sense of the data information provided by the sensors therefore, usual values are chosen close to zero, however, this might degrade the filter's performance. Since our work does not involve discussing optimal methods of choice of values towards the filter's noise covariance, we will adopt a simple solution consisting of the sensor's data variance of the position measurement errors (since our work is related to POM data), as adopted by the authors in [91] and assumed to be available, taking the following form

$$\boldsymbol{R} = \begin{bmatrix} \sigma_x & 0 & 0 \\ 0 & \sigma_y & 0 \\ 0 & 0 & \sigma_z \end{bmatrix} \tag{4.12}$$

where σ_x, σ_y and σ_z denote the variance of position measurements' errors in the horizontal (x and y) and vertical axis (z).

4.3.3 A Kalman Filter Solution

Given all this discussion and implementation of a target tracking filter implementation, we can then proceed to estimate the state of a moving diver driven by a state-space dynamic system (**??**) in a mean-square sense using noisy position measurements, driven by the measurement model (4.10). The Kalman filter algorithm

based on these models recursively estimates the state vectors via the Kalman filter equations of prediction and estimation, respectively given by

$$\tilde{\boldsymbol{x}}_k = \boldsymbol{\Phi}\hat{\boldsymbol{x}}_{k-1} \tag{4.13}$$

$$\hat{\boldsymbol{x}}_k = \tilde{\boldsymbol{x}}_k + \boldsymbol{K}_k(\boldsymbol{z}_k - \boldsymbol{H}\tilde{\boldsymbol{x}}_k) \tag{4.14}$$

where the parameter $\boldsymbol{K}_k$ denotes the Kalman gain that minimizes the steady-state expected value of the error covariance, given by $\lim_{t\to\infty} E[(\boldsymbol{x}_k - \hat{\boldsymbol{x}}_k)(\boldsymbol{x}_k - \hat{\boldsymbol{x}}_k)^T]$. We will not expand the algorithm behind computing such gain as this is a well known procedure in the literature, however, it is important to note that the way this gain is obtained is what makes this filter a Kalman filter. If other ways are used to compute this gain, then we can think of this filter as an Observer instead.

4.4 Cooperation Architecture Proposal

In this last section, we condense and use all the information gathered throughout this Chapter proposing a cooperation architecture between diver and an AUV that will promote cooperation strategies with a diver, and it will serve as a basis of development and motivation for the control system of an AUV derived in Chapter 5.

This cooperation architecture is focused on the diving operations, mentioned in Section 4.1, and is intended to be a general-purpose architecture allowing for different approaches to be implemented under the same objectives. Overall, we desire the AUV to have the following capabilities:

1. Follow and accompany the diver during diving operations, maintaining a safe distance, e.g., carrying cargo alongside a diver.
2. Position itself accordingly, in any given desired location according to mission requirements, e.g., indicate direction of mission location.
3. Orient itself accordingly, independently of position, according to mission requirements, e.g., facing and monitoring the diver with the AUV forward sensors, illuminate the surrounding area increasing diver visibility levels.

Under this architecture, with an overview diagram presented in Fig. 4.8, we assume that we have a capable and robust navigation system to obtain the vehicle state (pose and velocity) and also the diver state, via a tracking filter mentioned in Section 4.3 with the help of measurement of the diver location with sensors and algorithms discussed in Section 4.2. Moreover, the guidance system will vary depending on the mission requirements, but it will provide the necessary reference signals, by processing the information of the mission requirements and diver state. Therefore we present a brief example during the implementation phase on Chapter 6. AS mentioned before, we assume that our vehicle is fully-actuated, allowing us to decouple the robot positioning and orientation mechanisms to divide our control design task and provide an easy way the respective controllers. This will allow an extension of these capabilities for additional objectives, such as facing the ocean currents direction while approaching the diver to reduce drag and power consumption from the

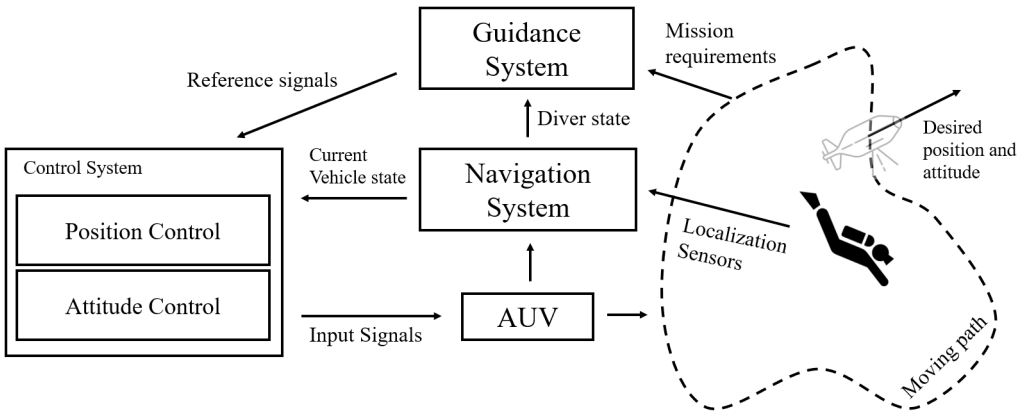

Figure 4.8: An overview of the cooperation strategy implemented in this thesis, formulated in this architecture diagram.

motors, facing the diver with the AUV frontal sensor or other surrounding structures, while keeping a specific position, etc.

Keeping this general cooperation architecture in mind, we now proceed to derive a control system that can accomplish this type of cooperation in Chapter 5.

Chapter 5

AUV 6DOF Motion Control

In this chapter the control problem of stabilizing the position and attitude of a single AUV at arbitrary references is discussed. The controller is designed taking into account the cooperation architecture proposed in Chapter 4 and follows an inner-outer loop strategy, effectively dividing the problem into two tasks. Considering that the vehicle used throughout this work is fully-actuated and the kinematics of the outer-loop are decoupled from the inner-loop (but not the opposite), the control architecture can be decoupled into translational and rotational motion, using the former to position the vehicle at a desired location near the diver, and the latter to change the vehicle attitude at an arbitrary reference. Then, the inner-loops provides the necessary forces and torques for the vehicle to follow the references signals from the outer-loop. A stability analysis of the outer-loop is performed in section 5.1, as well as the respective inner-loop in section 5.2. Finally, the derived controller is coupled together and the respective stability analysis of the interconnected closed-loop system is performed in section 5.4. In the following Fig. 5.1, we provide an overview perspective of the guidance, navigation and control architecture where our control system derivation (inner-outer loop and ocean observer) will be fitted into, assuming we already have implemented a navigation and guidance system capable of providing the vehicle state and reference signals, respectively.

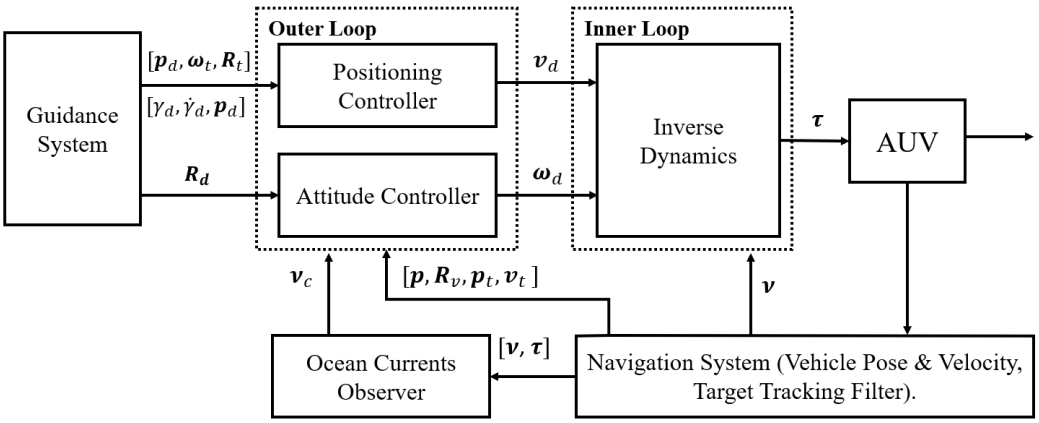

Figure 5.1: The guidance, navigation and control architecture where the inner and outer loop controllers, as well as ocean current observer will be implemented.

5.1 Outer Loop Controller

The outer loop controller concerns the vehicle kinematics and the higher level requirements for the mission performance, providing speed assignments, as linear and angular velocities, to the inner loop controller that will position and orient the AUV according to the control objectives. As previously mentioned in Chapter 4, we want to promote a cooperation relationship between the diver and robot, more specifically, develop a control architecture such that the robot positions itself in desired arbitrary points, along a predefined path, as well as stabilizing its attitude at a desired arbitrary reference. The outer loop controller is assigned to provide linear and angular velocity signals to the inner loop controller. Due to vehicle fully actuation capabilities, the control task is divided in two parts: position and attitude. Each part is handled such that the vehicle position reaches a desired location and the vehicle attitude stabilizes at a certain configuration. Two control laws are proposed to solve each respective problem.

5.1.1 Positioning Controller

Consider an inertial frame of reference $\{N\}$ and a body frame $\{B\}$ attached to the center of mass of the AUV. The kinematics of the vehicle in (3.16) can be rewritten taking ocean currents into account, expressed as follows

$$\begin{cases} \dot{\boldsymbol{p}} = \boldsymbol{R}_v \boldsymbol{v}_r + \boldsymbol{V}_{c_v} & \text{(5.1a)} \\ \dot{\boldsymbol{R}}_v = \boldsymbol{R}_v \boldsymbol{S}(\boldsymbol{\omega}_r) & \text{(5.1b)} \end{cases}$$

where $\boldsymbol{v}_r$ and $\boldsymbol{\omega}_r$ represent the linear and angular relative velocities of the vehicle in the water, and $\boldsymbol{V}_{c_v}$ the ocean current linear velocity expressed in the inertial frame. Notice that the ocean current angular velocity is not taken into account on the vehicle kinematics, since the ocean currents are considered to be irrotational, as mentioned in Chapter 3.

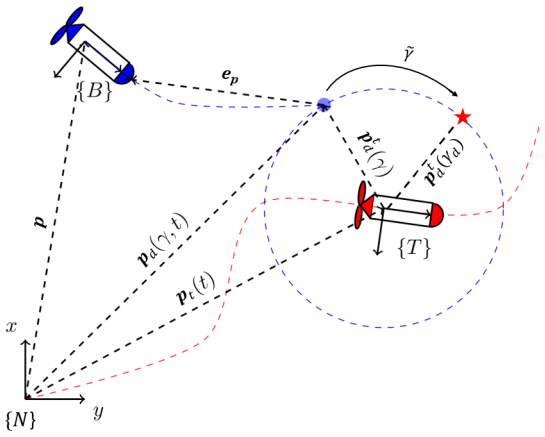

Figure 5.2: Representation of the *moving path-following* problem, where our vehicle is represented in blue, and an arbitrary target is represented in red, e.g., diver, other vehicle, etc. (adapted from [36]).

The control problem, as illustrated in Fig. 5.2, can be regarded as a *moving path-following* problem, where the vehicle is tasked to follow an *a-priori* specified path expressed with respect to a moving target. This path is

a parametric closed $\mathcal{C}^2$ continuous curve, that is, a curve that share the same parametric second derivatives with no self-intersecting points, and it is parameterized by a continuous variable $\gamma \in \mathbb{R}$. We define a target frame $\{T\}$ whose origin is attached to the target position $\boldsymbol{p}_t \in \mathbb{R}^3$.

Let the virtual point $\boldsymbol{p}_d^t(\gamma) \in \mathbb{R}^3$ denote the position of the virtual reference point to follow, expressed in the target frame. To obtain the inertial position and velocity, we can express its virtual position, as follows for a given γ,

$$\boldsymbol{p}_d(\gamma) = \boldsymbol{p}_t + \boldsymbol{R}_t \boldsymbol{p}_d^t(\gamma) \tag{5.2}$$

$$\dot{\boldsymbol{p}}_d(\gamma) = \boldsymbol{v}_t + \boldsymbol{R}_t \left(\frac{\partial \boldsymbol{p}_d^t(\gamma)}{\partial \gamma} \dot{\gamma} + \boldsymbol{S}(\boldsymbol{w}_t) \boldsymbol{p}_d^t(\gamma) \right) \tag{5.3}$$

where $\boldsymbol{R}_t \in SO(3)$ is the rotation matrix of frame $\{T\}$ with respect to the inertial frame $\{N\}$ provided by the guidance system (since we assume the diver does not have an inherent orientation in space), $\boldsymbol{v}_t = \dot{\boldsymbol{p}}_t$ is the target linear velocity, and $\boldsymbol{\omega}_t \in \mathbb{R}^3$ is the angular velocity of the target frame, expressed in its body frame $\{T\}$. In addition to this, we want the virtual position to converge to a desired virtual position $\boldsymbol{p}_d^t(\gamma_d) \in \mathbb{R}^3$, where $\gamma_d \in \mathbb{R}$ is a desired parameterization variable. This is possible by deriving a control law for the derivative of the parameterization variable, $\dot{\gamma}$

With this in mind, the positioning control problem can be formulated as a *moving path-following* problem, as follows:

Problem 1. *Consider an AUV with kinematics equation given by* (5.1a)-(5.1b)*. Let $\boldsymbol{p}_t$ be the target known position, $\boldsymbol{R}_t \in SO(3)$ its attitude, $\boldsymbol{v}_t, \boldsymbol{\omega}_t \in \mathbb{R}^3$ the linear and angular velocity of the target frame $\{T\}$, respectively, and $\boldsymbol{p}_d^t(\gamma)$ a desired virtual position in $\{T\}$. Suppose also that $\boldsymbol{p}_d^t(\gamma)$ is sufficiently smooth and its derivatives with respect to γ are bounded. Derive a control law for $\boldsymbol{v}_r$ and $\dot{\gamma}$ such that i) the position of the vehicle $\boldsymbol{p}$ converges to the desired position $\boldsymbol{p}_d(\gamma)$, i.e., the positioning error $\boldsymbol{p} - \boldsymbol{p_d}$ has a GAS equilibrium point at the origin and ii) the path parameterization variable γ stabilizes at the desired monitoring position parameterized by γ_d, i.e, the virtual particle position error $\gamma - \gamma_d$ has a GAS equilibrium point at the origin.*

The error associated with the vehicle and the desired position can be defined in the body-fixed frame as

$$\boldsymbol{e}_p = \boldsymbol{R}_v^T (\boldsymbol{p} - \boldsymbol{p_d}) \tag{5.4}$$

Taking the time derivative of the error, and using the vehicle's and the virtual point kinematics we obtain

$$\dot{\boldsymbol{e}}_p = -\boldsymbol{S}(\boldsymbol{\omega}_r)\boldsymbol{e}_p + \boldsymbol{v}_r + \boldsymbol{R}_v^T \left(\boldsymbol{V}_{c_v} - \boldsymbol{v}_t - \boldsymbol{R}_t \left(\frac{\partial \boldsymbol{p}_d^t(\gamma)}{\partial \gamma} \dot{\gamma} + \boldsymbol{S}(\boldsymbol{w}_t) \boldsymbol{p}_d^t(\gamma) \right) \right) \tag{5.5}$$

where $\boldsymbol{v}_r$ is the available control signal, to be fed onto the inner loop. An expression for the path position error and respective dynamics are, respectively, given by

$$\tilde{\gamma} = \gamma - \gamma_d \tag{5.6}$$

$$\dot{\tilde{\gamma}} = \dot{\gamma} - \dot{\gamma_d} \tag{5.7}$$

where $\dot{\gamma}$ is an extra direct control input.

Additionally, following the definition used in [92], define a saturation function δ according to the following definition:

Definition 6 (Saturation Function)**.** *A saturation function is a differentiable mapping function* $\sigma : \mathbb{R}^n \Rightarrow \mathbb{R}^n$ *satisfying for* $n = 1$*:*

$$
\begin{aligned}
&|\sigma'(s)| := \left|\frac{d\sigma(s)}{ds}\right| \leq 2 \quad \forall s \in \mathbb{R}, \\
&s\sigma(s) > 0 \quad \forall s \neq 0, \quad \sigma(0) = 0, \\
&\sigma(s) = \operatorname{sgn}(s) \quad \forall |s| \geq 1 \\
&|s| < |\sigma(s)| < 1 \quad \forall |s| < 1
\end{aligned}
$$

For $n > 1$*,*

$$
\boldsymbol{\sigma} : \boldsymbol{s} = [s_1, ..., s_n]^T \Rightarrow [\sigma(s_1), ..., \sigma(s_n)]^T
$$

The following Fig. 5.3 represents a possible saturation function $\lambda\sigma\left(\frac{k}{\lambda}x\right)$, for $n = 1$, highlighting its possible regions of operation via the parameters λ and k are nonnegative parameters.

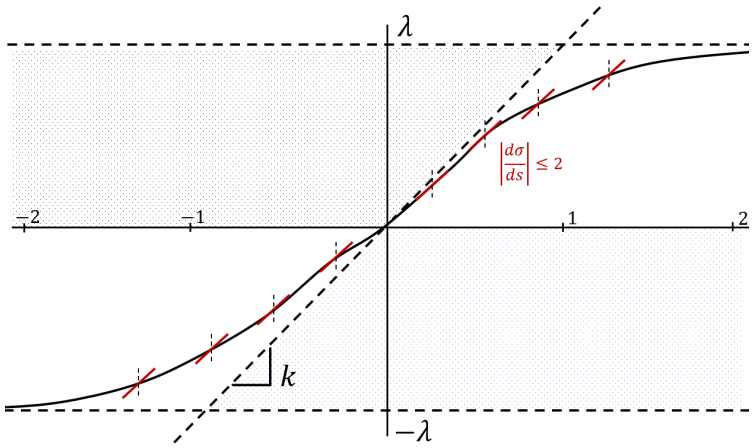

Figure 5.3: Example of an arbitrary saturation function, represented in black, where the dotted area are regions where the function does not take values $\forall k, \lambda > 0$.

With this, the following control law is proposed to solve the *moving path-following* Problem 1, as follows:

Proposition 1. *Consider the system described in* (5.1a) *in closed-loop with the control laws*

$$
\boldsymbol{v}_d = -\lambda_p \boldsymbol{\sigma}\left(\frac{k_p}{\lambda_p}\boldsymbol{e}_p\right) - \boldsymbol{R}_v^T\left(\boldsymbol{V}_{c_v} - \boldsymbol{v}_t - \boldsymbol{R}_t\left(\frac{\partial \boldsymbol{p}_d^t(\gamma)}{\partial \gamma}\dot{\gamma}_d + \boldsymbol{S}(\boldsymbol{w}_t)\boldsymbol{p}_d^t(\gamma)\right)\right) \tag{5.8}
$$

$$
\dot{\gamma} = \dot{\gamma}_d - k_\gamma\left(\rho_{\tilde{\gamma}}\sigma(k_{\tilde{\gamma}}\tilde{\gamma}) - \boldsymbol{e}_p^T\boldsymbol{R}_v^T\boldsymbol{R}_t^n\frac{\partial p_d^t(\gamma)}{\partial \gamma}\right) \tag{5.9}
$$

where it is assumed that $\boldsymbol{v}_d = \boldsymbol{v}_r$ *at a kinematic level. Aditionally,* $\rho_{\tilde{\gamma}}$ *and* $k_{\tilde{\gamma}}$ *are positive parameter gains, and* k_γ*,* λ_p *and* k_p *are positive controller gains. Then, the origin of positioning error system* $\boldsymbol{e}_p = \boldsymbol{0}$ *and path*

parameterization position error system $\tilde{\gamma} = 0$ are GAS.

Proof. Define a Lyapunov candidate for the vehicle positioning and path parameterization variable error dynamics

$$V_p(\tilde{\gamma}, \boldsymbol{e}_p) = \frac{1}{2}\boldsymbol{e}_p^T\boldsymbol{e}_p + \frac{\rho_{\tilde{\gamma}}}{k_{\tilde{\gamma}}}\int_0^{\tilde{\gamma}} \sigma(k_{\tilde{\gamma}} s)\, ds > 0, \quad \forall \boldsymbol{e}_p \in \mathbb{R}^3\backslash\{\boldsymbol{0}\}, \tilde{\gamma} \in \mathbb{R}\backslash\{0\} \tag{5.10}$$

.

Note that $V_p(\tilde{\gamma}, \boldsymbol{e}_p)$ is a valid energy function since it is continuous, has continuous first derivatives, is strictly positive, $V_p(0,0) = 0 + \int_0^{\tilde{\gamma}} \sigma(0)\, ds = 0$, and $V_p(\tilde{\gamma}, \boldsymbol{e}_p) \Rightarrow \infty$ when $\|\boldsymbol{e}_p\|, \|\tilde{\gamma}\| \Rightarrow \infty$.

In [93], the authors propose a similar scheme relative to the path paramaterization error $\tilde{\gamma}$, defining two Lyapunov candidates as

$$V(\tilde{\gamma}) = \begin{cases} \frac{1}{2}k_{\tilde{\gamma}}\tilde{\gamma}^2 \\ \frac{\rho_{\tilde{\gamma}}}{k_{\tilde{\gamma}}}\ln\left(\cosh\left(k_{\tilde{\gamma}}\tilde{\gamma}\right)\right) \end{cases} \tag{5.11}$$

where both cases represent a valid energy function, according to the above mentioned conditions. The reason behind this choice is that, to some extent, the transient between desired points can be shaped using the parameter gains $\rho_{\tilde{\gamma}}$, $k_{\tilde{\gamma}}$, k_{γ}. The authors performed different experiments to show a comparison between the two choices. In this work, we follow a similar approach as author's because the logarithmic/hyperbolic function provides a fast transient and negligible undershoot when γ_d alternates. Moreover, in this work, we extended their results by considering the integral of the saturation function $\sigma(\cdot)$ instead of an explicit logarithmic/hyperbolic function $\ln(\cosh(\cdot))$.

The time derivative of (5.10) and using the error dynamics (5.5) and (5.7) is given by

$$\begin{aligned} \dot{V}_p &= \boldsymbol{e}_p^T\dot{\boldsymbol{e}}_p + \rho_{\tilde{\gamma}}\sigma(k_{\tilde{\gamma}}\tilde{\gamma})\dot{\tilde{\gamma}} \\ &= \boldsymbol{e}_p^T\left(\boldsymbol{v}_r + \boldsymbol{R}_v^T\left(\boldsymbol{V}_{c_v} - \boldsymbol{v}_t - \boldsymbol{R}_t\left(\frac{\partial \boldsymbol{p}_d^t(\gamma)}{\partial\gamma}\dot{\gamma} + \boldsymbol{S}(\boldsymbol{w}_t)\boldsymbol{p}_d^t(\gamma)\right)\right)\right) + \rho_{\tilde{\gamma}}\sigma(k_{\tilde{\gamma}}\tilde{\gamma})\dot{\tilde{\gamma}} \end{aligned} \tag{5.12}$$

Rewriting the time derivative of (5.12), gives the following

$$\begin{aligned} \dot{V}_p = \boldsymbol{e}_p^T\left(\boldsymbol{v}_r + \boldsymbol{R}_v^T\left(\boldsymbol{V}_{c_v} - \boldsymbol{v}_t - \boldsymbol{R}_t\left(\frac{\partial \boldsymbol{p}_d^t(\gamma)}{\partial\gamma}\dot{\gamma}_d + \boldsymbol{S}(\boldsymbol{w}_t)\boldsymbol{p}_d^t(\gamma)\right)\right)\right) + \\ + \dot{\tilde{\gamma}}\left(\rho_{\tilde{\gamma}}\sigma(k_{\tilde{\gamma}}\tilde{\gamma}) - \boldsymbol{e}^T\boldsymbol{R}_v^T\boldsymbol{R}_t^n\frac{\partial \boldsymbol{p}_d^t(\gamma)}{\partial\gamma}\right) \end{aligned} \tag{5.13}$$

Substituting the control law (5.8)-(5.9) in (5.13) yields

$$\dot{V}_p = -\boldsymbol{e}_p^T\lambda_p\boldsymbol{\sigma}\left(\frac{k_p}{\lambda_p}\boldsymbol{e}_p\right) - k_{\gamma}\left(\rho_{\tilde{\gamma}}\sigma(k_{\tilde{\gamma}}\tilde{\gamma}) - \boldsymbol{e}^T\boldsymbol{R}_v^T\boldsymbol{R}_t^n\frac{\partial p_d^t(\gamma)}{\partial\gamma}\right)^2 \tag{5.14}$$

Observe the proposed control law (5.9) and assume the $\dot{\gamma_d} = 0$ without loss of generalization. The remaining factors $\rho_{\tilde{\gamma}}\sigma(k_{\tilde{\gamma}}\tilde{\gamma})$ and $\boldsymbol{e}^T\boldsymbol{R}_v^T\boldsymbol{R}_t\frac{\partial \boldsymbol{p}_d^t(\gamma)}{\partial\gamma}$ govern $\dot{\gamma}$. When governed by the first factor only, it forces convergence to γ_d. On the other hand, the second factor forces converge of γ to the point of projection of the vehicle's position onto the path. The last statement can be better understood in [94] where the authors define a similar

error vector

$$\boldsymbol{\epsilon} = \boldsymbol{R}_t^T(\boldsymbol{p} - \boldsymbol{p}_d) = \boldsymbol{R}_t^T \boldsymbol{R}_b^n \boldsymbol{e}_p \tag{5.15}$$

where $\boldsymbol{\epsilon} = [s, e, h]^T$ consists of the *along-track error*, the *cross-track error* and *vertical-track-error*, respectively. The along-track error represents the distance from $\boldsymbol{p}_d$ to $\boldsymbol{p}$ along the *x*-axis of target frame $\{T\}$, the cross-track error represents the distance along the *y*-axis, and the vertical-track error represents the distance along the *z*-axis. Now, it is straightforward to see that the factor $\boldsymbol{e}^T \boldsymbol{R}_v^T \boldsymbol{R}_t^n \frac{\partial \boldsymbol{p}_d^t(\gamma)}{\partial \gamma}$ represents the vehicle own projection on the path.

Knowing that the following inequality is satisfied

$$\dot{V}_p = -\boldsymbol{e}_p^T \lambda_p \boldsymbol{\sigma}\left(\frac{k_p}{\lambda_p}\boldsymbol{e}_p\right) - k_\gamma \left(\rho_{\tilde{\gamma}}\sigma(k_{\tilde{\gamma}}\tilde{\gamma}) - \boldsymbol{e}^T \boldsymbol{R}_v^T \boldsymbol{R}_t^n \frac{\partial p_d^t(\gamma)}{\partial \gamma}\right)^2 \leq 0, \quad \forall \boldsymbol{e}_p \in \mathbb{R}^3 \backslash \{\boldsymbol{0}\}, \tilde{\gamma} \in \mathbb{R} \backslash \{0\} \tag{5.16}$$

all conditions of Theorem 2 are verified and the origin of both systems $\boldsymbol{e} = \boldsymbol{0}$ and $\tilde{\gamma} = 0$ are GAS. □

5.1.2 Attitude Controller

Consider the rotational kinematics of the vehicle (5.1b) and a target rotation matrix $\boldsymbol{R}_d \in SO(3)$ defined as the rotation matrix of an arbitrary desired frame $\{D\}$, with origin equal to frame $\{B\}$ origin, with respect to the inertial frame $\{N\}$. In broad terms, the problem at hand consists controlling the vehicle body frame $\{B\}$, with respective rotation matrix $\boldsymbol{R}_v$, via the body angular velocity $\boldsymbol{\omega}_r$, assumed available to the system for feedback control, to ensure convergence of $\boldsymbol{R}_v$ to $\boldsymbol{R}_d$. Although it is not trivial for an end-user to define a desired rotation matrix $\boldsymbol{R}_d$ according to the mission specification, one can easily parameterize $\boldsymbol{R}_d(\boldsymbol{\Theta}_d)$ via Euler angles $\boldsymbol{\Theta}_d = [\phi_d, \theta_d, \psi_d]^T \in \mathbb{R}^3$, which is a more intuitive approach.

Additionally, suppose there exist a matrix $\boldsymbol{Q}$ such that is satisfies the following assumption:

Assumption 1. *The matrix $\boldsymbol{Q} \in \mathbb{M}(3, m)$ with $m > 0$ is such that the singular values are all distinct.*

Given this, the attitude control problem can be defined as follows:

Problem 2. *Consider an AUV with rotational kinematics equation given by 5.1b. Let $\boldsymbol{R}_d(\boldsymbol{\Theta}_d)$ be a target rotation matrix, parameterized by a constant reference, defined a-priori, $\boldsymbol{\Theta}_d = [\phi_d, \theta_d, \psi_d]^T$. Additionally suppose that there exists a matrix $\boldsymbol{Q}$ that satisfies Assumption 1. Derive a feedback control for $\boldsymbol{\omega}_r$ such that the body frame rotation matrix $\boldsymbol{R}_v$ converges to $\boldsymbol{R}_d$, i.e, the rotational error $\boldsymbol{R}_v^T \boldsymbol{R}_d$ has an AGAS equilibrium point at $\boldsymbol{I}_3$, where $\boldsymbol{I}_3$ is the identity matrix in three dimensions.*

For this purpose, define the error rotation matrix

$$\boldsymbol{R}_e = \boldsymbol{R}_b^{n^T} \boldsymbol{R}_d \tag{5.17}$$

with the respective dynamics as follows

$$\dot{\boldsymbol{R}}_e = -\boldsymbol{S}(\boldsymbol{\omega}_r)\boldsymbol{R}_e \tag{5.18}$$

Since the error evolves on $SO(3)$, it is convenient to express error as an function on $SO(3)$, as follows

$$e_\Theta(\boldsymbol{R}_e) = \mathrm{Tr}\left((\boldsymbol{I}_3 - \boldsymbol{R}_e)\,\boldsymbol{Q}\boldsymbol{Q}^T\right) \tag{5.19}$$

where $\mathrm{Tr}(\cdot)$ denotes the trace of a square matrix, defined as the sum of all elements in the matrix diagonal. If Assumption 1 holds, the error function is a Morse function i.e, it is a function with nondegenerate isolated critical points [95], [96]. A critical point of a (differentiable) function maybe a local maximum, local minimum or a saddle point. In other words, the function e_Θ corresponds to the modified trace function studied in [96] which is positive definite with a global minimum at $\boldsymbol{R}_e = \boldsymbol{I}_3$, a maximum and two saddle points. These properties are fundamental, as mentioned in the work done by the authors in [42] and [12], where it will also be valuable to the proof of our controller. Then, following the same approach, it is possible to compute the time derivative as follows

$$\dot{e}_\Theta(\boldsymbol{R}_e) = -\boldsymbol{S}^{-1}(\boldsymbol{R}_e\boldsymbol{Q}\boldsymbol{Q}^T - \boldsymbol{Q}\boldsymbol{Q}^T\boldsymbol{R}_e^T)^T\boldsymbol{\omega}_r \tag{5.20}$$

where $\boldsymbol{S}^{-1} : SO(3) \mapsto \mathbb{R}^3$ corresponds to the inverse of the cross-product operator and the available control input is $\boldsymbol{\omega}_r$.

Note that, it is possible to define the error with same approach as done in section 5.1.1, as follows

$$\boldsymbol{e}_\Theta = \boldsymbol{\Theta} - \boldsymbol{\Theta}_d \tag{5.21}$$

where $\boldsymbol{\Theta} \in \mathbb{R}^3$ is the vehicle body frame $\{B\}$ orientation with respect to the inertial frame $\{N\}$, and $\boldsymbol{\Theta}_d \in \mathbb{R}^3$ the desired orientation, both expressed in Euler angles. Then, taking into account the vehicle angular kinematic equation using Euler angles parameterization (3.6), the error dynamics can be expressed as follows

$$\dot{\boldsymbol{e}}_\Theta = \dot{\boldsymbol{\Theta}} - \dot{\boldsymbol{\Theta}}_d = \boldsymbol{T}_b^n(\phi, \theta, \psi)\boldsymbol{\omega}_r - \dot{\boldsymbol{\Theta}}_d \tag{5.22}$$

It immediately follows that, because $\boldsymbol{T}_b^n(\phi, \theta, \psi)$ is not fully defined for $\theta \neq 90°$, it only allows the design of locally stable control laws and not globally/almost globally stable control laws, deteriorating the controller stability performance, as briefly mentioned in Chapter 1.

With this, the following control law is proposed to solve the *path-following* problem 2, as follows:

Proposition 2. *Consider the system given by* (5.1b) *and the following control law in closed-loop*

$$\boldsymbol{\omega}_d = \boldsymbol{K}_\omega \boldsymbol{S}^{-1}(\boldsymbol{R}_e\boldsymbol{Q}\boldsymbol{Q}^T - \boldsymbol{Q}\boldsymbol{Q}^T\boldsymbol{R}_e^T) \tag{5.23}$$

where $\boldsymbol{K}_\omega$ is a positive definite gain matrix, and it is assumed that $\boldsymbol{\omega}_d = \boldsymbol{\omega}_r$ at a kinematic level. Then, the equilibrium point of the error rotation matrix $R_e = \boldsymbol{I}_3$ is almost GAS. Moreover, there exists a neighborhood of $\boldsymbol{R}_e = \boldsymbol{I}_3$, such that all solutions starting inside it converge exponentially fast to $\boldsymbol{R}_e = \boldsymbol{I}_3$.

Proof. The proof will follow previous works done towards attitude stabilization [42], but only considering the rotational kinematic of the vehicle and disregarding its inherent dynamics, since we follow an inner-outer loop approach.

Define the following Lyapunov candidate

$$V_\Theta(\boldsymbol{R}_e) = e_\Theta(\boldsymbol{R}_e) = \mathrm{Tr}\left((\boldsymbol{I}_3 - \boldsymbol{R}_e)\,\boldsymbol{Q}\boldsymbol{Q}^T\right) \tag{5.24}$$

Under Assumption 1, V_Θ is positive definite being a valid energy function, as previously explained. Then, the derivative of (5.24) and using the attitude error dynamics (5.20) in closed-loop with the control law (5.23) is given by

$$\begin{aligned}\dot{V}_\Theta &= \frac{d}{dt}\left(e_\Theta(\boldsymbol{R}_e)\right) \\ &= -\boldsymbol{S}^{-1}(\boldsymbol{R}_e\boldsymbol{Q}\boldsymbol{Q}^T - \boldsymbol{Q}\boldsymbol{Q}^T\boldsymbol{R}_e^T)^T\boldsymbol{K}_\omega\boldsymbol{S}^{-1}(\boldsymbol{R}_e\boldsymbol{Q}\boldsymbol{Q}^T - \boldsymbol{Q}\boldsymbol{Q}^T\boldsymbol{R}_e^T) \leq 0\end{aligned} \tag{5.25}$$

It follows immediately that $\dot{V}_\Theta$ is negative semi-definite. This however, does not provide sufficient conditions regarding stability conditions of the equilibrium points. So, rather than focus on the question of stability of an equilibrium solution as in Lyapunov's method again, LaSalle's Invariance Principle provides simple intuitive conditions that describe their behavior, similarly to what the author did in [42]. For convenience purposes, we will mention briefly the theory behind this principle, using this proof as an application example.

We know that V_Θ has exactly four critical points: one minimum at $\boldsymbol{R}_e = \boldsymbol{I}_3$, one maximum and two saddle points. Considering the level sets of (5.24) $\mathcal{C}$, we know from (5.25) that

$$\dot{V}_\Theta \leq 0 \text{ on } V_\Theta = \mathcal{C} \tag{5.26}$$

Therefore, for a sufficiently large $\mathcal{C}$, the corresponding set of V_Θ bounds a compact positive and invariant set $\mathcal{M}$ that contains the four equilibrium points of (5.20). The next natural step is to find such set, that is

$$\mathcal{M} = \{\boldsymbol{R}_e \in SO(3) \mid \dot{V}_\Theta = 0\} \tag{5.27}$$

It follows immediately that the largest invariant set $\mathcal{M}$ is the set of points $\boldsymbol{R}_e$ that are critical points of $V_\Theta = e_\Theta$, which are the global minimum $\boldsymbol{R}_e = \boldsymbol{I}_3$, a maximum and two saddle points. The actual expression of these critical points are mentioned by the authors in [42].

Then, LaSalle's Invariance Principle states that for all $\boldsymbol{R}_e \in SO(3)$, the closed-loop trajectories of the error system (5.20) converge to $\mathcal{M}$ as $t \to \infty$ for any given initial condition in $\mathcal{C}$. Informally, this means that, with the control law (5.23), the trajectories of this system, starting at that initial condition, approach one of the four equilibrium points as $t \Rightarrow \infty$.

Additionally, the authors in [42] and [12] prove that except for the point $\boldsymbol{R}_e = \boldsymbol{I}_3$ all equilibrium points $\boldsymbol{R}_e = \boldsymbol{R}_c \in \mathcal{M}$ have an unstable manifold. In loose terms, this prevent trajectories remaining in this manifold, allowing them to asymptotically converge to the desired equilibrium. However, it may happen that the convergence to the equilibrium can be affected near this *thin* set [97]. With this, the equilibrium point $\boldsymbol{R}_e = \boldsymbol{I}_3$ is proven to be AGAS.

□

5.2 Dynamics Controller

In an inner-outer loop architecture, the task of the inner loop is to follow the outer loop speed requirements as close as possible, in order to move the vehicle at that desired speed. These speed requirements are given in terms of the relative velocity of the vehicle in the water. This allows us to simplify the computations from the dynamic point of view, because, as explained in the previous chapter, the AUV dynamics are related to the vehicle's relative velocity with respect to the water.

The control problem can be formulated as follows:

Problem 3. *Consider the dynamical model of the vehicle given by* (3.17). *Let* $\boldsymbol{\nu}_d = [\boldsymbol{v}_d, \boldsymbol{\omega}_d]^T \in \mathbb{R}^6$ *be a desired speed requirement from the outer loop, and suppose that* $\boldsymbol{\nu}_d$ *is sufficiently smooth and its derivative is bounded. Derive a feedback control law* $\boldsymbol{\tau}$ *such that the relative velocity error* $\boldsymbol{\nu}_r - \boldsymbol{\nu}_d$ *has a GES equilibrium point at the origin.*

Notice that the speed requirement is given both for linear and angular velocities. We consider the 6 DOF vectorial dynamical equation in the inner loop control due to rotational and translational motion dynamic coupling. The inner-loop will output the desired forces and moments $\boldsymbol{\tau}$.

For this purpose, we first define the error $\boldsymbol{e}_d = \boldsymbol{\nu}_r - \boldsymbol{\nu}_d \in \mathbb{R}^3$. With this, we can rewrite the AUV equations of motion in error form, as follows

$$\boldsymbol{M}\dot{\boldsymbol{e}}_d = \boldsymbol{\tau} - \boldsymbol{M}\dot{\boldsymbol{\nu}}_d - \boldsymbol{C}(\boldsymbol{\nu}_r)\boldsymbol{\nu}_r - \boldsymbol{D}(\boldsymbol{\nu}_r)\boldsymbol{\nu}_d - \boldsymbol{D}(\boldsymbol{\nu}_r)\boldsymbol{e}_d \tag{5.28}$$

Then, the following inner loop control law is proposed:

Proposition 3. *Consider the system described by* (5.28) *and the following control law in closed-loop*

$$\boldsymbol{\tau} = -\boldsymbol{K}_d\boldsymbol{e}_d + \boldsymbol{M}\dot{\boldsymbol{\nu}}_d + \boldsymbol{D}(\boldsymbol{\nu}_r)\boldsymbol{\nu}_d + \boldsymbol{C}(\boldsymbol{\nu}_r)\boldsymbol{\nu}_r \tag{5.29}$$

where $\boldsymbol{K}_d$ *is a positive definite gain matrix. Then, the origin of the relative velocity error system* $\boldsymbol{e}_d = \boldsymbol{0}$ *has a GES equilibrium point.*

Proof. By substituting the control law (5.29) into (5.28) yields

$$\dot{\boldsymbol{e}}_d = -\boldsymbol{M}^{-1}\left(\boldsymbol{K}_d + \boldsymbol{D}(\boldsymbol{\nu}_r)\right)\boldsymbol{e}_d \tag{5.30}$$

which shows that the error dynamics have an equilibrium point of $\boldsymbol{e}_d = \boldsymbol{0}$. Consider the following Lyapunov candidate

$$V_d(\boldsymbol{e}_d) = \frac{1}{2}\boldsymbol{e}_d^T\boldsymbol{M}\boldsymbol{e}_d \tag{5.31}$$

The time derivative of $V_d(\boldsymbol{e}_d)$ and using the error dynamics (5.30) is given by

$$\dot{V}_d = \boldsymbol{e}_d^T\boldsymbol{M}\dot{\boldsymbol{e}}_d = -\boldsymbol{e}_d^T\left(\boldsymbol{K}_d + \boldsymbol{D}(\boldsymbol{\nu}_r)\right)\boldsymbol{e}_d \tag{5.32}$$

Knowing that $\boldsymbol{D}(\boldsymbol{\nu}_r))$ is a matrix of damping forces, satisfying Property 2, the following inequality is always satisfied

$$\dot{V}_d \leq -\boldsymbol{e}_d^T \left(\boldsymbol{K}_d + \boldsymbol{D}(\boldsymbol{0})\right) \boldsymbol{e}_d \tag{5.33}$$

With this, we can define the following conditions

$$\frac{1}{2}\lambda_{\mathsf{min}}(\boldsymbol{M}) \left\|\boldsymbol{e}_d\right\|^2 \leq V_d(\boldsymbol{e}_d) \leq \frac{1}{2}\lambda_{\mathsf{max}}(\boldsymbol{M}) \left\|\boldsymbol{e}_d\right\|^2 \tag{5.34a}$$

$$\dot{V}_d \leq -\lambda_{\mathsf{min}}(\boldsymbol{A}) \left\|\boldsymbol{e}_d\right\|^2 \tag{5.34b}$$

where $\boldsymbol{A} = \boldsymbol{K}_d + \boldsymbol{D}(\boldsymbol{0})$ is the sum of two positive definite matrices, since $\boldsymbol{D}(\boldsymbol{0})$ is also positive definite, rendering $\lambda_{\mathsf{min}}\boldsymbol{A} > 0$. Then, according to Theorem 3, if this assumptions hold globally, then the equilibrium point $\boldsymbol{e}_d = \boldsymbol{0}$ is GES.

□

5.3 Ocean Currents Observer

An AUV moving through water is generally subject to ocean currents, which influence the motion of the vehicle. The intensity of such currents affect the kinematic control of the vehicle, modifying the total velocity of the vehicle itself. Such disturbances are not easy to sense, however, there are clever ways to approach this problem using some known variables.

In [24], the authors use the vehicle relative velocity from the vehicle's kinematic model, deriving a simple fixed gain observer whose error dynamics equilibrium point are exponentially stable, where the observer ocean currents estimates converge to the true values. However, this approach assumes available measurements of the vehicles' relative velocity, which is hard to obtain. One way of obtaining these measurements is via a Doppler Velocity Logger (DVL) that has 2 modes of operation, one of which that outputs the vehicle's relative body velocity via reflection from acoustic waves in the surrounding fluid and the other that provides measurements of the vehicle's body velocity. But a problem arises from the fact that the DVL only operates on one mode at a time, and in addition the former mode usually exhibits a slow bandwidth and prone to high levels of noise. Therefore, this mode is only used in certain scenarios and the common approach is to have the latter mode of operation.

So, to avoid the use of relative velocities as measurements for estimating the ocean current intensity, one can use a model-based observer for ocean current estimation, as proposed by the authors in [98]. Considering the AUV DOF dynamic model (3.17) and the assumptions made in the scope of this thesis, that is, mass and inertia matrix being positive definite (Property 1), a non symmetric and strictly positive damping matrix (Property 2) and irrotational and constant ocean currents in the inertial frame, the authors derive an observer for the ocean current velocity $\boldsymbol{\nu}_c$ as follows

$$\boldsymbol{M}\dot{\hat{\boldsymbol{\nu}}} = -\boldsymbol{C}_{RB}(\boldsymbol{\nu})\boldsymbol{\nu} + \boldsymbol{\tau} + \hat{\boldsymbol{\tau}}_H + \boldsymbol{K}_1(\boldsymbol{\nu} - \hat{\boldsymbol{\nu}}) \tag{5.35}$$

$$\dot{\hat{\boldsymbol{\nu}}}_c = -\bar{\boldsymbol{S}}(\boldsymbol{\omega})\hat{\boldsymbol{\nu}}_c + \boldsymbol{K}_2(\boldsymbol{\nu} - \hat{\boldsymbol{\nu}}) \tag{5.36}$$

where $\boldsymbol{K}_1$ and $\boldsymbol{K}_2$ are the observer gain matrices, and $\bar{\boldsymbol{S}}(\boldsymbol{\omega}) = \begin{bmatrix} \boldsymbol{S}(\boldsymbol{\omega}) & \boldsymbol{0}_{3x3} \\ \boldsymbol{0}_{3x3} & \boldsymbol{0}_{3x3} \end{bmatrix}$. The last term accounts for the evolution of the ocean current velocity in the body-fixed frame, that is, $\dot{\boldsymbol{\nu}}_c = -\bar{\boldsymbol{S}}(\boldsymbol{\omega})\boldsymbol{\nu}_c$. Usually, the ocean current velocity is assumed to be constant or slowly-varying in the body frame, i.e. $\dot{\boldsymbol{\nu}}_c = \boldsymbol{0}$. But this is only valid during course-keeping and is easily violated during turning maneuvers. This term allows relaxing this assumption and account for constant ocean currents velocities in the inertial frame.

The observer is structured in a way to also provide a filtered velocity estimate $\hat{\boldsymbol{\nu}}$ besides the ocean current velocity $\hat{\boldsymbol{\nu}}_c$. Furthermore, different from the dynamic model used in this thesis, the observer separates the rigid body and hydrodynamic components of the Coriolis-Centripetal matrix, giving rise to the term of hydrodynamic forces and moments estimates

$$\hat{\boldsymbol{\tau}}_H = -\boldsymbol{M}\bar{\boldsymbol{S}}(\boldsymbol{\omega}) \cdot \hat{\boldsymbol{\nu}}_c - \boldsymbol{C}_A(\hat{\boldsymbol{\nu}} - \hat{\boldsymbol{\nu}}_c) \cdot (\hat{\boldsymbol{\nu}} - \hat{\boldsymbol{\nu}}_c) - \boldsymbol{D}(\hat{\boldsymbol{\nu}} - \hat{\boldsymbol{\nu}}_c) \cdot (\hat{\boldsymbol{\nu}} - \hat{\boldsymbol{\nu}}_c) \tag{5.37}$$

Defining the error variables as $\boldsymbol{e}_1 = (\boldsymbol{\nu} - \hat{\boldsymbol{\nu}}) - (\boldsymbol{\nu}_c - \hat{\boldsymbol{\nu}}_c)$ and $\boldsymbol{e}_2 = \boldsymbol{\nu}_c - \hat{\boldsymbol{\nu}}_c$, the observer error dynamics are described by

$$\boldsymbol{M}\dot{\boldsymbol{e}}_1 = -2\boldsymbol{C}_A(\boldsymbol{\nu}_r) \cdot \boldsymbol{e}_1 + \boldsymbol{C}_A(\boldsymbol{e}_1) \cdot \boldsymbol{e}_1 - \boldsymbol{D}\boldsymbol{e}_1 - [\boldsymbol{d}(\boldsymbol{\nu}_r) - \boldsymbol{d}(\boldsymbol{\nu}_r - \boldsymbol{e}_1)] - (\boldsymbol{K}_1 - \boldsymbol{M}\boldsymbol{K}_2)(\boldsymbol{e}_1 + \boldsymbol{e}_2) \tag{5.38a}$$

$$\dot{\boldsymbol{e}}_2 = -\bar{\boldsymbol{S}}(\boldsymbol{\omega})\boldsymbol{e}_2 - \boldsymbol{K}_2(\boldsymbol{e}_1 + \boldsymbol{e}_2) \tag{5.38b}$$

If the above assumptions hold and the observer gains $\boldsymbol{K}_1$ and $\boldsymbol{K}_2$ are chosen according to

$$\boldsymbol{K}_1 = (\boldsymbol{I} + \boldsymbol{M})\boldsymbol{K}, \quad \boldsymbol{K}_2 = \boldsymbol{K} \tag{5.39}$$

where $\boldsymbol{K} = \boldsymbol{K}^T > \boldsymbol{0}$, then the observer error dynamics (5.38) have GAS equilibrium points $(\boldsymbol{e}_1, \boldsymbol{e}_2) = (\boldsymbol{0}, \boldsymbol{0})$. The proof is shown in [98], therefore the proof is not derived in this thesis.

5.4 Closed-Loop Stability Analysis

The idea behind the inner-outer loop control architecture is to design the two controllers independently. This simplifies the computations and stability analysis of both systems. For LTI systems global stability of the interconnection of both systems can be guaranteed. However, global stability in close-loop form is not always the case for the interconnection of non-linear systems. This last sections analyses the overall system stability and prove that, even under interconnection terms between each loop, affecting their respective dynamics, we can still prove converge to the desired equilibrium points of each system.

The closed-loop stability analysis starts by considering a simple interconnection of both systems and we assume we access to the true states of the system, that is, the vehicle position $\boldsymbol{p}$ and linear and angular velocities $\boldsymbol{\nu} = [\boldsymbol{v}, \boldsymbol{\omega}]^T$ and ocean current velocity $\boldsymbol{V}_c$. Additionally, we assume that the target position $\boldsymbol{p}_t$ and velocity $\boldsymbol{v}_t$ are given by a time parameterized variable $\boldsymbol{p}_d(t)$ and its respective time derivative $\dot{\boldsymbol{p}}_d(t)$ to

facilitate the proof analysis. The proof is finalized by considering that the ocean current velocity are provided via the observer derived in Section 5.3 with the estimation error dynamics regarded as a disturbance to the interconnected system. This proof can be viewed as the derivation of a controller solution to a *trajectory tracking* problem.

After the main proof is established, we extend these results to now consider a *moving path stabilization* problem, considering the desired position $\boldsymbol{p}_d(\gamma)$ of the path to be parameterized by a continuous variable $\gamma(t)$, and lift the temporal constraints relative to the desired trajectory $\boldsymbol{p}_d(t)$. In addition, we also lift the assumption that we have true access to the target velocity $\boldsymbol{v}_t$ and instead have access to its estimate $\hat{\boldsymbol{v}}_t$ provided by a tracking filter, mentioned in Section 4.3. We only consider the estimate of the target linear velocity and not its angular velocity $\boldsymbol{\omega}_t$ since the tracking filter regards a target with linear motion. The orientation is intrinsically related with the mission requirements, where the associated guidance system provides not only an associated rotation matrix $\boldsymbol{R}_t$ but also $\boldsymbol{\omega}_t$.

5.4.1 Trajectory Tracking Controller

Given the speed requirements $\boldsymbol{\nu}_d = [\boldsymbol{v}_d, \boldsymbol{\omega}_d]^T$ produced by the outer loop, composed of the position and attitude controller, the inner loop will try to provide the necessary forces and moments to the vehicle to satisfy these requirements. However, because the inner loop has associated error dynamics $\boldsymbol{e}_d = \boldsymbol{\nu}_r - \boldsymbol{\nu}_d$, the outer loop error dynamics will also be affected assigning the following speed requirement $\boldsymbol{\nu}_d = \boldsymbol{\nu}_r - \boldsymbol{e}_d = [\boldsymbol{v}_r - \boldsymbol{e}_v, \boldsymbol{\omega}_r - \boldsymbol{e}_\omega]^T$. The error dynamics of the position (5.5) and attitude (5.20) system become, respectively

$$\dot{\boldsymbol{e}}_p = \boldsymbol{f}_p(\boldsymbol{e}_p + \boldsymbol{e}_v) = -\boldsymbol{S}(\boldsymbol{\omega}_r)\boldsymbol{e}_p + (\boldsymbol{v}_d + \boldsymbol{e}_v) + \boldsymbol{R}_v^T\left(\boldsymbol{V}_{c_v} - \dot{\boldsymbol{p}}_d\right) \tag{5.40}$$

$$\dot{e}_\Theta(\boldsymbol{R}_e) = \boldsymbol{f}_\Theta(\boldsymbol{R}_e + \boldsymbol{e}_\omega) = -\boldsymbol{S}^{-1}(\boldsymbol{R}_e\boldsymbol{Q}\boldsymbol{Q}^T - \boldsymbol{Q}\boldsymbol{Q}^T\boldsymbol{R}_e^T)^T(\boldsymbol{\omega}_d + \boldsymbol{e}_\omega) \tag{5.41}$$

Additionally, the term $\dot{\boldsymbol{\nu}}_d = [\dot{\boldsymbol{v}}_d, \dot{\boldsymbol{\omega}}_d]^T$ is not available to inner loop controllers since the outer-inner loop scheme keeps both controllers independent. Moreover, an heuristic regarding the tuning of gains is such that the inner loop has a ~ 10x larger bandwidth than the outer loop, that is, its dynamics need to be faster to adapt the rate of change of the speed requirements from the outer loop. In the end it will be proven that certain gains the system is stable. Therefore, new control laws without the derivative term $\dot{\boldsymbol{v}}_d$ and $\dot{\boldsymbol{\omega}}_d$ are defined. The following assumptions are made.

Assumption 2. *The vehicle position $\boldsymbol{p} \in \mathbb{R}^3$, orientation $\boldsymbol{R}_v \in SO(3)$ and relative velocities $\boldsymbol{\nu}_r \in \mathbb{R}^6$ are known.*

Assumption 3. *There exists a continuously differentiable bounded time-varying desired trajectory $\boldsymbol{p}_d(t) \in \mathbb{R}^3$ and respective time derivative $\dot{\boldsymbol{p}}_d(t) \in \mathbb{R}^3$ that hold information relative to the target position $\boldsymbol{p}_t \in \mathbb{R}^3$, orientation $\boldsymbol{R}_t^n \in SO(3)$, linear $\boldsymbol{v}_t \in \mathbb{R}^3$, and angular $\boldsymbol{\omega}_t \in \mathbb{R}^3$ velocities.*

Theorem 9. *Consider the system described by* (3.16) *and* (3.17) *in closed-loop with the following control law*

$$\boldsymbol{\tau} = -\boldsymbol{K}_d\boldsymbol{e}_d + \boldsymbol{D}(\boldsymbol{\nu}_r)\boldsymbol{\nu}_d + \boldsymbol{C}(\boldsymbol{\nu}_r)\boldsymbol{\nu}_r \tag{5.42}$$

$$\boldsymbol{\omega}_d = \boldsymbol{K}_\omega \boldsymbol{S}^{-1}(\boldsymbol{R}_e \boldsymbol{Q}\boldsymbol{Q}^T - \boldsymbol{Q}\boldsymbol{Q}^T \boldsymbol{R}_e^T) \tag{5.43}$$

$$\boldsymbol{v}_d = -\lambda_p \boldsymbol{\sigma}\left(\frac{k_p}{\lambda_p}\boldsymbol{e}_p\right) - \boldsymbol{R}_v^T\left(\hat{\boldsymbol{V}}_{c_v} - \dot{\boldsymbol{p}}_d\right) \tag{5.44}$$

where $\boldsymbol{K}_d$ and $\boldsymbol{K}_{p_\omega}$ are positive definite gain matrices, and k_p and λ_p are positive parameter gains. Let $\dot{\boldsymbol{p}}_d$, $\ddot{\boldsymbol{p}}_d$ and $\boldsymbol{V}_{c_v}$ be bounded signals and consider Assumption 2 and 3. Then, there are sufficiently large gains $\boldsymbol{K}_d$ such that the closed-loop system is finite-gain $\mathcal{L}$ stable, with restrictions on $\boldsymbol{e}_v(0)$ initial conditions.

Proof. The proof will follow a step-by-step approach: 1) we define a bound to the relative velocity of the vehicle to help the follow up ISS proof; 2) the inner loop and positioning subsystem dynamics are proven to be ISS under certain conditions and we extend these results to prove IOS, resorting to the small-gain theorem, proving stability of their respective interconnection; 3) the attitude subsystem is proven to be ISS but do not extended it to prove IOS, as this is quite difficult, leaving this as motivation for future work towards a more complete stability analysis of our controller; 4) we lift the assumption that $\hat{\boldsymbol{V}}_{c_v} = \boldsymbol{V}_{c_v}$ and take into account the observer error dynamics.

Boundedness of relative linear and angular velocity $\boldsymbol{v}_r$, $\boldsymbol{\omega}_r$

Consider the dynamics of $\boldsymbol{\nu}_r = \boldsymbol{\nu}_d + \boldsymbol{e}_d$. From (5.28) with the control law (5.42) we obtain

$$\dot{\boldsymbol{\nu}}_r = -\boldsymbol{M}^{-1}\boldsymbol{A}\boldsymbol{\nu}_r + \boldsymbol{M}^{-1}\boldsymbol{A}\boldsymbol{\nu}_d \tag{5.45}$$

where $\boldsymbol{A}$ is a positive definite matrix, previously defined (5.34b).

Define the Lyapunov function, relative to the relative velocity system (5.45), as follows

$$V_d(t, \boldsymbol{\nu}_r) = \frac{1}{2}\boldsymbol{\nu}_r^T \boldsymbol{M}\boldsymbol{\nu}_r \tag{5.46}$$

whose time derivative is

$$\dot{V}_d = \boldsymbol{\nu}_r^T \boldsymbol{M}\dot{\boldsymbol{\nu}}_r = -\boldsymbol{\nu}_r^T \boldsymbol{A}\boldsymbol{\nu}_r + \boldsymbol{\nu}_r^T \boldsymbol{A}\boldsymbol{\nu}_d \tag{5.47}$$

The following inequalities can be satisfied

$$\frac{1}{2}\lambda_{\mathsf{min}}(\boldsymbol{M})\left\|\boldsymbol{\nu}_r\right\|^2 \leq V_d(\boldsymbol{\nu}_r) \leq \frac{1}{2}\lambda_{\mathsf{max}}(\boldsymbol{M})\left\|\boldsymbol{\nu}_r\right\|^2 \tag{5.48a}$$

$$\begin{aligned}
\dot{V}_d &\leq -\lambda_{\mathsf{min}}(\boldsymbol{A})\left\|\boldsymbol{\nu}_r\right\|^2 + \lambda_{\mathsf{max}}(\boldsymbol{A})\left\|\boldsymbol{\nu}_r\right\|\left\|\boldsymbol{\nu}_d\right\| \\
&\leq -(1-\theta_d)\lambda_{\mathsf{min}}(\boldsymbol{A})\left\|\boldsymbol{\nu}_r\right\|^2 - \theta_d\lambda_{\mathsf{min}}(\boldsymbol{A})\left\|\boldsymbol{\nu}_r\right\|^2 + \lambda_{\mathsf{max}}(\boldsymbol{A})\left\|\boldsymbol{\nu}_r\right\|\left\|\boldsymbol{\nu}_d\right\| \\
&\leq -(1-\theta_d)\lambda_{\mathsf{min}}(\boldsymbol{A})\left\|\boldsymbol{\nu}_r\right\|^2, \quad \forall \left\|\boldsymbol{\nu}_r\right\| \geq \frac{\lambda_{\mathsf{max}}(\boldsymbol{A})}{\lambda_{\mathsf{min}}(\boldsymbol{A})}\frac{1}{\theta_d}\left\|\boldsymbol{\nu}_d\right\|
\end{aligned} \tag{5.48b}$$

where $0 < \theta_d < 1$. Additionally, given the velocity loop control law (5.44)-(5.43), the following bounds are established, for the desired linear and angular velocity

$$\left\|\boldsymbol{v}_d\right\| \leq \lambda_p + \left\|\boldsymbol{c}_v\right\| \tag{5.49a}$$

$$\left\|\boldsymbol{\omega}_d\right\| \leq \lambda_{\mathsf{max}}(\boldsymbol{K}_\omega)(\lambda_1(\boldsymbol{Q}\boldsymbol{Q}^T) + \lambda_2(\boldsymbol{Q}\boldsymbol{Q}^T)) \tag{5.49b}$$

where $\boldsymbol{c}_v = \boldsymbol{R}_v^T(\boldsymbol{V}_{c_v} - \dot{\boldsymbol{p}}_d)$ is a bounded term, and $\lambda_1(\boldsymbol{Q}\boldsymbol{Q}^T)$ and $\lambda_2(\boldsymbol{Q}\boldsymbol{Q}^T)$ are the largest and second largest eigenvalues of the matrix $\boldsymbol{Q}\boldsymbol{Q}^T$.

With this, according to Theorem 4, the solution of (5.45) satisfies

$$\|\boldsymbol{\nu}_r\| \leq \sqrt{\frac{\lambda_{\max}(\boldsymbol{M})}{\lambda_{\min}(\boldsymbol{M})}}\mu \quad \forall t \geq t_0 \tag{5.50}$$

where $\mu = \frac{\lambda_{\max}(\boldsymbol{A})}{\lambda_{\min}(\boldsymbol{A})}\frac{1}{\theta_d}\max\{\lambda_p + \|\boldsymbol{c}_v\|, \lambda_{\max}(\boldsymbol{K}_\omega)(\lambda_1(\boldsymbol{Q}\boldsymbol{Q}^T) + \lambda_2(\boldsymbol{Q}\boldsymbol{Q}^T))\}$.

In addition, since the trajectories are defined in $D = \mathbb{R}^6$ and $\alpha_1(\|\boldsymbol{\nu}_r\|)$ belongs to $\mathcal{K}_\infty$, then (5.50) holds for any initial state $\boldsymbol{\nu}_r(0)$, that is, the solutions are globally ultimately bounded.

Notice that we dropped the use of T referenced in Theorem 4 since we are dealing with autonomous systems, therefore the solution depends only on $t - t_0$. The bounds defined in (5.50) and (5.49a)-(5.49b) provide a choice of gains λ_p, $\boldsymbol{K}_{p\Theta}$ and $\boldsymbol{K}_d$, recalling that $\boldsymbol{A} = \boldsymbol{K}_d + \boldsymbol{D}(\boldsymbol{0})$.

Input-to-Output Stability of Inner-Loop and Positioning Subsystem

At this point we make a key observation of the inner-outer loop interconnection, depicted in Fig. 5.4, providing a visual aid to our closed-loop interconnection problem. The outer loop system H_1 can be further divided into two independent parts, namely the positioning subsystem $H_{1p} : \boldsymbol{e}_v \to \dot{\boldsymbol{v}}_d$ and the attitude subsystem $H_{1\theta} : \boldsymbol{e}_\omega \to \dot{\boldsymbol{\omega}}_d$, since we assume our vehicle to be fully-actuated, independently controlling its attitude and position. The inner loop system $H_2 : \dot{\boldsymbol{\nu}}_d \to \boldsymbol{e}_d$ is then interconnected with system H_1. This interconnection of the inner-outer loop block can be further abstracted to the scheme represented in Fig. 5.5.

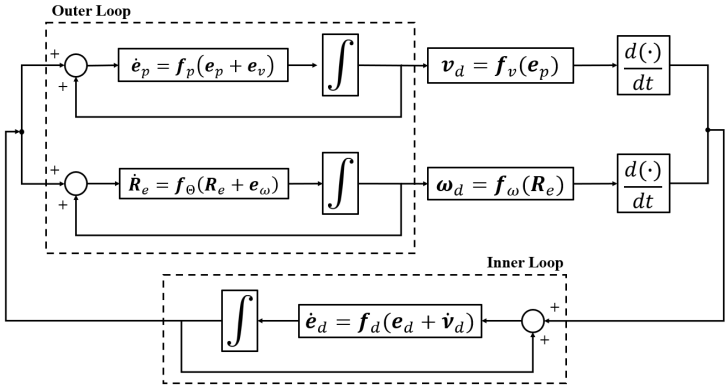

Figure 5.4: Inner-outer interconnection, where the outer loop consists in two independent systems related with position and attitude.

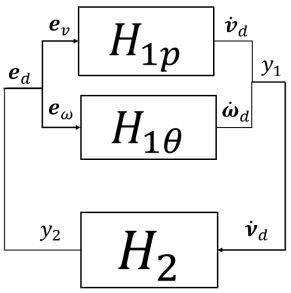

Figure 5.5: A more simple visualization of inner-outer loop feedback interconnection.

Relative to the outer loop positioning subsystem H_{1p}, the position error dynamics (5.40), coupled with the control law (5.44), are as follows

$$\dot{\boldsymbol{e}}_p = -\boldsymbol{S}(\boldsymbol{\omega}_r)\boldsymbol{e}_p - \lambda_p\boldsymbol{\sigma}\left(\frac{k_p}{\lambda_p}\boldsymbol{e}_p\right) + \boldsymbol{e}_v \tag{5.51}$$

Define a candidate Lyapunov function for the system (5.51)

$$V_{1p} = \frac{1}{2}\boldsymbol{e}_p^T\boldsymbol{e}_p \tag{5.52}$$

whose time derivative is given by

$$\begin{aligned}\dot{V}_{1p} &= \boldsymbol{e}_p^T\left(-\boldsymbol{S}(\boldsymbol{\omega}_r)\boldsymbol{e}_p - \lambda_p\boldsymbol{\sigma}\left(\frac{k_p}{\lambda_p}\boldsymbol{e}_p\right)\right) + \boldsymbol{e}_p^T\boldsymbol{e}_v \\ &= -\boldsymbol{e}_p^T\lambda_p\boldsymbol{\sigma}\left(\frac{k_p}{\lambda_p}\boldsymbol{e}_p\right) + \boldsymbol{e}_p^T\boldsymbol{e}_v\end{aligned} \tag{5.53}$$

The following inequalities are verified

$$\frac{1}{2}\left\|\boldsymbol{e}_p\right\|^2 \leq V_{1p}(\boldsymbol{e}_p) \leq \frac{1}{2}\left\|\boldsymbol{e}_p\right\|^2 \tag{5.54}$$

$$\dot{V}_{1p} \leq -\lambda_p\boldsymbol{\sigma}\left(\frac{k_p}{\lambda_p}\boldsymbol{e}_p\right), \quad \forall\left\|\boldsymbol{e}_p\right\| \geq \frac{\lambda_p}{k_p}\boldsymbol{\sigma}^{-1}\left(\frac{\left\|\boldsymbol{e}_v\right\|}{\lambda_p}\right) \tag{5.55}$$

where $\alpha_1(\|\boldsymbol{e}_p\|) = \alpha_2(\|\boldsymbol{e}_p\|) = \frac{1}{2}\|\boldsymbol{e}_p\|^2$ are class $\mathcal{K}_\infty$ functions, $W(\boldsymbol{e}_p) = \lambda_p\boldsymbol{\sigma}\left(\frac{k_p}{\lambda_p}\boldsymbol{e}_p\right)$ is a continuous positive definite function and $\rho(\|\boldsymbol{e}_v\|) = \frac{\lambda_p}{k_p}\boldsymbol{\sigma}^{-1}\left(\frac{\|\boldsymbol{e}_v\|}{\lambda_p}\right)$ is a class $\mathcal{K}$ function, but only when the input $\boldsymbol{e}_v$ satisfies

$$\|\boldsymbol{e}_v\| < \lambda_p$$

which is valid as the input $\boldsymbol{e}_v = \boldsymbol{v}_r - \boldsymbol{v}_d$ is a sum of bounded terms, proven in (5.50) and (5.49a), respectively. Then, according to Theorem 5 the system H_{1p} satisfies the ISS condition with restrictions, according to Definition 4, with respect to input $\boldsymbol{e}_v$

$$\begin{aligned}\|\boldsymbol{e}_p\| &\leq \gamma_{11}(\|\boldsymbol{e}_v\|) + \beta_p(\|\boldsymbol{e}_p(0)\|), \quad \forall\|\boldsymbol{e}_v\| < \lambda_p, t \geq t_0 \\ &\leq \frac{\lambda_p}{k_p}\boldsymbol{\sigma}^{-1}\left(\frac{\|\boldsymbol{e}_v\|}{\lambda_p}\right) + \beta_p(\|\boldsymbol{e}_p(0)\|), \quad \forall\|\boldsymbol{e}_v\| < \lambda_p, t \geq t_0\end{aligned} \tag{5.56}$$

where β_p is a class $\mathcal{KL}$ function.

In addition, keeping in mind the expression for the desired linear velocity time derivative, given by

$$\dot{\boldsymbol{v}}_d = \lambda_p\boldsymbol{\sigma}'\left(\frac{k_p}{\lambda_p}\boldsymbol{e}_p\right)\left(\boldsymbol{S}(\boldsymbol{\omega}_r)\boldsymbol{e}_p + \lambda_p\boldsymbol{\sigma}\left(\frac{k_p}{\lambda_p}\boldsymbol{e}_p\right)\right) - \lambda_p\boldsymbol{\sigma}\left(\frac{k_p}{\lambda_p}\boldsymbol{e}_p\right)\boldsymbol{e}_v - \dot{\boldsymbol{c}}_v \tag{5.57}$$

where a bound can be easily obtained using Definition 6 of a saturation function and the bound for relative velocities in (5.50). With $\|\sigma'(\boldsymbol{s})\| \leq \sqrt{6}$ and $\|\sigma(\boldsymbol{s})\| \leq \sqrt{3}$ for all $\boldsymbol{s} \in \mathbb{R}^3$, $\dot{\boldsymbol{v}}_d$ is bounded by

$$\begin{aligned}\|\dot{\boldsymbol{v}}_d\| &\leq \lambda_p\sqrt{6}\,\|\boldsymbol{\omega}_r\| \cdot \|\boldsymbol{e}_p\| + \lambda_p\sqrt{3} \cdot \|\boldsymbol{e}_v\| + k_p\lambda_p\sqrt{6}\sqrt{3} + \|\dot{\boldsymbol{c}}_v\| \\ &\leq k_p\nu_{max}\sqrt{6} \cdot \|\boldsymbol{e}_p\| + \lambda_p\sqrt{3} \cdot \|\boldsymbol{e}_v\| + k_p\lambda_p\sqrt{6}\sqrt{3} + \|\dot{\boldsymbol{c}}_v\|\end{aligned} \tag{5.58}$$

With this, we can establish a bound for system H_{1p} output, as follows

$$
\begin{aligned}
y_{1p} &= h_{1p}(\boldsymbol{e}_p, \boldsymbol{e}_v) = \dot{\boldsymbol{v}}_d \\
&= \lambda_p \boldsymbol{\sigma}'\left(\frac{k_p}{\lambda_p}\boldsymbol{e}_p\right)\left(\boldsymbol{S}(\boldsymbol{\omega}_r)\boldsymbol{e}_p + \lambda_p \boldsymbol{\sigma}\left(\frac{k_p}{\lambda_p}\boldsymbol{e}_p\right)\right) - \lambda_p \boldsymbol{\sigma}\left(\frac{k_p}{\lambda_p}\boldsymbol{e}_p\right)\boldsymbol{e}_v - \dot{\boldsymbol{c}}_v
\end{aligned} \tag{5.59}
$$

Keeping in mind the expression for y_{1v} a bound can be easily obtained using Definition 6 of a saturation function and the bound for relative velocities in (5.50). With $\|\sigma'(\boldsymbol{s})\| \leq \sqrt{6}$ and $\|\sigma(\boldsymbol{s})\| \leq \sqrt{3}$ for all $\boldsymbol{s} \in \mathbb{R}^3$, the output can be bounded as

$$
\begin{aligned}
\|H_{1p}(\boldsymbol{e}_p, \boldsymbol{e}_v)\| &\leq \lambda_p\sqrt{6}\,\|\boldsymbol{\omega}_r\| \cdot \|\boldsymbol{e}_p\| + \lambda_p\sqrt{3} \cdot \|\boldsymbol{e}_v\| + k_p\lambda_p\sqrt{6}\sqrt{3} + \|\dot{\boldsymbol{c}}_v\| \\
&\leq k_p\nu_{max}\sqrt{6} \cdot \|\boldsymbol{e}_p\| + \lambda_p\sqrt{3} \cdot \|\boldsymbol{e}_v\| + k_p\lambda_p\sqrt{6}\sqrt{3} + \|\dot{\boldsymbol{c}}_v\|
\end{aligned} \tag{5.60}
$$

where we define the following class $\mathcal{K}$ functions $\alpha_6(\|\boldsymbol{e}_p\|) = \lambda_p\sqrt{6}\nu_{max} \cdot \|\boldsymbol{e}_p\|$, $\alpha_7(\|\boldsymbol{e}_v\|) = \lambda_p\sqrt{3} \cdot \|\boldsymbol{e}_v\|$ and a nonnegative constant $\eta = k_p\lambda_p\sqrt{6}\sqrt{3} + \|\dot{\boldsymbol{c}}_v\|$ since the term $\|\dot{\boldsymbol{c}}_v\|$ is bounded by bounded terms

$$
\|\dot{\boldsymbol{c}}_v\| \leq \|\boldsymbol{\omega}_r\| \cdot (\|\boldsymbol{V}_{c_v}\| + \|\dot{\boldsymbol{p}}_d\|) + \|\ddot{\boldsymbol{p}}_d\| \tag{5.61}
$$

As we have proven the system H_{1p} to be ISS under the restriction of $\|\boldsymbol{e}_v\| < \lambda_p$, according to Theorem 6, system H_{1p} is $\mathcal{L}_\infty$ stable with the output satisfying the following condition

$$
\begin{aligned}
\|y_{1p}\|_\infty &\leq \alpha_6(2\gamma_{11}(\|\boldsymbol{e}_v\|_\infty)) + \alpha_7(\|\boldsymbol{e}_v\|_\infty) + \beta \\
&\leq \gamma_{1p}(\|\boldsymbol{e}_v\|) + \beta \\
&\leq 2\lambda_p\left(\nu_{max}\sqrt{6} \cdot \frac{\lambda_p}{k_p}\boldsymbol{\sigma}^{-1}\left(\frac{\|\boldsymbol{e}_v\|_\infty}{\lambda_p}\right) + \frac{\sqrt{3}}{2}\|\boldsymbol{e}_v\|_\infty\right) + \beta
\end{aligned} \tag{5.62}
$$

where β is a nonnegative constant bias term.

Note that, this is not similar to finite-gain $\mathcal{L}$ stability, which is a stronger condition than $\mathcal{L}$ stability. However, it is still possible to prove that system H_{1p} gain is finite, allowing us to prove finite-gain $\mathcal{L}$ stability.

The proof analysis of system H_{1p} being $\mathcal{L}$ stable is presented for its operation in the unsaturated region defined by $|\boldsymbol{e}_{p,i}| < \frac{\lambda_p}{k_p}, \quad i = 1, 2, 3$. However, even if the system enters the saturated region of operation, the system will enter the unsaturated region of operation in finite time, analogous to the work in [13], [51], assuming the restriction $\|\boldsymbol{e}_v\| < \lambda_p\Delta$ still hold. The term $\Delta < 1$ was purposely added to avoid $\|\boldsymbol{e}_v\|$ being infinitely close to λ_p and fulfill the restriction in finite time. For example, in [51], the authors follow an architecture of inner-outer loop, whose outer loop error dynamics have similar structure as ours, except for the non existing skew symmetric term (in our case $\boldsymbol{S}(\boldsymbol{\omega}_r)$), which can be disregarded in a Lyapunov analysis since $\boldsymbol{e}_p^T\boldsymbol{S}(\cdot)\boldsymbol{e}_p = \boldsymbol{0}$. Similar to the author analysis, by looking at the error dynamics (ignoring the skew-symmetric term, as explained before)

$$
\dot{\boldsymbol{e}}_p = -\lambda_p\boldsymbol{\sigma}\left(\frac{k_p}{\lambda_p}\boldsymbol{e}_p\right) + \boldsymbol{e}_v
$$

if $\boldsymbol{\sigma}\left(\frac{k_p}{\lambda_p}\boldsymbol{e}_p\right)$ saturates the error derivative will still be negative under the restriction $\|\boldsymbol{e}_v\| < \lambda_p\Delta$ and $\|\boldsymbol{e}_p\|$ will diminish until it reaches the unsaturated region of operation in finite time. Then, within the restriction $\|\boldsymbol{e}_v\| < \lambda\Delta$, it allows us to prove that system H_{1p} is finite-gain $\mathcal{L}$ stable.

Now, regarding the inner-loop system H_2, the relative velocity error dynamics 5.28, coupled with the control law (5.42), are as follows

$$\dot{\boldsymbol{e}}_d = \boldsymbol{f}_d(\boldsymbol{e}_d + \dot{\boldsymbol{\nu}}_d) = -\boldsymbol{M}^{-1}(\boldsymbol{K}_d + \boldsymbol{D}(\boldsymbol{\nu}_r))\boldsymbol{e}_d - \dot{\boldsymbol{\nu}}_d \tag{5.63}$$

Define a Lyapunov function relative to system (5.63)

$$V_2(\boldsymbol{e}_d) = \frac{1}{2}\boldsymbol{e}_d^T\boldsymbol{M}\boldsymbol{e}_d \tag{5.64}$$

and its respective time derivative,

$$\dot{V}_2 = -\boldsymbol{e}_d^T(\boldsymbol{K}_d + \boldsymbol{D}(\boldsymbol{\nu}_r))\boldsymbol{e}_d - \boldsymbol{e}_d^T\boldsymbol{M}\dot{\boldsymbol{\nu}}_d \tag{5.65}$$

Before proceeding to prove ISS stability condition of system H_2, we first need to prove that the input $\dot{\boldsymbol{\nu}}_d = [\dot{\boldsymbol{v}}_d, \dot{\boldsymbol{\omega}}_d]^T$ is bounded. We already expressed a bound for $\dot{\boldsymbol{v}}_d$ in terms of $\boldsymbol{e}_p$ and $\boldsymbol{e}_v$, shown in (5.58), and following immediately from the conclusion that the position error system H_{1p} is ISS and $\boldsymbol{e}_v = \boldsymbol{v}_r - \boldsymbol{v}_d$ being a sum of bounded terms, we can prove that the input $\dot{\boldsymbol{v}}_d$ is indeed bounded.

Relative to the desired angular velocity time derivative $\dot{\boldsymbol{\omega}}_d$, this is not straightforward to obtain an explicit bound and we will not consider this case, leaving this as future work towards a more complete proof. An initial approach could pass by expanding and discussion the tangent spaces of rotational groups [99] since $\boldsymbol{\omega}_d : SO(3) \mapsto \mathbb{R}^3$. For now, we assume that $\|\dot{\boldsymbol{\omega}}_d\|$ is bounded.

Then, the following inequalities can be verified

$$\frac{1}{2}\lambda_{\mathsf{min}}(\boldsymbol{M})\|\boldsymbol{e}_d\|^2 \leq V_2(\boldsymbol{e}_d) \leq \frac{1}{2}\lambda_{\mathsf{max}}(\boldsymbol{M})\|\boldsymbol{e}_d\|^2 \tag{5.66}$$

$$\dot{V}_2 \leq -(1-\theta_d)\lambda_{\mathsf{min}}(\boldsymbol{A})\|\boldsymbol{e}_d\|^2, \quad \forall\|\boldsymbol{e}_d\| \geq \frac{\lambda_{\mathsf{max}}(\boldsymbol{M})}{\lambda_{\mathsf{min}}(\boldsymbol{A})}\frac{1}{\theta_d}\cdot\|\dot{\boldsymbol{\nu}}_d\| \tag{5.67}$$

It is possible to define the following class $\mathcal{K}_\infty$ functions $\alpha_1(\|\boldsymbol{e}_d\|) = \frac{1}{2}\lambda_{\mathsf{min}}(\boldsymbol{M})\|\boldsymbol{e}_d\|^2$, $\alpha_2(\|\boldsymbol{e}_d\|) = \frac{1}{2}\lambda_{\mathsf{max}}(\boldsymbol{M})\|\boldsymbol{e}_d\|^2$, a class $\mathcal{K}$ function $\rho(\|\dot{\boldsymbol{\nu}}_d\|) = \frac{\lambda_{\mathsf{max}}(M)}{\theta_d\lambda_{\mathsf{min}}(\boldsymbol{A})}\cdot\|\dot{\boldsymbol{\nu}}_d\|$ and a positive definite function $W_3(\boldsymbol{e}_d) = (1-\theta_d)\lambda_{\mathsf{min}}(\boldsymbol{A})\|\boldsymbol{e}_d\|^2$. Then, according to Theorem 5 the system H_2 is ISS with respect to a bounded input $\dot{\boldsymbol{\nu}}_d$ satisfying the following condition

$$\begin{aligned}\|\boldsymbol{e}_d\| &\leq \gamma_2(\|\dot{\boldsymbol{\nu}}_d\|) + \beta_2(\|\boldsymbol{e}_d(0)\|), \quad \forall t \geq t_0 \\ &\leq \frac{\lambda_{\mathsf{max}}(\boldsymbol{M})\sqrt{\lambda_{\mathsf{max}}(\boldsymbol{M})}}{\lambda_{\mathsf{min}}(\boldsymbol{A})\sqrt{\lambda_{\mathsf{min}}(\boldsymbol{M})}}\cdot\|\dot{\boldsymbol{\nu}}_d\| + \beta_2(\|\boldsymbol{e}_d(0)\|, t), \quad \forall t \geq t_0\end{aligned} \tag{5.68}$$

where β_2 is a class $\mathcal{KL}$ function.

Since the output of this system is the state itself $\boldsymbol{e}_d$, it satisfies the IOS condition, that is, the system

(5.63) is finite-gain $\mathcal{L}$ stable with the output satisfying the following condition

$$\begin{aligned}\|y_2\|_\infty &\leq \gamma_2 \cdot \|\dot{\boldsymbol{\nu}}_d\|_\infty + \beta \\ &\leq \frac{\lambda_{\max}(\boldsymbol{M})\sqrt{\lambda_{\max}(\boldsymbol{M})}}{\lambda_{\min}(\boldsymbol{A})\sqrt{\lambda_{\min}(\boldsymbol{M})}} \cdot \|\dot{\boldsymbol{\nu}}_d\|_\infty + \beta\end{aligned} \tag{5.69}$$

where β is a nonnegative constant bias term. And it makes sense that it is proven to be finite-gain $\mathcal{L}$ immediately stable in contrast with the added conditions of system H_{1p} towards proving finite-gain $\mathcal{L}$ stability. This occurs because we have proven, previously in Section 5.2, that the inner loop system equilibrium point is GES, in contrast to the outer loop positioning subsystem H_{1p} equilibrium point which is proven to be GAS.

The, using the Small-Gain Theorem 7, we can show that the interconnection between system H_{1p} and H_2 is stable if $\gamma_{1p} \cdot \gamma_2 < 1$, that is, with the previously obtained results,

$$\lambda_p \left(2\frac{\lambda_p}{k_p}\sqrt{6}\left(\nu_{max} + \|\boldsymbol{V}_{c_\omega}\|\right)\boldsymbol{\sigma}^{-1}\left(\frac{\|\boldsymbol{e}_v\|}{\lambda_p}\right) + \sqrt{3}\right) \cdot \frac{\lambda_{\max}(\boldsymbol{M})\sqrt{\lambda_{\max}(\boldsymbol{M})}}{\lambda_{\min}(\boldsymbol{A})\sqrt{\lambda_{\min}(\boldsymbol{M})}} < 1 \tag{5.70}$$

For each parameter λ_p and k_p, there exists bounds on the desired position $\boldsymbol{p}_d$ and its respective derivatives, bounds on ocean currents velocities $\boldsymbol{V}_c$ and a choice of gains $\boldsymbol{K}_d$ sufficiently large, such that the positioning error closed-loop system is stable. Since all these terms are known according to the mission design and, most importantly, related to the controller gains, this final result provides a framework for tuning the inner-outer loop controller stability, by choice k_p and λ_p. This can be allied to the common practice and heuristic of inner-outer loop structures, where the inner loop bandwidth is designed to be approximately 10 times larger than the outer loop bandwidth.

Input-to-State Stability of Attitude system

Now, relative to the outer loop attitude subsystem $H_{1\Theta}$, its error dynamics (5.41), coupled with the control law (5.43), are as follows

$$\dot{\boldsymbol{e}}_\Theta = f_{1\Theta}(\boldsymbol{e}_\Theta) = -\boldsymbol{z}^T\boldsymbol{K}_\omega\boldsymbol{z} - \boldsymbol{z}^T\boldsymbol{e}_\omega \tag{5.71}$$

where $\boldsymbol{z}(\boldsymbol{R}_e) = \boldsymbol{S}^{-1}(\boldsymbol{R}_e\boldsymbol{Q}\boldsymbol{Q}^T - \boldsymbol{Q}\boldsymbol{Q}^T\boldsymbol{R}_e^T)$.

Proving ISS is not straightforward as the proof done for system H_{1p} since our attitude error dynamics live in $SO(3)$, the space of rotation matrices, and most tools referenced in Chapter 2 are relative to Euclidean space. Instead, we resort to the definition of *Almost Globally Input-to-state Stable* (aISS), which appears as Definition 1 of [46], that is, ISS except on a set of measure zero, much like the definition of AGAS.

The proof is supported on recent developments of generalized ISS for different topological spaces and besides those of euclidean geometry, and with multiple equilibrium points [46], [47]. The proof of the attitude error system satisfying aISS follows from certain assumptions and the boundedness properties of the state $\boldsymbol{R}_e$. The assumptions are defined by the authors in [46], referenced in their work from A0 to A2. We will not expand them here, but we can easily prove our system satisfies these same assumptions. First, our system evolves on $SO(3)$ therefore assumption A0 is satisfied. Second, as shown in Section 5.1.2, we have proven that (5.24) is

semi-definite negative therefore assumption A1 is also satisfied. Finally, also mentioned in Section 5.1.2, all four equilibrium points of the unperturbed system (5.19) are non-degenerate and consequently isolated, when satisfying Assumption 1, and the three equilibrium points that are not asymptotically stable exhibit at least one positive eigenvalue, as pointed out by the authors in [42], allowing us to conclude that assumption A2 is also satisfied. Allied to the fact that attitude error $\boldsymbol{R}_e$ is naturally bounded since it lives in the compact space of $SO(3)$, we can then conclude from the authors Proposition 2 [46] that our perturbed attitude error subsystem (5.71) satisfies aISS with respect to the set of asymptotically stable equilibria, in our case $\boldsymbol{R}_e = \boldsymbol{I}_3$.

Closed-Loop Stability with Observer System

Finally, we proceed to prove stability of our system out of the assumption that we have access to true states of the ocean current velocity V_c. We now consider that this variable is provided by an observer system, where we only have access to its estimate $\hat{\boldsymbol{V}}_c$. This translates to the existence of errors on the true values of these variables, which need to be taken into account on the stability analysis of the system, and prove that it is ISS relative to the input disturbance signal $\tilde{\boldsymbol{V}}_c = \boldsymbol{V}_c - \hat{\boldsymbol{V}}_c$, as depicted in Fig. 5.6.

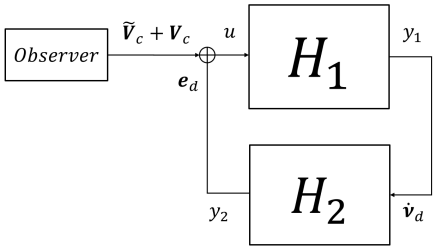

Figure 5.6: The observer system in cascade connection with the outer loop system.

It is possible to conclude that system H_1 is still stable with GAS equilibrium points. This follows immediately from the fact that the connection with the observer can be viewed as a cascade system between an ISS system and an observer with GAS equilibrium points. Then, according to Lemma 1, the equilibrium point of system H_1 is still GAS and the system interconnection H_1 and H_2 is still finite-gain $\mathcal{L}$ stable.

□

5.4.2 Path-following Controller

Until now, the main proof as been established for the inner-outer loop system under Assumption 3. As our final proof, we proceed to lift this assumption and assume that the desired position $\boldsymbol{p}_(\gamma)$ is instead parameterized by some continuous variable γ, as done in Section 5.1.1, meaning that $\dot{\boldsymbol{p}}_d(\gamma) = \boldsymbol{v}_t + \boldsymbol{R}_t \left(\frac{\partial \boldsymbol{p}_d^t(\gamma)}{\partial \gamma} \dot{\gamma} + \boldsymbol{S}(\boldsymbol{w}_t) \boldsymbol{p}_d^t(\gamma) \right)$. This translates to the positioning error dynamics now given by

$$\dot{\boldsymbol{e}}_p = -\boldsymbol{S}(\boldsymbol{\omega}_r)\boldsymbol{e}_p + (\boldsymbol{v}_d + \boldsymbol{e}_v) + \boldsymbol{R}_v^T \left(\boldsymbol{V}_{c_v} - \boldsymbol{v}_t + \boldsymbol{R}_t \left(\frac{\partial \boldsymbol{p}_d^t(\gamma)}{\partial \gamma} \dot{\gamma} + \boldsymbol{S}(\boldsymbol{w}_t) \boldsymbol{p}_d^t(\gamma) \right) \right) \tag{5.72}$$

With this, Theorem 9 is reformulated to take into account the parameterization variable dynamics given by $\dot{\gamma}$.

Theorem 10. *Consider the system described by* (3.16) *and* (3.17) *in closed-loop with the following control law*

$$\boldsymbol{\tau} = -\boldsymbol{K}_d \boldsymbol{e}_d + \boldsymbol{D}(\boldsymbol{\nu}_r)\boldsymbol{\nu}_d + \boldsymbol{C}(\boldsymbol{\nu}_r)\boldsymbol{\nu}_r \tag{5.73}$$

$$\boldsymbol{\omega}_d = \boldsymbol{K}_\omega \boldsymbol{S}^{-1}(\boldsymbol{R}_e \boldsymbol{Q}\boldsymbol{Q}^T - \boldsymbol{Q}\boldsymbol{Q}^T \boldsymbol{R}_e^T) \tag{5.74}$$

$$\boldsymbol{v}_d = -\lambda_p \boldsymbol{\sigma}\left(\frac{k_p}{\lambda_p}\boldsymbol{e}_p\right) - \boldsymbol{R}_v^T\left(\hat{\boldsymbol{V}}_{c_v} - \hat{\boldsymbol{v}}_t - \boldsymbol{R}_t\left(\frac{\partial \boldsymbol{p}_d^t(\gamma)}{\partial \gamma}\dot{\gamma_d} + \boldsymbol{S}(\boldsymbol{w}_t)\boldsymbol{p}_d^t(\gamma)\right)\right) \tag{5.75}$$

$$\dot{\gamma} = \dot{\gamma_d} - k_\gamma\left(\rho_{\tilde{\gamma}}\sigma(k_{\tilde{\gamma}}\tilde{\gamma}) - \boldsymbol{e}_p^T \boldsymbol{R}_v^T \boldsymbol{R}_t^n \frac{\partial p_d^t(\gamma)}{\partial \gamma}\right) \tag{5.76}$$

where $\boldsymbol{K}_d$ *and* $\boldsymbol{K}_{p_\omega}$ *are positive definite gain matrices, and* k_p, $\rho_{\tilde{\gamma}}$, $k_{\tilde{\gamma}}$ *and* λ_p *are positive parameter gains. Let* $\frac{\partial \boldsymbol{p}_d^t(\gamma)}{\partial \gamma}$, $\frac{\partial^2 \boldsymbol{p}_d^t(\gamma)}{\partial \gamma^2}$ *and* $\boldsymbol{V}_{c_v}$ *be bounded signals. Then, there are sufficiently large gains* $\boldsymbol{K}_d$ *such that the closed-loop system is finite-gain* $\mathcal{L}$ *stable, with restriction on* $\boldsymbol{e}_v(0)$ *and* $\tilde{\boldsymbol{v}}_t(0)$ *initial conditions.*

Proof. This proof is done similarly to the proof done previously for 9, with the added term of the parameterization variable dynamics $\dot{\gamma}$ in the outer-loop positioning subsystem. Then, as done previously in Section 5.1, we can see that our Lyapunov function (5.52) has an added term $\frac{\rho_{\tilde{\gamma}}}{k_{\tilde{\gamma}}}\int_0^{\tilde{\gamma}} \sigma(k_{\tilde{\gamma}} s)\, ds$. With the control law (5.76) this translates into a negative quadratic term $k_\gamma\left(\rho_{\tilde{\gamma}}\sigma(k_{\tilde{\gamma}}\tilde{\gamma}) - \boldsymbol{e}^T \boldsymbol{R}_v^T \boldsymbol{R}_t^n \frac{\partial p_d^t(\gamma)}{\partial \gamma}\right)^2$ in the Lyapunov function time derivative which does not change the convergence properties of system H_{1p}, allowing us to maintain the proof of finite-gain $\mathcal{L}$ stability of the system interconnection H_1 and H_2, with the suitable restriction of $\boldsymbol{e}_v(0)$ initial conditions.

Although we do not derive an explicit stability condition for the target filter system derived in Section 4.3, we can view the estimate $\hat{\boldsymbol{v}}_t$ as disturbance input signals to system H_1. And similar to the proof done for Theorem 9 relative to the ISS condition established for the positioning subsystem H_{1p}, it is possible to follow the same approach and establish that it is locally-ISS under the restriction of $\tilde{\boldsymbol{v}}_t = \boldsymbol{v}_t - \hat{\boldsymbol{v}}_t \leq \lambda_p$. Therefore, the same conclusion can be established, that is, the system interconnection H_1 and H_2, with suitable restriction of $\boldsymbol{v}_t(0)$ initial conditions, is finite-gain $\mathcal{L}$ stable.

□

5.5 Summary

In this Chapter we presented a position and attitude solution to the problem of *path-following* and stabilization in $SO(3)$. The derived controller follows an inner-outer loop approach, considering both the vehicle kinematics and dynamics. The outer and inner loop controller guarantees GAS and AGAS of the desired equilibrium points for the positioning and attitude error dynamics, and GES for the relative velocity equilibrium points. The dependence of gain choices and initial conditions is specified for the stability of the inner-outer loop interconnection.

Chapter 6

Results

This last chapter will bridge the work discussed and presented in previous chapters, from the underwater robot mathematical models discussed in Chapter 3 and the cooperation architecture proposed in Chapter 4 to the control architecture derived in Chapter 5 that can satisfy the generalized cooperation schemes in compliance with the proposed cooperation architecture.

We will start by discussing the vehicle specifications in which this work will be developed on, with fully actuation capabilities and a suite of on-board sensors that are essential to perform the cooperation missions with a diver, from guidance, navigation and control. Afterwards, we present some brief simulations regarding the inner and outer loop controllers to corroborate the stability characteristics of the system and illustrate the properties discussed in the preceding sections. Finally, we also simulate a cooperative scenario under the proposed cooperation architecture, to demonstrate the derived control system capabilities. A guidance system is briefly presented providing the necessary references signals for the control system, according to the mission requirements.

6.1 FUSION

The developed work in this thesis will focus around a six DOF UUV named FUSION. This vehicle was developed by the company *Strategic Robotic System* (SRS) and is capable of operating as a ROV or as an AUV.

The FUSION robot is fully actuated, carrying seven thrusters, four for horizontal motion that are symmetric about the xz plane and three for vertical motion. Furthermore, one of the vertical thrusters, located in the rear of the vehicle, allows for pitch control. To identify each thruster, we numbered them accordingly, as seen in Fig. 6.1.

6.1.1 Hardware and Sensors

The FUSION robot possesses various instruments for navigation and measurement. Depending on the mission at hand, different sensors might provide useful data for different applications. Some of them can be useful to us in terms of applicability of cooperation strategies, as discussed and explained in Chapter 4.

In terms of *navigation*, FUSION carries a Doppler Velocity Log (DVL) that provides velocity measurements

Figure 6.1: Perspective of the FUSION vehicle and identification of its seven thrusters. (source: https://www.srsfusion.com/srs-fusion)

relative to seabed and/or relative to the fluid (water), inertial sensors such as an Attitude and Heading Reference System (AHRS) for vehicle attitude measurements, a Global Navigation Satellite System (GNSS) device for global positioning, and pressure and temperature sensors.

FUSION can also be equipped with a Multibeam SONAR, a Side-Scan Sonar (SSS), a magnetometer, an HD camera and an Ultra-Short Baseline (USBL) (USBL) system.

6.1.2 System Inertia and Coriolis-Centripetal Parameters

FUSION geometry and characteristics allows us simplify the system Inertia modelling. Assuming the craft body has homogeneous mass distribution and symmetry about the xy, xz and yz planes (port/starboard, fore/aft and bottom/top symmetries), results in a diagonal system inertia matrix $\boldsymbol{M} = \text{diag}\{m_{\dot{u}}, m_{\dot{v}}, m_{\dot{w}}, m_{\dot{p}}, m_{\dot{q}}, m_{\dot{r}}\}$ where

$$m_{\dot{u}} = m - X_{\dot{u}}, \quad m_{\dot{v}} = m - Y_{\dot{v}}, \quad m_{\dot{w}} = m - Z_{\dot{w}}$$
$$m_{\dot{p}} = I_x - K_{\dot{p}}, \quad m_{\dot{q}} = I_y - M_{\dot{q}}, \quad m_{\dot{r}} = I_z - N_{\dot{r}}$$

where m is the mass of the vehicle, $I_{x,y,z}$, are the moments of inertia of the vehicle about the x, y and z *body-fixed* frame axes, respectively, and $X_{\dot{u}}$, $Y_{\dot{v}}$, $Z_{\dot{w}}$, $K_{\dot{p}}$, $M_{\dot{q}}$ and $N_{\dot{r}}$ are *hydrodynamic derivative* coefficients of the vehicle in the its six DOF in the SNAME notation (1950).

Having defined the system inertia matrix, one can easily model the respective Coriolis-centripetal forces from Theorem 8.

From the FUSION datasheet, it is possible to obtain some parameters, such as mass, length, width and height. To define the moment of inertia, we consider the FUSION geometry to be that of an ellipsoid, allowing us to compute the moments of inertia about the xyz axis. Moreover, because not all hydrodynamic parameters are available, additional FUSION hydrodynamic parameters were taken from another similar AUV called REMUS [100], which for now emulates the unknown vehicle parameters. The most recent updated values of the FUSION vehicle parameters can be seen in Table 6.1.

6.1.3 Hydrodynamic Damping and Hydrostatic Parameters

A moving vehicle underwater will have highly non-linear coupled damping terms in its dynamic equations of motion. However, one can assume that FUSION performs non-coupled motion, that is, the hydrodynamic damping cross-terms can be neglected. This way, one can simply model the hydrodynamic damping forces as a

m = 27.5 Kg		
I_x = 0.417 Kg·m^2	I_y = 0.751 Kg·m^2	I_z = 0.960 Kg·m^2
X_u = -21.41 Kg/s	Y_v = -21.41Kg/s	Z_w = -21.41 Kg/s
X_{uu} = -83.72 Kg/m	Y_{vv} = -83.72 Kg/m	Z_{ww} = -83.72 Kg/m
$X_{\dot{u}}$ = -123.05 Kg	$Y_{\dot{v}}$ = -123.05 Kg	$Z_{\dot{w}}$ = -123.05 Kg
K_p = -0.543 Kg·m^2/s	M_q = -6.15 Kg·m^2/s	N_r = -2.247Kg·m^2/s
K_{pp} = -0.013 Kg·m^2/rad^2	M_{qq} = -9.4 Kg·m^2/rad^2	N_{rr} = -2.448 Kg·m^2/rad^2
$K_{\dot{p}}$ = -0.0141 Kg·$\gg^2$/rad	$M_{\dot{q}}$ = -4.88 Kg·$\gg^2$/rad	$N_{\dot{r}}$ = -0.324 Kg·$\gg^2$/rad

Table 6.1: Model parameters for the FUSION vehicle.

matrix with a diagonal structure $\boldsymbol{D}(\boldsymbol{\nu}) = -\mathrm{diag}\{D_u(u), D_v(v), D_w(w), D_p(p), D_q(q), D_r(r)\}$ where

$$D_u(u) = X_u + X_{uu}|u|, \quad D_v(v) = Y_v + Y_{vv}|v|, \quad D_w(w) = Z_w + Z_{ww}|w|$$

$$D_p(p) = K_p + K_{pp}|p|, \quad D_q(q) = M_q + M_{qq}|q|, \quad D_r(r) = N_r + N_{rr}|r|$$

with $X_u, Y_v, Z_w, K_p, M_q, N_r$ and $X_{uu}, Y_{vv}, Z_{ww}, K_{pp}, M_{qq}, N_{rr}$ being the linear and quadratic hydrodynamic damping coefficients of the vehicle, respectively.

The hydrostatic forces, as mentioned before, concern the forces of gravity and buoyancy $\boldsymbol{g}$ of the vehicle, and also the restoration forces of a given ballast system incorporated in the vehicle $\boldsymbol{g}_0$.

However, because FUSION is neutrally buoyant (weight and buoyancy forces are equal) and does not possess a ballast system to rise or descend in depth, instead using the vertical thrusters, we can define the respective hydrostatic vector of forces as $\boldsymbol{g}(\boldsymbol{\eta}) = \boldsymbol{g}_0 = \boldsymbol{0}$.

6.1.4 Control Allocation

The subject of control allocation concerns the transformation of the control law output $\boldsymbol{\tau} \in \mathbb{R}^n$, where $n = 6$ in 6 DOF, into a control input signal $\boldsymbol{u} \in \mathbb{R}^r$, where $r = 7$ is the number of thrusters of the working vehicle, as shown in Fig. 6.2. Because $r > n$, we consider the problem of control allocation to be *overactuated*, that is, there are many possible ways of effectively selecting the optimal thrusters input's to produce the desired forces and moments.

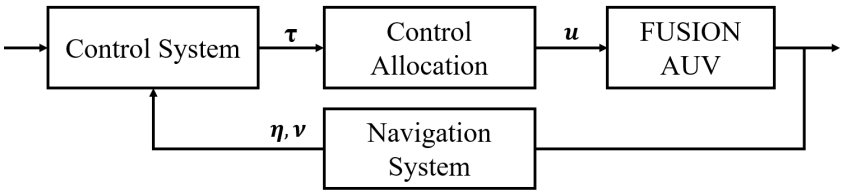

Figure 6.2: Block diagram showing the control allocation system coupled with the AUV control and navigation system.

The configuration of the thrusters are embedded in the configuration matrix $\boldsymbol{T}$, according to their position and angle of orientation. With this, we can define $\boldsymbol{T}$ as follows

$$\boldsymbol{T} = \begin{bmatrix} \boldsymbol{t}_1 & \cdots & \boldsymbol{t}_7 \\ \boldsymbol{r_1} \times \boldsymbol{t}_1 & \cdots & \boldsymbol{r_7} \times \boldsymbol{t}_7 \end{bmatrix} \tag{6.1}$$

where $\boldsymbol{t}_i, i = 1, 2, ..., 7$ are the thrusters force vector given by

$$\boldsymbol{t}_1 = \begin{bmatrix} \cos\alpha \\ -\sin\alpha \\ 0 \end{bmatrix}, \boldsymbol{t}_2 = \begin{bmatrix} 0 \\ \sin\beta \\ \cos\beta \end{bmatrix}, \boldsymbol{t}_3 = \begin{bmatrix} \cos\alpha \\ \sin\alpha \\ 0 \end{bmatrix}, \boldsymbol{t}_4 = \begin{bmatrix} \cos\alpha \\ \sin\alpha \\ 0 \end{bmatrix}, \boldsymbol{t}_5 = \begin{bmatrix} 0 \\ -\sin\beta \\ \cos\beta \end{bmatrix}, \boldsymbol{t}_6 = \begin{bmatrix} \cos\alpha \\ -\sin\alpha \\ 0 \end{bmatrix}, \boldsymbol{t}_7 = \begin{bmatrix} 0 \\ 0 \\ 1 \end{bmatrix}$$

with $\alpha = \frac{35}{180}\pi$ and $\beta = \frac{10}{180}\pi$ being the horizontal and vertical thrusters angles, respectively, and $\boldsymbol{r}_i, i = 1, 2, ..., 7$ the thruster positions expressed in the *body-fixed* frame.

Having defined T we can obtain a control signal $\boldsymbol{u} = [u_1, u_2, u_3, u_4, u_5, u_6, u_7]^T$ for each thruster that best fits a desired vector of forces and moments $\boldsymbol{\tau}$ from the controller.

There exist many approaches towards optimally solving the control allocation problem. A simple approach to the problem of control allocation is using an *unconstrained control allocation* approach. The term *unconstrained* is used because it is assumed that there are no constraints on the input signals vector, In this formulation, having more control inputs than DOFs, as is our case, it is possible to find an optimal solution of $\boldsymbol{u}$ for the desired $\boldsymbol{\tau}$, by considering a unconstrained least-squares optimization problem proposed [32]

$$\begin{aligned} \min_{\boldsymbol{u}} \quad & \boldsymbol{u}^T\boldsymbol{u} \\ \text{subject to} \quad & \boldsymbol{\tau} - \boldsymbol{T}\boldsymbol{u} = \boldsymbol{0} \end{aligned} \tag{6.2}$$

The respective solution is valid only if the thrusters angles are static (not time-varying), and is given by

$$\boldsymbol{u} = \boldsymbol{T}^T(\boldsymbol{T}\boldsymbol{T}^T)^{-1}\boldsymbol{\tau} \tag{6.3}$$

This solution is easy to implement and compute as it is provided in explicit form. However, such optimization problem does not take into consideration certain constraints, eg. saturation, wear and tear, etc, that plague actuators and differences that might exist between the available actuators, e.g., vehicles might possess fins as actuator devices which are far less "expensive energetically" than rotor thrusters. For that, other optimization problems have been proposed in the literature of control allocation [101] such as direct allocation method that preserves the direction of $\boldsymbol{\tau}$ and at the same time minimize the power consumption by taking advantage of the additional control forces, and a mixed optimization method that minimizes the error between the desired and the achieved moments as well as the control effort. Within the scope of this thesis, it is acceptable to only consider the *unconstrained* approach to the control allocation problem and, in future work, study and solve the problem in a *constrained* approach to optimize directionality and consider motor non-linearity's.

6.2 Simulation Results

Different simulation results were carried out to illustrate the performance of the control schemes proposed for vehicle position and attitude in the presence of model parameter uncertainty and/or constant ocean current disturbances.

6.2.1 Inner Loop Control

Two simulation were performed where the speed reference was changed over time to validate the control law of the inner loop controller, according to the results obtained in Section 5.2. The AUV initial velocity is zero, and assume we have access to model parameters true values, as well as no ocean currents affecting the system. The second simulation was similar to the first one, but instead with a 50% uncertainty in the model parameters of the vehicle. The results of these simulations are presented in Fig. 6.3.

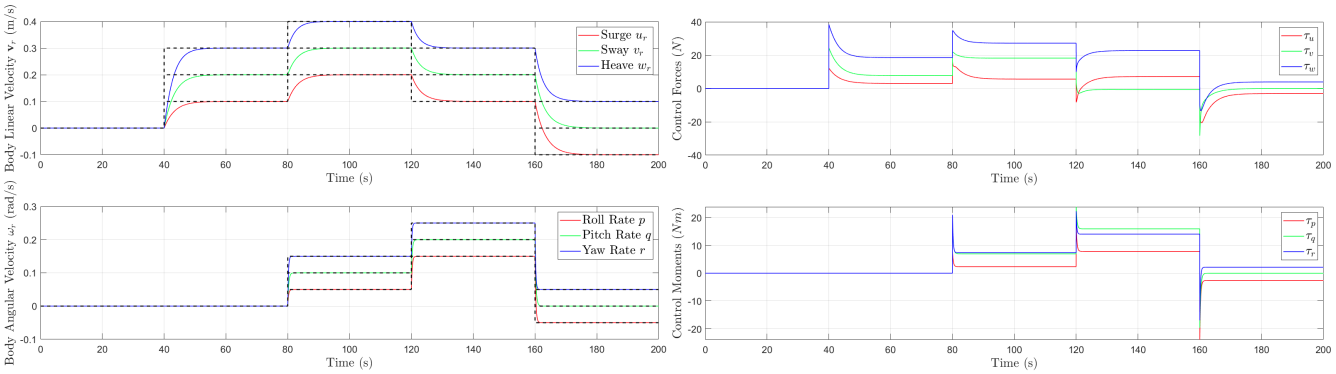

(a) No model parameter uncertainty.

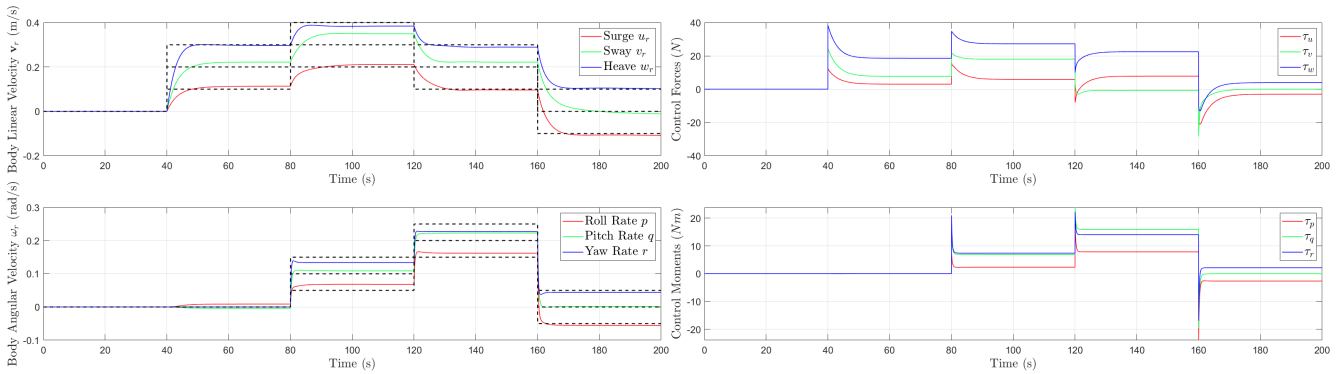

(b) With model parameters uncertainty of 50%.

Figure 6.3: Two simulations of the inner-loop controller stability properties, as well as actuation forces and moments.

In the first simulation, as shown in Fig. 6.3a, the desired relative velocities are met, with the origin of the relative velocity error dynamics being exponentially stable as expected (it is possible to deduce that the error decays exponentially by taking the "inverse" of the relative velocity curves, taking form of an exponential curve). Regarding the last simulation, shown in Fig. 6.3b, it is possible to observer that the velocity error dynamics no longer converge to the desired value but instead are bounded in a neighborhood of the desired value, due to the added model parameter uncertainty as expected. If it is required to meet precisely these reference values, future work could pass through a common practice of adding an integral term of the velocity error to the control law, compensating this offset. Since we will deal with the vehicle converging to certain points via the outer loop controller, and not meet certain velocities overall, this is not a major issue The control actuation is also kept bounded, in both scenarios, even in the presence of disturbances on the model parameters, maintaining a constant input towards a constant velocity reference.

6.2.2 Inner-Outer Loop with Ocean Currents Observer

Now, regarding the outer and inner loop and ocean currents observer convergence properties and stability, we demonstrate the results obtained in Chapter 5 by having the vehicle converge to an arbitrary desired point $\boldsymbol{p}_d(\gamma_d)$, parameterized by $\gamma_d = 1.5$, and a fixed arbitrary attitude reference $\boldsymbol{R}_d(\phi_d, \theta_d, \psi_d)$, parameterized by arbitrary desired Euler angles $[\phi_d, \theta_d, \psi_d] = [0, 0, 1]^T$, along a circular path, as shown in Fig. 6.4. The AUV initial position and attitude is $\boldsymbol{\eta} = [20, 15, 25, 0, 0, 0]^T$ with an initial velocity $\boldsymbol{\nu} = [0, 0, 0, 0, 0, 0]^T$, and the target position is $\boldsymbol{p}_t = [10, 5, 15]^T$. Additionally, there exists an irrotational ocean current (which is unknown from the point of view of the controller) that has an inertial velocity of $\boldsymbol{V}_c = [0.3, 0.2, 0.1, 0, 0, 0]^T$. For demonstration purposes of the stability properties of our proposed controller, we assume to have access to the vehicle position and attitude $\boldsymbol{\eta}$, velocity $\boldsymbol{\nu}$, target position $\boldsymbol{p}_t$ and no vehicle model parameter uncertainty. We implement our inner-outer controller such as to satisfy the condition requirements derived in Theorem 10.

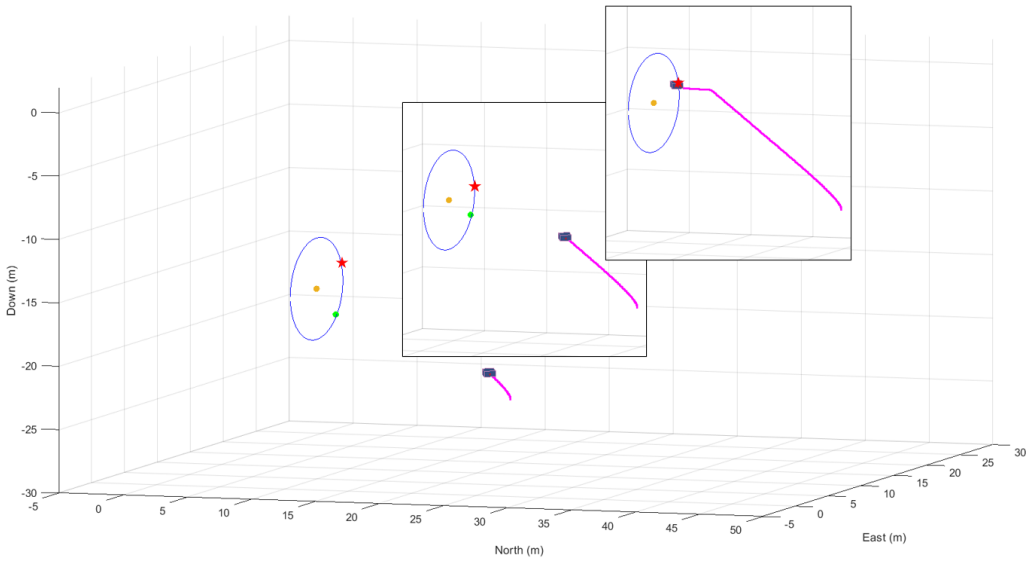

Figure 6.4: The simulation scenario, where a target in yellow is stationary and the AUV, with its trajectory in pink, is required to converge to $\boldsymbol{p}_d$, represented here in green. The red star represents the desired point of convergence $\boldsymbol{p}_d(\gamma_d)$.

The results obtained are shown in Fig. 6.5 and corroborate the results shown in Chapter 5 relative to the inner-outer loop interconnection, coupled with an ocean current observer, namely:

- The positioning error $\boldsymbol{e}_p$ and the path parameterization error $\tilde{\gamma} = \gamma - \gamma_d$ converge asymptotically to the origin.
- The attitude error $\boldsymbol{R}_e = \boldsymbol{R}^T \boldsymbol{R}_d$ converges to the equilibrium point $\boldsymbol{I}_3$ asymptotically. For the attitude error, we consider the angle of rotation θ_e from the angle-axis representation of $\boldsymbol{R}_e$ given by $\text{rot}(\theta_e, \boldsymbol{n})$, translating to the desired equilibrium point being the origin.
- The ocean current observer error dynamics norm $\|\boldsymbol{e}_2\| = \|\boldsymbol{\nu}_c - \hat{\boldsymbol{\nu}}_c\|$ converges asymptotically to the origin.

Another simulation was also carried out in the same scenario to illustrate the controller performance if no ocean currents observer was designed, i.e control law assumes no existing ocean currents disturbing the system.

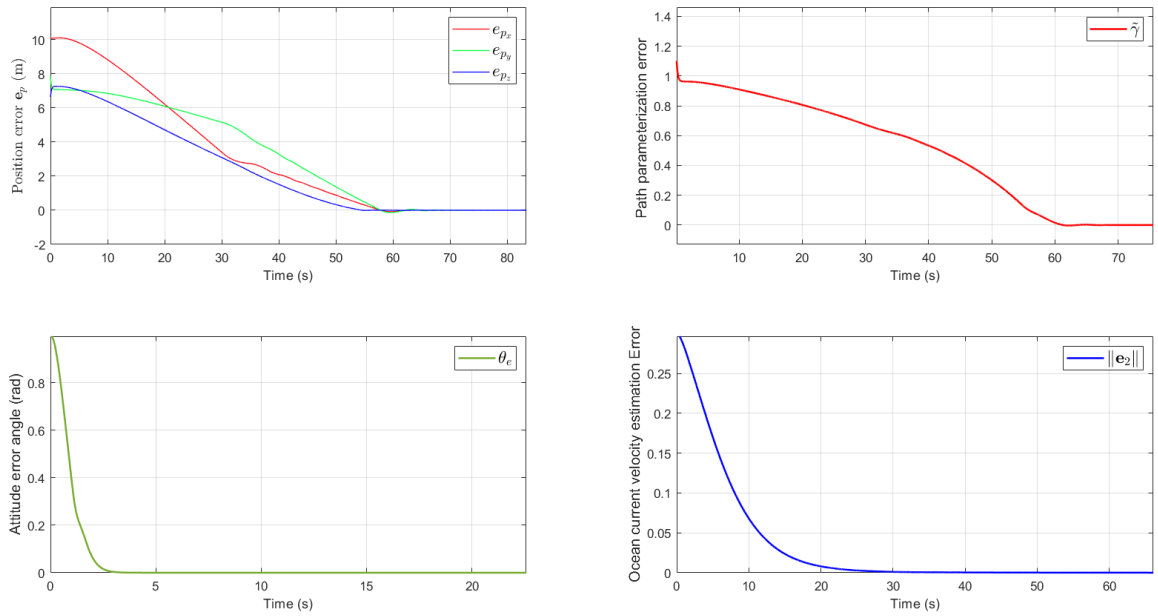

Figure 6.5: Evolution in time of position error $\boldsymbol{e}_p = \boldsymbol{p} - \boldsymbol{p}_d = [e_{p_x}, e_{p_y}, e_{p_z}]^T$, path parameterization variable error $\tilde{\gamma}$, attitude error θ_e and the norm of ocean current velocity estimate error $\|\boldsymbol{e}_2\|$.

The results for the position error evolution are presented in Fig. 6.6, and it clearly shows the degrade in the convergence rate of the vehicle position to the desired location. Additionally, it is possible to observe that $\tilde{\gamma}$ does not decrease that much from 70 to 140 seconds into the simulation. Recalling our positioning control law (5.76) related to $\dot{\gamma}$, we can see that it is governed by two factors which concern the convergence to γ_d and the converge of γ to the point of projection of the vehicle's position onto the path, both conditioned the position error $\boldsymbol{e}_p$, as explained in Section 5.1.1.

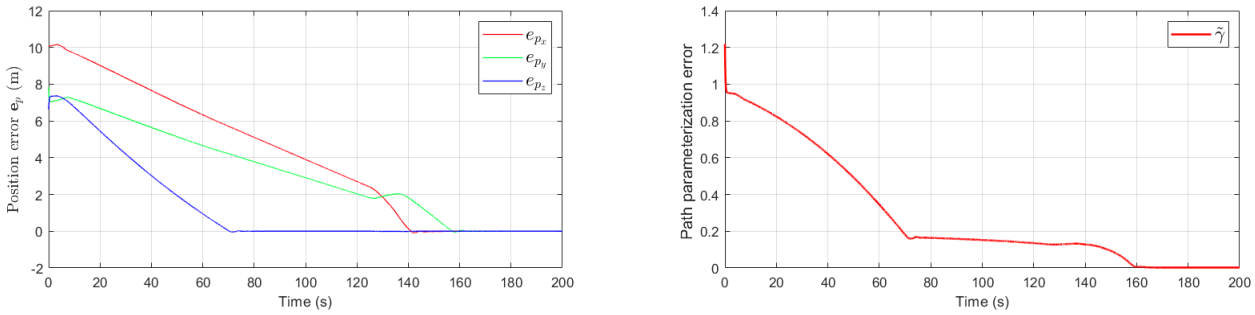

Figure 6.6: Evolution in time of position error $\boldsymbol{e}_p = \boldsymbol{p} - \boldsymbol{p}_d = [e_{p_x}, e_{p_y}, e_{p_z}]^T$ and path parameterization variable error $\tilde{\gamma}$ with no estimation of the ocean current velocity $\boldsymbol{V}_c$.

6.2.3 Cooperation Scenario

Finally, we implement our controller system and tracking filter in a more realistic scenario with a moving target, i.e, a diver. Similar to the previous scenario, the simulation consists on having the AUV join the diver and position itself on a desired point $\boldsymbol{p}_d(\gamma_d)$, parameterized by γ_d, along a circular path with a predefined safety radius R. Note that, here we parameterize a circular path centered on the diver, but the control system can work with other types of curve parameterizations, e.g., ellipses, taking the mission objectives in mind, extending the

original work [93]. The AUV starts from the initial condition $\boldsymbol{\eta} = [15, 15, 30, 0, 0, 0]^T$ and $\boldsymbol{\nu}] = [0, 0, 0, 0, 0, 0]^T$, and the target initial position $\boldsymbol{p}_t = [5, 5, 20]^T$ and velocity $\boldsymbol{v}_t = [0.1, 0.1, 0]^T$. This time, γ_d is not arbitrary but concerns the closest point between the circular path and the mission site, as shown in Fig. 6.7. Additionally, the AUV must maintain an attitude such as to point towards the mission site location $\boldsymbol{p}_m = [x_m, y_m, z_m]$, providing a sense of direction to the nearby diver. Finally, we consider that the diver position measurements are imbued with zero-mean Gaussian noise with standard deviation of $\sigma_t = 0.4$ m all three directions, with an observation time of 1 second, the vehicle possesses model parameter uncertainties of 10% and there exists some sort of ocean current with unknown initial values. The tracking filter is designed with a process noise variance $\sigma_q = 0.1$ and a measurement noise variance of $\sigma_x = \sigma_y = \sigma_z = 0.1$ m, following the choices of the tracking filter implementation of the authors in [36], within a context of a real marine mission. The filter target state is initialized at zero except for its position which is initialized around the initial measured target position $\boldsymbol{p}_t$.

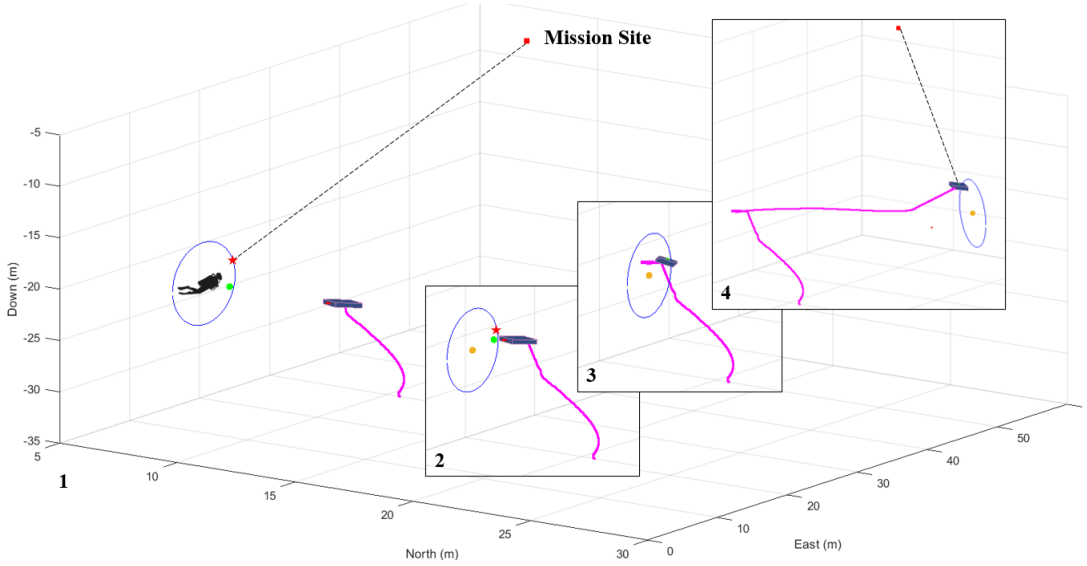

Figure 6.7: The cooperation scenario, where the AUV is initially deployed far away from the diver, represented in yellow. In the initial approach (1), the AUV converges to the closest point $\boldsymbol{p}_d(\gamma)$, represented in green, between it and the diver while the attitude controller keeps the roll and pitch stabilized and the heading aligned with the velocity vector. Then, in (2), the AUV follows $\boldsymbol{p}_d(\gamma)$ along the circular path, where $\boldsymbol{p}_d(\gamma)$ is converging to the closest point between the diver and the mission site $\boldsymbol{p}_d(\gamma_d)$, represented as a red star. At the same time (3), the AUV heading changes to face the mission site. In the end (4), when the vehicle has approached the diver, it maintains its heading and follows the diver, maintaining a safe distance.

Guidance System

With all of this in mind, a guidance system was developed providing the reference signals to the control system that satisfy our mission requirements. Related to the positioning controller, the circular path radius R is parameterized by

$$\boldsymbol{p}_d^t(\gamma) = R \begin{bmatrix} \boldsymbol{i} & \boldsymbol{j} \end{bmatrix} \begin{bmatrix} \cos(\gamma) \\ \sin(\gamma) \end{bmatrix} \tag{6.4}$$

where $\boldsymbol{i}$ and $\boldsymbol{j}$ are orthogonal unit vectors that define the circular plane of the path. Then, taking the derivative with respect to γ we obtain

$$\frac{\partial \boldsymbol{p}_d^t(\gamma)}{\partial \gamma} = R \begin{bmatrix} \boldsymbol{i} & \boldsymbol{j} \end{bmatrix} \begin{bmatrix} -\sin(\gamma) \\ \cos(\gamma) \end{bmatrix} \tag{6.5}$$

Regarding the convergence point γ_d, since γ is a parameterization of a 2D circle, this can be seen as an angular location of the mission site projection onto the circular path. Therefore, γ_d is the angle between the distance of the mission site and the diver in the horizontal plane $d_{xy} = \left\| \begin{bmatrix} x_m - x_t & y_m - y_t \end{bmatrix} \right\|$, and the vertical distance $d_z = z_m - z_t$ where $\boldsymbol{p}_m = [x_m, y_m, z_m]^T \in \mathbb{R}^3$. is the inertial position of our mission site. With this, we have that $\gamma_d = \text{atan2}(d_z, d_{xy})$, where atan2 stands for the "2-argument arctangent".

Relative to the attitude controller, we want the vehicle to stabilize its attitude around zero in roll $\phi_d = 0$ and pitch $\theta_d = 0$, and change its yaw such as to point towards the mission site position, specifying $\Delta_d = \text{atan2}\,(y_m - y, x_m - x)$. Then, this is fed to the controller by parameterization of the desired rotation matrix via the desired Euler angles $\boldsymbol{R}_d(\phi_d, \theta_d, \psi_d)$. Additionally, during the AUV initial approach with the diver, we do not want the vehicle to immediately face the mission site, but instead face the desired point to converge reducing the side-slip angle, and consequently lessening the actuators strain. For that, we adopt a similar approach implemented by the authors in [55], where the desired yaw angle ψ_d is a mix between δ_d and $\zeta_d = \text{atan2}(v_y - y, v_x - x)$ where the latter allows the vehicle yaw to align with its body velocity vector in surge. This mixing is then made by merging both angles with a sigmoid function, defining the desired yaw as

$$\psi_d = k\zeta_d + (1-k)\Delta_d \tag{6.6}$$

where $k = \frac{1}{2}\left(\tanh\left(\frac{\|\boldsymbol{p}_t - \boldsymbol{p}\| - \sigma_m}{k_\psi}\right) + 1\right)$, and σ_m and k_ψ are control parameters with the former denoting maximum distance in which the change in the desired yaw angle occurs, and the latter representing how "fast" this change should occur.

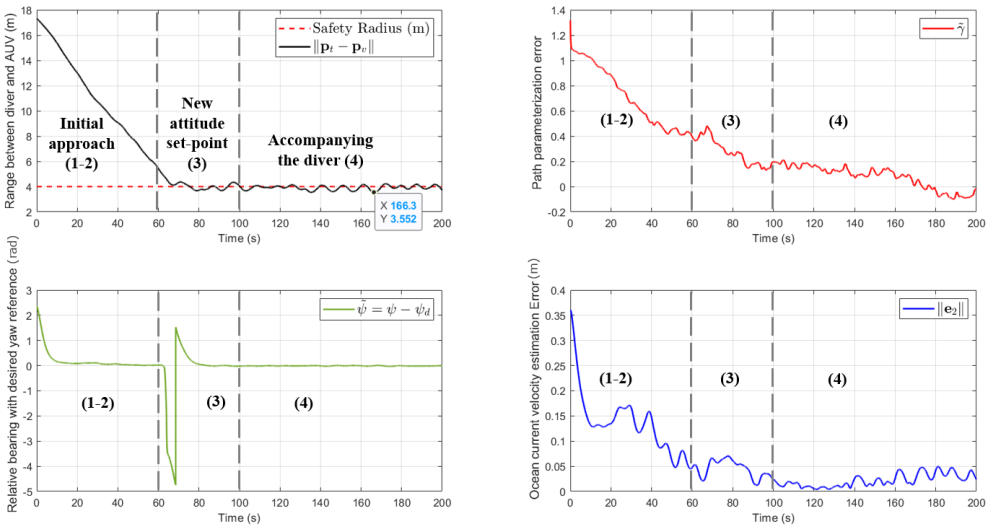

Figure 6.8: Evolution in time of the range between the diver and the AUV true positions given by $\|\boldsymbol{p}_t - \boldsymbol{p}_v\|$, the path parameterization variable error $\tilde{\gamma}$, the relative bearing between the AUV attitude and the mission site $\tilde{\psi}$, as well as the ocean current velocity estimate error $\boldsymbol{e}_2$. The slightly drastic change in yaw reference is related with the output of the guidance system yaw reference, given by (6.6).

The obtained results, presented in Fig. 6.8, show that even under model parameter uncertainty and noisy data from the diver's position, the positioning controller is able to track the diver, maintaining a safety distance around 4 meters with a maximum error of ≈0.5 meters. The oscillations that are evidenced in the range plot, in the upper-left graph, are due to these model parameter uncertainty and noisy data, which translates into oscillations on the desired position for the AUV to follow. However, this is not a fault or undesired effect from the controller, but instead due to the nature of the obtained data, which naturally our control system can not have authority. The attitude controller is also able to reduce the relative bearing between the AUV attitude and mission site. However, due to the existence of model uncertainty parameters, as expected from the fact that our observer is model-based, the ocean current estimation error $\boldsymbol{e}_2$ is bounded and does not converge to the origin.

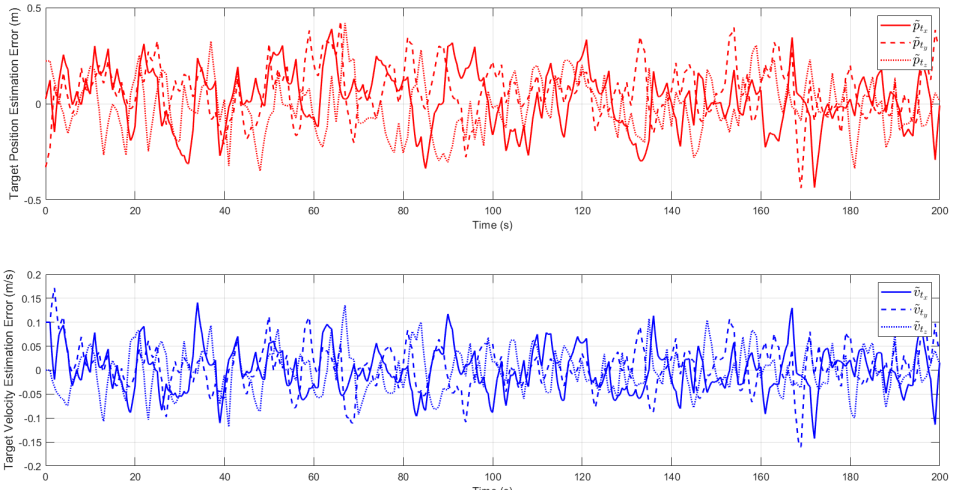

Figure 6.9: Evolution in time of estimation errors of diver position $\tilde{\boldsymbol{p}}_t$ and diver velocity $\tilde{\boldsymbol{v}}_t$.

Finally, in Fig. 6.9it is also possible to validate the fact that our controller can operate without access to measurements of diver velocity $\boldsymbol{v}_t$. The tracking filter provides estimates of the diver state $\hat{x}_t = [\hat{\boldsymbol{p}}_t^T, \hat{\boldsymbol{v}}_t^T]^T$ via periodic noisy measurements of the target position from an on-board sensor. Ultimately this allows us to not only obtain a continuously filtered version of the diver position, but also the target inertial velocity estimate $\hat{\boldsymbol{v}}_t$.

Chapter 7

Conclusions

This thesis addressed a number of modeling, navigation and control problems to promote cooperation synergies between a diver and a robot in order to reduce diving operation risks and increase operation efficiency and versatility. Beginning with Chapter 2, we defined some mathematical notations that were used in this thesis and introduced important concepts regarding theory of stability of non-linear systems, which supported the work of subsequent chapters. More specifically, we introduced the notions of autonomous and non-autonomous systems, with their respective differences, the different stability properties of equilibrium points, and important tools towards proving stability of individual systems and possible interconnections between them.

In Chapter 3, we introduced a general vehicle model for an underwater vehicle traveling in three dimensions, requiring a 6 DOF description. For that, we defined the frames of reference require to represent such vehicle motions, as well as their equations of motion regarding the kinematic components and dynamics that arise when moving submerged in an water medium.

In Chapter 4, we discussed the tasks that divers perform during different types of diving operations, and highlighted possible cooperation strategies between the diver and AUV, enabling a more safe way to carry out these operations, possible reducing associated mission costs and complexity, and most importantly, increase versatility and efficiency via the different capabilities that an AUV can provide underwater via its onboard sensors. Given this discussion, we established mechanisms for the AUV to "see" the diver and locate him/her. Without this, a great part of the cooperation synergy between the AUV and the diver would be lost. We presented classical and novel solutions to solve this problem of diver localization and discussed their different implementations, as well as respective advantages and disadvantages. Then, we introduced the concept of diver tracking which builds on top of the previously discussed localization solutions, in which the kinematic components of the diver (position, velocity, etc.) can be obtained via filtering techniques. We proposed a simple tracking Kalman filter for the diver, based on their position measurement provided by one of the diver localization solution, giving the necessary information for an AUV control system towards promoting cooperation with a diver. We finalized this chapter with the proposal of a cooperation architecture, with the AUV different systems (guidance, navigation and control) that promote a specific cooperation strategy, and the necessary requirements for the design of a control system.

In Chapter 5, we derived a control system that met necessary requirements presented in our proposed cooperation architecture using Lyapunov based techniques. For that, we formulated the design strategy for our

controller, which followed an inner-outer loop approach allowing us to separate and aid us in solving the problems of controlling the vehicle kinematic and dynamic components independently. This translated into a problem of providing the desired velocities for the vehicle to achieve, in order to stabilize its kinematic components of attitude and position independently, since our vehicle is considered to be fully actuated. Regarding the position control, a *moving path-following* controller was proposed to solve the problem of stabilizing the vehicle position along a desired time-independent parameterized path. This methodology achieved a good path-following performance by: i) defining a path-dependent positioning error space that exhibits a GAS equilibrium point; ii) introducing the concept of saturation function, we achieve a generalized approach to control the desired position, resulting in better transients between points by shaping the control law parameters; iii) introducing the positioning error state in the path parameterization error space, the virtual particle evolves taking into account the distance with the vehicle, either evolving into the the vehicle's projection onto the path, or evolving to the desired path parameterization reference. The attitude control towards stabilizing at an arbitrary desired attitude was formulated as a set-point regulation problem, where the control design regarded the attitude error dynamics as a system evolving on the space of $SO(3)$. This allowed circumventing the usual setbacks posed on the local parameterization of rotation matrices using Euler angles, or via the use of quaternions. With that, we derived an attitude controller that achieved attitude error dynamics with AGAS equilibrium points, i.e. the point is stable and except for a set of zero measures all initial conditions converge to it. Then, given the velocity requirements given by the outer loop, the next step followed naturally of deriving an inner loop controller that provided the vehicle with the necessary forces and moments to achieve these velocity requirements. That was achieved via a simple model-based control strategy, taking advantage of knowing the vehicle model beforehand, deriving an inner loop controller that forced the velocity error dynamics to have GES equilibrium points. Now, having both inner and outer loops established, we proceed to analyze the stability of their interconnection due to the existence of interconnected terms between both systems. We approached this problem via concepts of ISS and IOS, where we proved that given arbitrary initial conditions, the system is always stable for a certain appropriate choice of gains.

Finally, in Chapter 6, we presented a brief overview on a fully-actuated vehicle in which the proposed cooperation architecture and related systems could be implemented. More specifically, we presented the known model parameters of this vehicle, and approximated other unknown parameters with known parameters from similar vehicles on the literature. Afterwards, the control allocation system, that is, the system that produced the necessary actuator input signals from the desired forces and moment given by the control system, was briefly discussed and an unconstrained control allocation solution was proposed. With this, the overall architecture of the vehicle control and navigation system was presented, towards implementation and simulation of the proposed strategies and derived control system. Results were established showing the controller performance and robustness regarding the desired equilibrium points stability and convergence properties, even in the presence of sensor noise and estimates of the diver state provided by a Kalman filter. We have also shown the controller and ocean current velocity observer dependence on the uncertainty of model parameters.

7.1 Future Work

The results presented in this thesis leave several avenues open for future research. Though the AUV model presented in Chapter 3 accurately represents an abstract underwater vehicle motion, it requires huge knowledge on its parameters. The next logical step is to use experimental data to validate this model and identify its parameters. However, this is not straightforward and requires intense experimentation and testing [100]. Therefore, a future approach to the types of controllers presented here that require knowledge of such models should be extended to take into account robustness against uncertainties in the model parameters. Work developing such strategies have already proven to be possible to implement [24].

The cooperation strategies presented in Chapter 4 can be approached in many fronts. In this thesis, we only presented a control and navigation architecture that approach a certain cooperation strategy in its most abstract form possible. Other control and navigation architecture should be presented tackling other different cooperation strategies highlighted in this work, such as having an autonomous vehicle performing underwater tasks such as valve turning, inspecting certain areas, collecting samples, etc, based on the diver's gestures serving as an higher authority for the AUV mission planner. For example, the European project SWARMs [102] developed work semi-autonomous manipulation with ROV, as well as the previously mentioned project Ocean One [23] developing an AUV platform capable of tool manipulation with hard and soft actuators. The diver then could reach a desired location with an AUV following him/her, and then redirect the robot to carry certain task and then return near the diver.

In Chapter 4, we also discussed available technology and architectures towards localization of diver via acoustic range measurements, or via image processing algorithms with optical sensors. However, there is barely any mention of obtaining velocity components of a diver (or even other arbitrary targets). This is not true for the case of obtaining velocity components of an AUV, since there exists available technology towards obtaining such data, e.g., DVL. That way, this would extended the use of diver tracking based on POM tracking filters to PVM filters, resulting in more accurate estimations of the position and velocity components of a diver.

In Chapter 5, was specifically applied to the motion control of a single vehicle. However, we can envision different applications where the present methodology can yield interesting results in different applications, such as target tracking with a drone or with others types of autonomous vehicles, to stabilize and change attitude in different requirements. Nonetheless, this controller is not perfect and further analysis is required to study the controller stability in a scenario where we do not have access to the vehicle true states but instead its estimates via robust and efficient state of the art navigation systems, a recurrent scenario in underwater autonomous missions, which we did not cover in this thesis. Additionally, we approached the attitude control problem as a *set-point regulation* of stabilizing in an arbitrary attitude value. Therefore, an additional challenge is to go from stabilization to reference-tracking (similar to the problem of *trajectory tracking* or *path-following*). Finally, the interconnection problem of dynamics and kinematics is not straightforward for systems evolving in $SO(3)$ and we did not prove IOS for the attitude subsystem. Recalling that our attitude subsystem output is a time-derivative of a mapping from $SO(3)$ to $\mathbb{R}^3$, an initial approach is suggested by considering tangent spaces in these rotational groups [99]. In the case of under-actuated underwater system this might prove even more difficult, as seen in [54], [103], therefore, a stability analysis of these interconnection terms.

Lastly, if possible, it is promising to apply the principles set forth in this thesis in a real vehicle with real conditions underwater to validate and test for comparison with the simulation results. The feedback obtained from such mission could provide huge insight and value to see if the actual cooperation strategies reduced the risks that divers undertake in diving operations, and increase their tasks productivity.

Bibliography

[1] S. Lucrezi, S. Egi, M. Pieri, *et al.*, "Safety Priorities and Underestimations in Recreational Scuba Diving Operations: A European Study Supporting the Implementation of New Risk Management Programmes", *Frontiers in Psychology*, vol. 9, p. 383, Mar. 2018.

[2] P. Denoble, J Caruso, G. Dear, C. Pieper, and R. Vann, "Common causes of open-circuit recreational diving fatalities", *Undersea and hyperbaric medicine : journal of the Undersea and Hyperbaric Medical Society, Inc*, vol. 35, pp. 393–406, Nov. 2008.

[3] E. Zereik, M. Bibuli, N. Mišković, P. Ridao, and A. Pascoal, "Challenges and future trends in marine robotics", *Annual Reviews in Control*, vol. 46, pp. 350–368, 2018.

[4] V. Huvenne, K. Robert, L. Marsh, C. Lo Iacono, T. Le Bas, and R. Wynn, "ROVs and AUVs", in Jul. 2018, pp. 93–108.

[5] N. Misković, u. N., and I. Rendulic, "Tracking Divers: An Autonomous Marine Surface Vehicle to Increase Diver Safety", *IEEE Robotics and Automation Magazine*, vol. 22, pp. 72–84, 2015.

[6] T. Nakatani, T. Hyakudome, T. Sawa, *et al.*, "Development of an autonomous surface vehicle for monitoring underwater vehicles", in *OCEANS 2015 - MTS/IEEE Washington*, 2015, pp. 1–5.

[7] B. Braginsky, A. Baruch, and H. Guterman, "Development of an Autonomous Surface Vehicle capable of tracking Autonomous Underwater Vehicles", *Ocean Engineering*, vol. 197, p. 106 868, 2020.

[8] M. Sasano, S. Inaba, A. Okamoto, *et al.*, "Development of a semi-submersible autonomous surface vehicle for control of multiple autonomous underwater vehicles", in *2016 Techno-Ocean (Techno-Ocean)*, 2016, pp. 309–312.

[9] P. Kimball, J. Bailey, S. Das, *et al.*, "The WHOI Jetyak: An autonomous surface vehicle for oceanographic research in shallow or dangerous waters", in *2014 IEEE/OES Autonomous Underwater Vehicles (AUV)*, 2014, pp. 1–7.

[10] L. Whitcomb, D. R. Yoerger, H. Singh, and J. Howland, "Advances in Underwater Robot Vehicles for Deep Ocean Exploration: Navigation, Control, and Survey Operations", in *Robotics Research*, J. M. Hollerbach and D. E. Koditschek, Eds., London: Springer London, 2000, pp. 439–448.

[11] G. Nootz, E. Jarosz, F. R. Dalgleish, and W. Hou, "Quantification of optical turbulence in the ocean and its effects on beam propagation", *Appl. Opt.*, vol. 55, no. 31, pp. 8813–8820, 2016.

[12] R. Cunha, C. Silvestre, and J. Hespanha, "Output-feedback control for stabilization on SE(3)", in *Proceedings of the 45th IEEE Conference on Decision and Control*, 2006, pp. 3825–3830.

[13] P. Maurya, A. P. Aguiar, and A. Pascoal, "Marine Vehicle Path Following Using Inner-Outer Loop Control", *IFAC Proceedings Volumes*, vol. 42, no. 18, pp. 38–43, 2009, 8th IFAC Conference on Manoeuvring and Control of Marine Craft.

[14] I. Fantoni, R. Lozano, and F. Kendoul, "Asymptotic Stability of Hierarchical Inner-Outer Loop-Based Flight Controllers", *IFAC Proceedings Volumes*, vol. 41, no. 2, pp. 1741–1746, 2008, 17th IFAC World Congress.

[15] D. D. R. A. Report, *Cooperative Cognitive Control for Autonomous Underwater Vehicles*. http://robotics.jacobs-university.de/projects/Co3-AUVs/publicdeliverables/D11-RequirementsAnalysis.pdf.

[16] *Cognitive Robotics: Cooperative Control and Navigation of Multiple Marine Robots for Assisted Human Diving Operations*, https://cordis.europa.eu/project/id/255216, Accessed: 2021-09-20.

[17] G. De Cubber and D. Doroftei, *Search and Rescue Robotics - From Theory to Practice*. Aug. 2017.

[18] N. Miskovic, M. Bibuli, A. Birk, *et al.*, "CADDY—Cognitive Autonomous Diving Buddy: Two Years of Underwater Human-Robot Interaction", *Marine Technology Society Journal*, vol. 50, pp. 54–66, Jul. 2016.

[19] A. Gomez Chavez, A. Ranieri, D. Chiarella, E. Zereik, A. Babić, and A. Birk, "CADDY Underwater Stereo-Vision Dataset for Human–Robot Interaction (HRI) in the Context of Diver Activities", *Journal of Marine Science and Engineering*, vol. 7, no. 1, p. 16, 2019.

[20] M. J. Islam, M. Ho, and J. Sattar, "Dynamic Reconfiguration of Mission Parameters in Underwater Human-Robot Collaboration", in *2018 IEEE International Conference on Robotics and Automation (ICRA)*, 2018, pp. 6212–6219.

[21] J. Hong, S. S. Enan, C. Morse, and J. Sattar, "Visual Diver Face Recognition for Underwater Human-Robot Interaction", *ArXiv*, vol. abs/2011.09556, 2020.

[22] K. de Langis and J. Sattar, "Real-Time Multi-Diver Tracking and Re-identification for Underwater Human-Robot Collaboration", *ArXiv*, 2019.

[23] O. Khatib, X. Yeh, G. Brantner, *et al.*, "Ocean One: A Robotic Avatar for Oceanic Discovery", *IEEE Robotics Automation Magazine*, vol. 23, no. 4, pp. 20–29, 2016.

[24] A. Aguiar and A. Pascoal, "Dynamic positioning and way-point tracking of underactuated AUVs in the presence of ocean currents", *International Journal of Control*, vol. 80, no. 7, pp. 1092–1108, 2007.

[25] P. Aguiar, J. Hespanha, and A. Pascoal, "Switched seesaw control for the stabilization of underactuated vehicles", *Automatica*, vol. 43, pp. 1997–2008, Dec. 2007.

[26] K. Pettersen and T. I. Fossen, "Underactuated dynamic positioning of a ship-experimental results", *IEEE Transactions on Control Systems Technology*, vol. 8, no. 5, pp. 856–863, 2000.

[27] A. Pascoal, C. Silvestre, and P. Oliveira, "Vehicle and Mission Control of Single and Multiple Autonomous Marine Robots", *Advances in Unmanned Marine Vehicles*, Jan. 2005.

[28] P. Aguiar and J. P. Hespanha, "Trajectory-Tracking and Path-Following of Underactuated Autonomous Vehicles With Parametric Modeling Uncertainty", *IEEE Transactions on Automatic Control*, vol. 52, no. 8, pp. 1362–1379, 2007.

[29] E. Lefeber, K. Pettersen, and H. Nijmeijer, "Tracking control of an underactuated ship", *IEEE Transactions on Control Systems Technology*, vol. 11, no. 1, pp. 52–61, 2003.

[30] P. Aguiar, J. Hespanha, and P. Kokotović, "Path-following for nonminimum phase systems removes performance limitations", *Automatic Control, IEEE Transactions on*, vol. 50, pp. 234 –239, Mar. 2005.

[31] C. Samson, "Time-varying Feedback Stabilization of Car-like Wheeled Mobile Robots", *The International Journal of Robotics Research*, vol. 12, no. 1, pp. 55–64, 1993.

[32] T. I. Fossen, *Handbook of Marine Craft Hydrodynamics and Motion Control*, First Edition. Wiley, May 2011.

[33] P. Encarnação and A. Pascoal, "3D path following for autonomous underwater vehicle", vol. 3, Feb. 2000, 2977 –2982 vol.3.

[34] P. Encarnação, A. Pascoal, and M Arcak, "Path Following for Marine Vehicles in The Presence of Unknown Currents", Sep. 2000.

[35] L. Lapierre, D. Soetanto, and A. Pascoal, "Nonlinear path following with applications to the control of autonomous underwater vehicles", vol. 2, Jan. 2004, 1256 –1261 Vol.2.

[36] M. F. Reis, R. P. Jain, P. Aguiar, and J. B. de Sousa, "Robust Moving Path Following Control for Robotic Vehicles: Theory and Experiments", *IEEE Robotics and Automation Letters*, vol. 4, no. 4, pp. 3192–3199, 2019.

[37] S. Sastry, *Nonlinear Systems: Analysis, Stability and Control*. Springer, 1998.

[38] D. Boskovic and M. Krstic, "Global attitude/position regulation for underwater vehicles", in *Proceedings of the 1999 IEEE International Conference on Control Applications (Cat. No.99CH36328)*, vol. 2, 1999, 1768–1773 vol. 2.

[39] S. Bhat and D. Bernstein, "A topological obstruction to continuous global stabilization of rotational motion and the unwinding phenomenon", *Systems and Control Letters*, vol. 39, pp. 63–70, 2000.

[40] J. Yu, J. Wang, and Q. Li, "A Condition for Almost Global Stability and Local Asymptotical Stability of Nonlinear System", *Procedia Engineering*, vol. 29, pp. 159–163, 2012, 2012 International Workshop on Information and Electronics Engineering.

[41] R. Cunha, "Advanced Motion Control for Autonomous Air Vehicles", Ph.D. dissertation, Instituto Superior Técnico, 2007.

[42] D. Cabecinhas, R. Cunha, and C. Silvestre, "Almost global stabilization of fully-actuated rigid bodies", *Systems and Control Letters*, vol. 58, no. 9, pp. 639–645, 2009.

[43] H. K. Khalil, *Nonlinear systems*, Third Edition. Upper Saddle River, NJ: Prentice-Hall, 2002.

[44] E. D. Sontag, "Input to State Stability: Basic Concepts and Results", in *Nonlinear and Optimal Control Theory: Lectures given at the C.I.M.E. Summer School held in Cetraro, Italy June 19–29, 2004*, P. Nistri and G. Stefani, Eds. Berlin, Heidelberg: Springer Berlin Heidelberg, 2008, pp. 163–220.

[45] E. D. Sontag and Y. Wang, "A notion of input to output stability", pp. 3862–3867, 1997.

[46] D. Angeli and L. Praly, "Stability Robustness in the Presence of Exponentially Unstable Isolated Equilibria", *IEEE Transactions on Automatic Control*, vol. 56, no. 7, pp. 1582–1592, 2011.

[47] D. Angeli and D. Efimov, "Characterizations of Input-to-State Stability for Systems With Multiple Invariant Sets", *IEEE Transactions on Automatic Control*, vol. 60, no. 12, pp. 3242–3256, 2015.

[48] A. Teel, "A nonlinear small gain theorem for the analysis of control systems with saturation", *IEEE Transactions on Automatic Control*, vol. 41, no. 9, pp. 1256–1270, 1996.

[49] R. M. Murray, Z. Li, and S. S. Sastry, *A Mathematical Introduction to Robotic Manipulation*, First Edition. CRC Press, 1994.

[50] E. D. Sontag, *Mathematical Control Theory*, Second Edition. Springer, 1998.

[51] L. Marconi and R. Naldi, "Robust full degree-of-freedom tracking control of a helicopter", *Automatica*, vol. 43, no. 11, pp. 1909–1920, 2007.

[52] *Mainstream Commercial Divers, Inc., Coal Pier Repair And Modifications*, https://www.mainstreamdivers.com/MoranSharedCmsContent/CaseStudyView.asp?NewsID=67, Accessed: 2021-09-08.

[53] *NEOSUB, Mira-Aquinova*, http://neosub.com, Accessed: 2021-09-08.

[54] P. Aguiar, J. Almeida, B. Bayat, *et al.*, "Cooperative Autonomous Marine Vehicle motion control in the scope of the EU GREX Project: Theory and Practice", Jun. 2009, pp. 1 –10.

[55] D. Nad, F. Mandić, and N. Mišković, "Using Autonomous Underwater Vehicles for Diver Tracking and Navigation Aiding", *Journal of Marine Science and Engineering*, vol. 8, no. 6, 2020.

[56] J. Baghdady, M. Incze, P. Dias, *et al.*, "Enabling Interoperability among Disparate Unmanned Vehicles via Coordinated Command, Control, and Communications Strategies", in *Global Oceans 2020: Singapore – U.S. Gulf Coast*, IEEE, Oct. 2020.

[57] T. Matsuda, T. Maki, Y. Sato, and T. Sakamaki, "Sea experiments and tank tests on alternating landmark navigation using multiple AUVs: Towards accurate and efficient survey of seafloor by AUVs", in *2016 IEEE/OES Autonomous Underwater Vehicles (AUV)*, 2016, pp. 213–221.

[58] M. Monteiro Marques, M. Gatta, M. Barreto, *et al.*, "Assessment of a Shallow Water Area in the Tagus Estuary Using Unmanned Underwater Vehicle (or AUV's), Vector-Sensors, Unmanned Surface Vehicles, and Hexacopters – REX'17", in *2018 OCEANS - MTS/IEEE Kobe Techno-Oceans (OTO)*, 2018, pp. 1–5.

[59] E. Simetti, S. Galeano, and G. Casalino, "Underwater vehicle manipulator systems: Control methodologies for inspection and maintenance tasks", Apr. 2016, pp. 1–7.

[60] S. Wehkamp and P. Fischer, "Impact of coastal defence structures (tetrapods) on a demersal hard-bottom fish community in the southern North Sea", *Marine environmental research*, vol. 83, Nov. 2012.

[61] *PIA - Platelet Ice Anthozoas*, https://www.awi.de/en/science/special-groups/scientific-diving/scientific-projects.html, Accessed: 2021-09-09.

[62] C. Chesher, "Robots and the Moving Camera in Cinema, Television and Digital Media", vol. 9549, Jul. 2016, pp. 98–106.

[63] D. Jóźwiak, P. Siermontowski, Z. DąbrowieckiI, and R. Olszański, "Analysis of the risk of diving accidents in military and recreational diving", *Polish Hyperbaric Research*, vol. 53, no. 4, 2016.

[64] A. Gómez-Espinosa, E. Cuan-Urquizo, and J. González-García, "Autonomous Underwater Vehicles: Localization, Navigation, and Communication for Collaborative Missions", *Applied Sciences*, vol. 10, p. 1256, Feb. 2020.

[65] T. Gode, "Long Baseline Ranging Acoustic Positioning System", Virginia Polytechnic Institute and State University, M.S. thesis, 2015.

[66] J. Zhang, Y. Han, C. Zheng, and D. Sun, "Underwater target localization using long baseline positioning system", *Applied Acoustics*, vol. 111, pp. 129–134, Oct. 2016.

[67] S. Smith and D. Kronen, "Experimental results of an inexpensive short baseline acoustic positioning system for AUV navigation", in *Oceans '97. MTS/IEEE Conference Proceedings*, vol. 1, 1997, pp. 714–720.

[68] H.-P. Tan, R. Diamant, W. K. Seah, and M. Waldmeyer, "A survey of techniques and challenges in underwater localization", *Ocean Engineering*, vol. 38, no. 14, pp. 1663–1676, 2011.

[69] W. Nodland, T. Ewart, W. Bendiner, J. Miller, and E. Aagaard, "SPURV II-An Unmanned, Free-Swimming Submersible Developed for Oceanographic Research", in *OCEANS 81*, 1981, pp. 92–98.

[70] P. H. Milne, *Underwater acoustic positioning systems*. Gulf Publishing Company, Jan. 1983.

[71] M. Morgado, "Advanced Ultra-Short Baseline Inertial Navigation Systems", Ph.D. dissertation, Instituto Superior Técnico, 2011.

[72] M. Morgado, P. Batista, P. Oliveira, and C. Silvestre, "Position USBL/DVL sensor-based navigation filter in the presence of unknown ocean currents", *Automatica*, vol. 47, no. 12, pp. 2604–2614, 2011.

[73] F. Mandić, I. Rendulić, N. Miskovic, and Đula Nađ, "Underwater Object Tracking Using Sonar and USBL Measurements", *Journal of Sensors*, vol. 2016, Jan. 2016.

[74] M. Carvalho, "Nonlinear Marine Animals Tracking System from Multiple USBL/INS Units", Instituto Superior Técnico, M.S. thesis, 2011.

[75] A. B. Figueiredo, B. M. Ferreira, and A. C. Matos, "Tracking of an underwater visual target with an autonomous surface vehicle", in *2014 Oceans - St. John's*, 2014, pp. 1–5.

[76] R. Schettini and S. Corchs, "Underwater Image Processing: State of the Art of Restoration and Image Enhancement Methods", *EURASIP J. Adv. Signal Process*, vol. 2010, Jan. 2010.

[77] D. Lee, G. Kim, D. Kim, H. Myung, and H.-T. Choi, "Vision-based object detection and tracking for autonomous navigation of underwater robots", *Ocean Engineering*, vol. 48, pp. 59–68, 2012.

[78] J. A. Monroy-Anieva, C. Rouviere, E. Campos-Mercado, T. Salgado-Jimenez, and L. G. Garcia-Valdovinos, "Modeling and Control of a Micro AUV: Objects Follower Approach", *Sensors*, vol. 18, no. 8, 2018.

[79] D. Dai, M. Chantler, D. Lane, and N. Williams, "A spatial-temporal approach for segmentation of moving and static objects in sector scan sonar image sequences", in *Fifth International Conference on Image Processing and its Applications, 1995.*, 1995, pp. 163–167.

[80] T. Zhang, S. Liu, X. He, H. Huang, and K. Hao, "Underwater Target Tracking Using Forward-Looking Sonar for Autonomous Underwater Vehicles", *Sensors*, vol. 20, no. 1, 2020.

[81] D. W. Krout, W. Kooiman, G. Okopal, and E. Hanusa, "Object tracking with imaging sonar", in *2012 15th International Conference on Information Fusion*, 2012, pp. 2400–2405.

[82] J. Saniie, M. Kupnik, and E. Oruklu, "Advances in Acoustic Sensing, Imaging, and Signal Processing", *Advances in Acoustics and Vibration*, vol. 2012, Sep. 2012.

[83] S. Sendra, J. Lloret, J. M. Jimenez, and L. Parra, "Underwater Acoustic Modems", *IEEE Sensors Journal*, vol. 16, no. 11, pp. 4063–4071, 2016.

[84] N. T. Hung, F. F. C. Rego, and A. Pascoal, "Cooperative Distributed Estimation and Control of Multiple Autonomous Vehicles for Range-Based Underwater Target Localization and Pursuit", *IEEE Transactions on Control Systems Technology*, pp. 1–15, 2021.

[85] A. Gadre and D. Stilwell, "A complete solution to underwater navigation in the presence of unknown currents based on range measurements from a single location", in *2005 IEEE/RSJ International Conference on Intelligent Robots and Systems*, 2005, pp. 1420–1425.

[86] P. Batista, C. Silvestre, and P. Oliveira, "Single range aided navigation and source localization: Observability and filter design", *Syst. Control. Lett.*, vol. 60, pp. 665–673, 2011.

[87] H. Nguyen and A. Pascoal, "Range-based Navigation and Target Localization: Observability Analysis and Guidelines for Motion Planning", Jun. 2020.

[88] M. Kumar and S. Mondal, "Recent developments on target tracking problems: A review", *Ocean Engineering*, vol. 236, p. 109 558, 2021.

[89] J. Luo, Y. Han, and L. Fan, "Underwater Acoustic Target Tracking: A Review", 1, vol. 18, 2018.

[90] K. Saho, "Kalman Filter for Moving Object Tracking: Performance Analysis and Filter Design", Feb. 2018.

[91] B. Ekstrand, "Some Aspects on Filter Design for Target Tracking", *Journal of Control Science and Engineering*, vol. 2012, May 2012.

[92] A. Isidori, L. Marconi, and A. Serrani, *Robust Autonomous Guidance: An Internal Model Approach*. Springer, 2003.

[93] u. n., F. Mandić, and N. Mišković, "Diver Tracking Using Path Stabilization - the Virtual Diver Experimental Results", *IFAC-PapersOnLine*, vol. 49, no. 23, pp. 214–219, 2016, 10th IFAC Conference on Control Applications in Marine SystemsCAMS 2016.

[94] M. Breivik and T. I. Fossen, "Principles of Guidance-Based Path Following in 2D and 3D", in *Proceedings of the 44th IEEE Conference on Decision and Control*, 2005, pp. 627–634.

[95] D. Koditschek, "The Application of Total Energy as a Lyapunov Function for Mechanical Control Systems", *Contemporary Mathematics, American Mathematical Society, 1989*, vol. 97, Feb. 1989.

[96] F. Bullo and A. D. Lewis, *Geometric Control of Mechanical Systems*, ser. Texts in Applied Mathematics. New York-Heidelberg-Berlin: Springer Verlag, 2004, vol. 49.

[97] N. A. Chaturvedi and N. H. McClamroch, "Attitude stabilization of the inverted 3D pendulum on TSO(3) with control saturation", in *2007 46th IEEE Conference on Decision and Control*, 2007, pp. 1910–1915.

[98] E. Børhaug, L. Pivano, K. Y. Pettersen, and T. A. Johansen, "A Model-Based Ocean Current Observer for a 6DOF Underwater Vehicle", *IFAC Proceedings Volumes*, vol. 40, no. 17, pp. 169–174, 2007, 7th IFAC Conference on Control Applications in Marine Systems.

[99] J. Mäkinen, "Rotation manifold SO(3) and its tangential vectors", *Computational Mechanics*, vol. 42, pp. 907–919, Nov. 2008.

[100] T. Prestero, "Verification of a six-degree of freedom simulation model for the REMUS autonomous underwater vehicle", 2001.

[101] M. Bodson, "Evaluation of Optimization Methods for Control Allocation", *Journal of Guidance Control and Dynamics - J GUID CONTROL DYNAM*, vol. 25, Jul. 2002.

[102] *Project SWARMs - Smart and Networking Underwater Robots in Cooperation Meshes*, http://www.swarms.eu/, Accessed: 2021-09-09.

[103] F. Vanni, "Coordinated Motion Control of Multiple Autonomous Underwater Vehicles", Ph.D. dissertation, Instituto Superior Técnico, 2007.

Appendix A

Cooperation Frameworks

The following table was created to summarize the different types of diving operations, associated risk/challenges and possible cooperation strategies.

Diving Operation	**Risks**		**Possible Human/Robot Cooperation Strategies**	**Benefits**	**Challenges**
	Common	Specific			
Commercial/ Industrial	Low visibility Limited breathing Nitrogen narcosis Decompression sickness Ocean currents Lacking sense of orientation	Interference of cabling systems Specialized and complex equipment Hazardous surrounding environment	Follow the diver within a safety radius and point towards the desired location underwater to aid the diver navigation. Observe the diver in the surrounding area to improve work conditions in a station-keeping manoeuvre. Monitor the diver towards a more controlled mission and checking of vital signs during work. Plan mission tasks online at the mission site according to the diver, via visual or acoustic signals, towards a more adaptive and responsive behaviour.	Reduced diver fatigue during diving operation. Faster diver worksite approach. Safer working environment. Stronger handling of harder-to-operate tools (e.g.,, valves, levers, etc). Faster approach to identified research sites. Quicker and safer delivery of research material to the surface team towards better and close examination. Better visualization of the research site. Search and observe new sites of interest that were not previously identified. Steadier recordings of videos and images via online tasks assignments from the diver. Self diver recording. Transportation of certain recording apparatus. Diver support towards search-and-rescue missions via acoustic, visual, or other suitable technology. Safe disposal of dangerous material found during the diving operation.	Hard and complex problem of autonomous control towards tool handling in underwater environments. Requires precise autonomous underwater navigation and localization. Multiple vehicles might need to operate co-jointly towards a better cooperation efficacy, complicating the overall cooperation strategy. Possible obstruction or making difficulty the diver diving operation with a nearby operating robot as well. Most cooperation strategies requires a fully-actuated vehicle to perform simultaneous tasks such as position and attitude control
Scientific		Overestimation of underwater diving skills Delicate and fragile environments			
Media		Overestimation of underwater diving skills			
Military		Handling of explosive ordnance Uncharted territory war scenarios Not enough planning time before diving operation			

Table A.1: Summary of the different types of diving operations, the associated risks faced by divers and identification of benefits/challenges arising from certain cooperation strategies.